THE EFFECT OF THE MUTAROTATION REACTION

ON THE CRYSTALLIZATION OF GLUCOSE

MONOHYDRATE

Sukanya Srisa-nga

A Thesis Submitted in Partial Fulfillment of the Requirements for the

Degree of Doctor of Philosophy in Chemical Engineering

Suranaree University of Technology

Academic Year 2005

ผลของปฏิกิริยามิวทาโรเทชันต่อการตกผลึกของกลูโคสโมโนไฮเดรต

นางสาวสุกัญญา ศรีสง่า
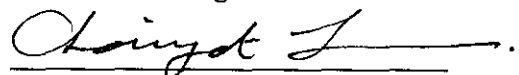
THE EFFECT OF THE MUTAROTATION REACTION ON THE

CRYSTALLIZATION OF GLUCOSE MONOHYDRATE

Suranaree University of Technology has approved this thesis submitted in partial fulfillment of the requirements for the Degree of Doctor of Philosophy.
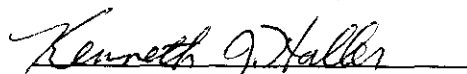
Thesis Examining Committee

_____

(Assoc. Prof. Dr. Chaiyot Tangsathitkulchai)
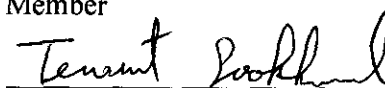
Chairperson

_____

(Asst. Prof. Dr. Adrian E. Flood)

Member (Thesis Advisor)

_____

(Assoc. Prof. Dr. Kenneth J. Haller)

Member

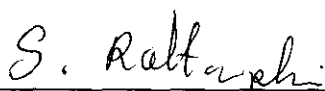_____

(Dr. Terasut Sookkumnerd)

Member

_____
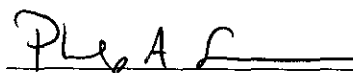
(Dr. Philip A. Schneider)

Member

_____   _____

(Assoc. Prof. Dr. Saowanee Rattanaphani)   (Assoc. Prof. Dr. Vorapot Khompis)

Vice Rector for Academic Affairs   Dean of Institute of Engineering

สุกัญญา ศรีสง่า : ผลของปฏิกิริยามิวทาโรเทชันต่อการตกผลึกของกลูโคสโมโนไฮเดรต
(THE EFFECT OF THE MUTAROTATION REACTION ON THE
CRYSTALLIZATION OF GLUCOSE MONOHYDRATE)
อาจารย์ที่ปรึกษา : ผศ. ดร.เอเดรียน ฟลัด, 191 หน้า. ISBN 974-533-487-1

น้ำตาลเป็นสินค้าที่จำเป็นในตลาดโลกแต่กลไกการตกผลึกของน้ำตาลหลาย ๆ ชนิดยังไม่
เป็นที่รู้จักแพร่หลายมากนัก ปัจจุบันนี้เป็นที่ทราบกันว่าปฏิกิริยามิวทาโรเทชันมีผลต่ออัตราการตก
ผลึกของน้ำตาลรีดิวซิง (reducing sugar) งานวิจัยนี้มีวัตถุประสงค์เพื่อสังเกตผลของปฏิกิริยามิว-
ทาโรเทชันต่ออัตราการตกผลึกรวมของน้ำตาลกลูโคสโมโนไฮเดรต ในการวิจัยใช้คาร์บอน 13-
เอ็นเอ็มอาร์ (^{13}C-NMR) วัดอัตราการเกิดปฏิกิริยามิวทาโรเทชันและค่าสมดุลปฏิกิริยาของกลูโคส
ในสารละลายที่มีน้ำเป็นตัวทำละลายในช่วงอุณหภูมิ 7 ถึง 35 องศาเซลเซียส และยังศึกษามิวทา-
โรเทชันของน้ำตาลชนิดอื่นๆ ด้วย เพื่อพิจารณาว่ามีข้อมูลใดบ้างที่จะยืนยันความสัมพันธ์ระหว่าง
ปฏิกิริยาและชนิดของน้ำตาล จุดเริ่มต้นของการเกิดนิวคลีเอชันแบบทุติยภูมิ (secondary
nucleation threshold) ในระบบการกวนแบบกะ (batch) ทำก่อนการทดลองหาอัตราการเติบโต
ของผลึก เพื่อให้แน่ใจว่าไม่มีนิวคลีเอชันเกิดในกระบวนการตกผลึก การตกผลึกแบบกะโดยใช้ตัว
ล่อทำในระบบที่มีการกวน ที่อุณหภูมิคงที่ในช่วงอุณหภูมิ 10 ถึง 40 องศาเซลเซียส

ผลการทดลองพบว่าค่าคงที่การเกิดปฏิกิริยามิวทาโรเทชันของน้ำตาลที่ศึกษาทุกชนิดเมื่อ
เทียบกับอุณหภูมิเป็นไปตามสมการของอาร์รีเนียส (Arrhenius equation) และไม่มีนัยสำคัญของ
ความสัมพันธ์ระหว่างค่าคงที่สมดุลปฏิกิริยาต่อความเข้มข้นของน้ำตาลหรืออุณหภูมิ อัตราการเกิด
มิวทาโรเทชันของน้ำตาลคีโตส (ketose sugar) เร็วกว่าอัตราการเกิดมิวทาโรเทชันของน้ำตาลอัล-
โดส (aldose sugar) และจำนวนของวงแหวนในโครงสร้างไม่มีผลต่ออัตราการเกิดปฏิกิริยามิว-
ทาโรเทชัน

ในช่วงอุณหภูมิที่ทดลองพบว่าช่วงของจุดเริ่มต้นของการเกิดนิวคลีเอชันแบบทุติยภูมิไม่
ขึ้นกับอุณหภูมิเมื่อพิจารณาความเข้มข้นยิ่งยวดสุทธิ (absolute supersaturation) เป็นแรง
ขับเคลื่อน (driving force) ข้อมูลนี้ใช้ในการบ่งชี้ช่วงของการตกผลึกในการทดลองตกผลึกแบบ
กะ การตกผลึกของผลึกกลูโคสโมโนไฮเดรตมีค่าคงที่การตกผลึกเป็นไปตามความสมการของอาร์-
รีเนียส และมีพลังงานกระตุ้นเท่ากับ 50 ± 2 กิโลจูลต่อโมล แรงขับเคลื่อนการตกผลึกถูกจำกัดโดย
จุดเริ่มต้นของการเกิดนิวคลีเอชันแบบทุติยภูมิที่ประมาณร้อยละ 10 ของความเข้มข้นยิ่งยวด
สัมพัทธ์ (relative supersaturation) ด้วยเหตุนี้รวมทั้งจลนพลศาสตร์การเติบโตค่อนข้างช้าดังนั้น
อัตราการเติบโตของผลึกที่วัดได้จึงน้อย นั่นคืออยู่ในช่วง 0.01 ถึง 0.10 ไมโครเมตรต่อนาที

II

แบบจำลองทางคณิตศาสตร์สร้างขึ้นโดยใช้ตัวแปรที่วัดได้จากทั้งการทดลองมิวทาโรเทชัน และอัตราการตกผลึก สมการอนุพันธ์สามัญ (ordinary differential equation) แสดงสมการ กลไกและสมการดุลยภาพ เขียนขึ้นเพื่ออธิบายระบบและจากนั้นก็แก้กลุ่มของสมการโดยใช้สภาวะ เริ่มต้นที่เหมาะสม พบว่าปริมาณการสะสมของมวล (mass deposition) บนพื้นผิวของผลึกเร็ว ขึ้นในกรณีที่ใช้ตัวล่อขนาดเล็ก ใช้อัตราการล่อสูง และใช้อุณหภูมิสูง การลดลงของปริมาณกลูโคส ชนิดแอลฟา (α-glucose) เป็นไปได้อย่างเร็วเมื่อใช้ตัวล่อขนาดเล็ก ใช้อัตราการล่อสูง และใช้ อุณหภูมิต่ำ สรุปได้ว่าสภาวะที่มิวทาโรเทชันจะเป็นขั้นตอนการกำหนดอัตรา (rate limiting step) หรือกำหนดอัตราการเกิดปฏิกิริยาบางส่วน (partially rate limiting) สามารถหาได้โดยง่ายโดย ใช้แบบจำลองทางคณิตศาสตร์ที่ได้นำเสนอไว้

สาขาวิชา<u>วิศวกรรมเคมี</u>   ลายมือชื่อนักศึกษา_____

ปีการศึกษา 2548   ลายมือชื่ออาจารย์ที่ปรึกษา_____

MUTAROTATION/BATCH CRYSTALLIZATION/GLUCOSE MONOHYDRATE

Crystalline sugars are significant commodities in the world market, however the crystallization mechanism of many sugars is still not well known. Recently it has been shown that the mutarotation reaction of reducing sugars plays a significant role in determining the crystallization rate of these sugars. This research aims to observe the effect of the mutarotation reaction on the overall crystallization rates of the α-glucose monohydrate. The mutarotation rate and equilibrium of glucose in aqueous solutions was measured over the temperature range of 7-35ºC, using ^{13}C-NMR. The mutarotation of other sugars was also studied to determine whether key data concerning the reaction could be correlated with the sugar type. Secondary nucleation thresholds were determined in an agitated batch system prior to the crystal growth experiment to ensure that no nucleation occurs in the crystallization process. Agitated seeded batch crystallizations were performed isothermally over the temperature range of 10-40°C.

The results show the that mutarotation rate constants of the sugars studied follow an Arrhenius relationship with respect to temperature, and there is no significant dependence of the equilibrium constant on the sugar concentration or the temperature. The mutarotation rate of ketose sugars is higher than the mutarotation

rate of aldose sugars, and the number of rings in the structure does not have a significant effect on the rate of mutarotation.

Over the experimental temperature range studied, the widths of the secondary nucleation thresholds were found to be temperature independent when supersaturation was based on the absolute concentration driving force. These data were used to specify the time dependent concentration limits in the batch crystallization experiments. Glucose monohydrate crystals have a growth rate constant that follows an Arrhenius relationship with respect to temperature, with an activation energy of 50 ± 2 kJ/mol. The driving force for crystal growth is limited to approximately 10% relative supersaturation by the secondary nucleation threshold, and because of this and the relatively slow growth kinetics, the growth rates measured were rather low, in the range of 0.01-0.10 μm/min.

A mathematical model was generated based on the mutarotation and crystal growth parameters measured in this study. Five ordinary differential equations, representing mechanistic and balance equations, were written to describe the system and then solved using reasonable values of the necessary initial conditions. The results show the mass deposition of glucose onto the crystal surface is faster in cases using smaller seed sizes, higher seeding rates, and higher temperatures. The depletion of α-glucose is rapid in cases using smaller seed size, higher seeding rate, and lower temperature. In summary, the conditions where the mutarotation may be the rate limiting step, or partially rate limiting, can be easily predicted via the model.

School of <u>Chemical Engineering</u>   Student's signature_____

Academic Year 2005   Advisor's signature_____

ACKNOWLEDGEMENTS

guidelines for use of the laboratory equipment, and occasional help in characterization of the properties of samples.

Thanks are also due to the Division of Chemical Engineering, the University of Queensland (UQ), Australia, for use of equipment and laboratory space during my research there. Various members of UQ have helped me during my time in the PSDC's laboratory and have made my stay a memorable and enjoyable one.

The support and encouragement of family and friends has also been of great benefit to me over the course of this project.

Sukanya Srisa-nga

TABLE OF CONTENTS

Page

TABLE OF CONTENTS (CONTINUED)

TABLE OF CONTENTS (CONTINUED)

TABLE OF CONTENTS (CONTINUED)

TABLE OF CONTENTS (CONTINUED)

TABLE OF CONTENTS (CONTINUED)

TABLE OF CONTENTS (CONTINUED)

Page

LIST OF TABLES

LIST OF TABLES (CONTINUED)

LIST OF TABLES (CONTINUED)

LIST OF FIGURES

Figure   **Page**

LIST OF FIGURES (CONTINUED)

LIST OF FIGURES (CONTINUED)

LIST OF FIGURES (CONTINUED)

Figure **Page**

LIST OF FIGURES (CONTINUED)

Figure   **Page**

SYMBOLS AND ABBREVIATIONS

A	$=$	particle surface area, μm^2 or m^2
B	$=$	birth rate distribution, $\#/\mu m.m^3.s$
B^0	$=$	nucleation rate, $\#/m^3.s$
BCF	$=$	Burton-Cabrera-Frank
$c(r)$	$=$	solubility of a particle of radius r, g/100 g solution
c^*	$=$	equilibrium or normal solubility, g/100 g solution
C	$=$	total glucose concentration, g/100 g solution
C^*	$=$	solubility, g/100 g solution
C_α	$=$	α-glucose concentration, g/100 g solution
C_α^*	$=$	concentration of α-glucose at equilibrium, g/100 g solution
C^{met}	$=$	metastable limit, g/100 g solution
CV	$=$	coefficient of variation, -
ΔC	$=$	absolute supersaturation, g/100 g solution
D	$=$	death rate distribution, $\#/\mu m.m^3.s$
$E°$	$=$	activation energy, kJ/mol
G	$=$	crystal growth rate, $\mu m/min$ or m/s
GC	$=$	gas chromatography
GLC	$=$	gas-liquid chromatography
h	$=$	step height, μm or m
k	$=$	overall mutarotation rate constant, s^{-1}

SYMBOLS AND ABBREVIATIONS (CONTINUED)

k	=	surface integration molecular-flux constant, m/s
k_1	=	forward mutarotation rate constant, s^{-1}
k_2	=	backward mutarotation rate constant, s^{-1}
K	=	mutarotation equilibrium constant, -
K_m	=	mass transfer coefficient, m/s
k_g	=	growth rate constant, μm/min or m/s
k_a	=	area shape factor, -
k_v	=	volume shape factor, -
L	=	crystal size, μm or m
L_0	=	particle size smaller than the smallest particle, μm or m
$\overline{L}$ and L_M	=	mean particle size, μm or m
$\overline{L}^{/}$	=	geometric mean particle size, μm or m
m_c	=	mass of glucose crystal, g or kg
m_{gluc}	=	mass of glucose in solution, g or kg
m_s	=	mass of solution, g or kg
m_j	=	j^{th} moment about mean
M_B	=	mass of crystallizer suspension, g or kg
M_T	=	suspension density, kg particle/m^3 solution
n	=	number density distribution, #/μm.m^3
n^0	=	number density distribution of nuclei, #/μm.m^3
N	=	number of particles, #

SYMBOLS AND ABBREVIATIONS (CONTINUED)

$N_{A(0)}$ =   molecular bulk concentration, mol/m^3

$N_{A(s)}$ =   molecular surface concentration, mol/m^3

$N_{A(eq.)}$ =   molecular equilibrium concentration, mol/m^3

NMR   =   nuclear magnetic resonance

PSD   =   particle size distribution

S =   supersaturation, -

SEM   =   scanning electron microscopy

SNT   =   secondary nucleation threshold, g/100 g solution

SNZW   =   secondary nucleation zone width, g/100 g solution

t =   time, s or hr

t_d =   delay time, s or hr

t_{ind} =   induction time for nucleation, s or hr

$t_{ind, hom}$ =   induction time for homogeneous primary nucleation, s or hr

$t_{ind, het}$ =   induction time for heterogeneous primary nucleation, s or hr

t_{SNT} =   induction time for secondary nucleation, s or hr

T =   temperature, °C or K

V =   volume, m^3

V_B =   crystallizer volume, ml or m^3

V_d =   volume of dispersant, ml or m^3

V_s =   volume of solution, ml or m^3

x_α =   α-glucose fraction, -

SYMBOLS AND ABBREVIATIONS (CONTINUED)

x_β^* = equilibrium fraction of β-glucose, -

x_α^* = equilibrium fraction of α-glucose, -

x_{gV} = median of the volume distribution, μm or m

x_{NL} = mean particle size, μm or m

σ = relative supersaturation, -

= arithmetic standard deviation, μm or m

σ_g and σ' = geometric standard deviation, μm or m

ρ and ρ_c = α-glucose monohydrate crystal density = 1,560 kg/m^3

β = surface area shape factor

ρ_s = specific surface energy of the solid particle, J/m^2

= slurry density, kg slurry/m^3 slurry

ω = agitation or stirring speed, rpm

$\mathfrak{I}_A$ = net-molecular growth flux, mol/m^{2}s

μ_j = jth moment about origin

Q_k = flow rate of stream k, m^3/s

τ = residence time, s or hr

CHAPTER I

Introduction

1.1 Glucose and Its Importance

Glucose is one of the most abundant organic compounds found in nature, especially in the juice of most fruits and berries, and in the bodies of animals and plants. It is the primary six-carbon sugar (hexose) having the chemical formula $C_6H_{12}O_6$ with a molecular weight of 180.59. Glucose is also called blood sugar, because it is present in human blood, and grape sugar, since pure glucose was first obtained from grape juice (Schenck, 1989). Honey, which has both been eaten as food and used as a medical substance, is probably the oldest and most widely known source of glucose (Hart, Craine, and Hart, 1999). Currently, most glucose is produced from the hydrolysis of starch.

Glucose (sometimes called dextrose) is used in both syrup (called glucose-containing syrup) and crystalline forms. It is used in many industries such as the food, confectionery, soft drink, and pharmaceutical industries, and also as a precursor to many other industrials and specialty chemicals. Glucose can be crystallized in both anhydrous (α- and β-) and monohydrate (α-) forms and used in different industries. The α-anhydrous and α-monohydrate forms are produced commercially, while the β-anhydrous form, which is unstable under normal atmospheric relative humidity (Hart, Craine, and Hart, 1999), is produced as a specialty chemical. From these three crystalline forms, glucose monohydrate is primary commercial product (Lloyd and

Nelson, 1984). Glucose monohydrate crystals produced by batch crystallization had the largest world market share in 1989 (Schenck, 1989).

Glucose is used as a sweetener in the form of glucose-containing syrup, which is normally composed of glucose and fructose for added sweetness. Currently dextrose is more important in the sweetener market since it is used as a raw material for many important sweeteners such as sorbitol, which is a low caloric sweetener used in toothpaste and chewing gum, and also used in cosmetic products, as well as used as a feedstock for the production of vitamin C. Schenck (1989) reported that in 1989, glucose-based sweeteners accounted for more than half of the total caloric sweeteners consumed in the United States.

Glucose in solution has six forms (or tautomers), α- and β-glucopyranose, α- and β-glucofuranose, an open chain form, and a hydrated open-chain form, which are present in different amounts in the solution, with the tautomeric composition of the solutions depending on the solvent used. The α- and β-glucopyranose forms dominate the composition in all solvents. These six forms (or in the simplified case, only the two dominant forms) undergo an interconversion reaction in solution, which is called the mutarotation reaction. Mutarotation is a property of all reducing sugars, and can be determined by their reaction with oxidizing agents such as cupric hydroxide: with the presence of the copper ion, red cuprous oxide is precipitated. This reducing property of glucose retards oxidative degradation in food; glucose maintains the bright red color of tomato catsup, red berry preserves, and red meats without the need for artificial antioxidants (Schenck, 1989).

1.2 Study Motivation and Research Objectives

Crystallization parameters are very important for choosing the operating conditions as well as the determination of optimum equipment designs. Suitable equipment and better operating conditions result in a higher product yield and better product properties; product size distribution, appearance, and shape. In addition, the mutarotation reaction occurs in the solution phase, and it is necessary to consider its effect especially where the crystallizer is operated using a very high seeding rate.

There are many publications on the mutarotation rates and mutarotation equilibrium compositions of D-glucose and other reducing sugars in aqueous solutions, but the different techniques used give different measured rates. Significant published information on the crystallization of α-D-glucose monohydrate in aqueous solutions is not available, and model, which include the effects of mutarotation on the overall crystallization of this sugar have not been produced. This research aims to improve the knowledge on the mutarotation kinetics of simple reducing sugars, especially for glucose in aqueous solution. The crystallization kinetic parameters and the secondary nucleation threshold for crystallization are also reported. A model is generated in order to observe the effect of the mutarotation reaction on the kinetics of crystallization. This model is used to specify whether mutarotation is the rate limiting step (over the crystallization rate) for this sugar.

1.3 Research Development

This research involves laboratory experiments and computational modeling based on the experimental parameters, and balance and mechanistic equations relating to the processes in the crystallizer. The experimental part involved observation of the

mutarotation of simple carbohydrates in the mixture of water and heavy water (D_2O) using carbon-13 nuclear magnetic resonance spectroscopy (^{13}C-NMR), the secondary nucleation threshold (SNT) of glucose monohydrate in aqueous solutions, and the crystallization of glucose monohydrate in aqueous solutions. Mutarotation data in the literature is reproduced to confirm the previous data, and to compare the mutarotation rates and equilibrium of the different types of sugars. The SNT is necessary to ensure the crystallization is operated in the correct region of the phase diagram (i.e. where crystals grow without nucleation). The crystallization kinetic parameters and mutarotation kinetic parameters obtained from the experiments will be used in a model of crystallization and mutarotation occurring simultaneously. A schematic diagram of the research procedure is shown in Figure 1.1. Chapter II is a review of the theoretical background required for this work. Specific details of the mutarotation, secondary nucleation, and crystal growth studies are revealed in Chapter III, IV, and V, respectively, while observations on the effect of the mutarotation reaction on crystallization, through the model, are explained in Chapter VI. Finally, Chapter VII shows the conclusions of this research and gives some recommendations for further work.

```
┌─────────────────────────────────────┐
│ SNT Experiment                      │
│                                     │
│  •  50 ml stirred bottle            │
│                                     │
│  •  isothermal at 10-40°C           │
│                                     │
│  •  presence of α-glucose           │
│                                     │
│     monohydrate crystals            │
└─────────────────────────────────────┘
                  │
                  ▼
┌─────────────────────────────────────┐      ┌─────────────────────────────────────┐
│ Crystal Growth Experiment           │      │ Mutarotation Experiment             │
│                                     │      │                                     │
│  •  1-litre batch, agitated crystallizer │  │  •  ¹³C-NMR                          │
│                                     │      │                                     │
│  •  isothermal at 10-40°C           │      │  •  isothermal at 7-35°C            │
│                                     │      │                                     │
│  •  small amount of seed            │      │  •  vary initial sugar content     │
│                                     │      │                                     │
│  •  operate within the SNT region   │      │                                     │
└─────────────────────────────────────┘      └─────────────────────────────────────┘
                  │                                          │
                  ▼                                          ▼
┌─────────────────────────────────────┐      ┌─────────────────────────────────────┐
│ Crystallization parameters          │      │ Mutarotation parameters             │
│                                     │      │                                     │
│  $k_g$, $n$ $(G=k_g\sigma^n)$       │      │  $k_\alpha$, $k_\beta$, $K$         │
└─────────────────────────────────────┘      └─────────────────────────────────────┘
                     \                          /
                      \                        /
                       ▼                      ▼
                  ┌─────────────────────────────────────┐
                  │ Modeling using MATLAB, based on     │
                  │                                     │
                  │ the experimental parameters         │
                  └─────────────────────────────────────┘
```

Figure 1.1 Research procedure overview.

1.4 Expected Results from the Study

According to the objectives of the research, this research expects to obtain accurate mutarotation kinetics and equilibrium of simple carbohydrates, and crystallization kinetics (including the secondary nucleation threshold) of glucose monohydrate in aqueous solutions. The data from both mutarotation and crystallization kinetic studies will be used to produce a mathematical model for the crystallization of α-glucose monohydrate from aqueous solutions over the range of

conditions operable in the crystallization. The model generated is expected to apply for the other types of reducing sugars with very little modification (although care needs to be taken depending on whether the crystal forms are hydrated or anhydrous), and much of the mutarotation data required for the other sugars is already determined in the current study.

1.5 References

Hart, H., Craine, L. E., and Hart, D. J. (1999). **Organic Chemistry: A Short Course** (10th ed.). Boston: Houghton Mifflin.

Lloyd, N. E. and Nelson, W. J. (1984). Glucose- and Fructose-Containing Sweeteners from Starch. In R. L., Whistler, J. N., Bemiller, and E. F., Paschall (eds). **Starch: Chemistry and Technology** (2nd ed., pp 611-660). San Diego: Academic Press.

Schenck, F. W. (1989). Glucose and Glucose-Containing Syrups. In **Ullmann's Encyclopedia of Industrial Chemistry** Vol. A 12 (pp 457-476). Weinheim: VCH.

CHAPTER II

Review of the Literature

2.1 Introduction

Crystallization is a separation and purification process used in a wide variety of industries. There are a number of crystallization mechanisms, which can be characterized into crystal growth from melts, solution, vapors and gases, supercritical fluids, and vapor phase epitaxy (Strickland-Constable, 1968). This thesis focuses on crystallization from solution, where the crystallizing species are contained within a liquid solvent, and the background for this subject is described here. Crystallization from solution is used in many industries, such as the food, pharmaceutical, and specialty chemicals industries. The latter two industries use crystallization since it gives a very high purity product and this is the most important requirement of products from these two industries. Crystallization may be used in the food industries due to a need for high purity, or for production of a convenient to use product, as in the cases of sugar and salt. Crystallization is considered to occur through two-processes, nucleation of new crystals (nuclei) and growth of these nuclei to larger sizes. A supersaturated environment is required for both processes. The phase diagram is necessary for the crystallization operation since it shows the region where the crystallizing species can crystallize out from solution. It is generally considered that there is a region on the phase diagram where crystal growth occurs, but nucleation does not. This region is known as the metastable region: it is larger for

primary nucleation than for the secondary nucleation and is highest for homogenous nucleation, as shown in Figure 4.5. The crystal growth process can be considered to occur via several steps, mainly the diffusion of solute molecules to the adsorbed layer and the integration of these molecules into the crystal lattice. In this chapter, the review of the literature is mainly the review of the theories that are concerned with the study of the above subjects.

The mutarotation reaction, which is the anomeric form transformation process in solution, can complicate the crystallization of reducing sugars, and will be reviewed in Chapter III. An introduction to nucleation will be given in this chapter and the theory is discussed more fully in Chapter IV. The crystal growth mechanism will be fully explained here.

The particle size distribution (PSD) is necessary for the crystallization product description and the theory relating to PSDs is also presented here. The population balance is required in crystallizer modeling, and the relevant theory is also given in this chapter. The review of previous work on each study will be presented in the particular chapter where that study is discussed.

2.2 General Considerations in Industrial Crystallizers

The general schematic of crystallization from solution can be drawn as in Figure 2.1. This review is focused on the crystallization unit. The phase separation process is also important for the overall crystallization process, since a good operating design gives a good appearance and minimizes the loss of the crystalline products. The particle size distribution, as well as the particle shape, of the product from a crystallization unit is significant for the phase separation operation, since a good

particle size distribution (a narrow distribution, uniform crystals) and good shape (no needle like crystals, no agglomerated aggregates) are required for good flow, easy handling, and easy phase separation.
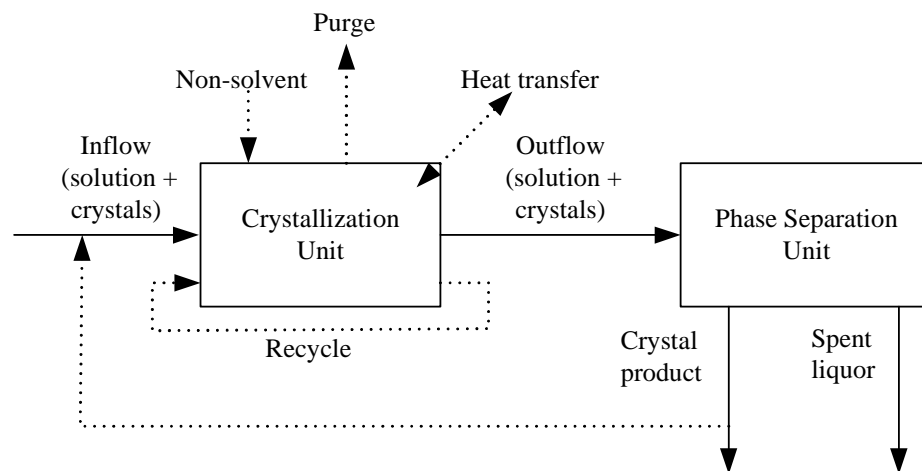
Figure 2.1 General schematic of a crystallization process.

Any of the streams may be present or absent from a particular crystallizer as considered below:

(a) *Continuous, steady-state crystallizer*: inflow and outflow are present with equal mass flow rates.

(b) *Batch crystallizer*: neither inflow nor outflow is present, except during the time required for filling at the beginning of the operation and for removal of the crystal product at the end of the batch. The fluid and crystal properties in the vessel will not be steady-state, but will vary with time during the batch.

(c) *Seeded crystallizer*: it is often preferred to add some crystalline product into the feed of the crystallizer to initiate the crystallization. This may be done to

remove the requirement of operation at a high driving force to produce nuclei (since crystals already exist in the liquor the nucleation step is not required), or to promote crystal breeding due to the secondary nucleation (described further).

(d) *Non-solvent and salting-out crystallizations*: a non-solvent or an anti-solvent (such as a polar species for sugar crystallization) is added to the solution to reduce the solubility of the crystallizing species. The addition of other solutes (other crystallizable species which are not considered as solvent) also aims to reduce the solubility and is known as salting out crystallization.

(e) *Cooling and heating crystallizations*: species, whose solubility increases with increasing temperature, may be crystallized in cooling crystallizers, where the supersaturated environment is reached by reducing the temperature of the solution. In a small number of other solutes, crystallization can occur via heating. The design of such crystallizers requires careful energy balances, which include consideration of the heats of crystallization.

(f) *Evaporative crystallization*: evaporation of solvent through a purge stream causes an increase in the solution concentration (solvent is evaporated out leaving solute in solution) which increases the driving force. This evaporation must occur at the boiling point of the solvent, which varies with the concentration of the solute, and the pressure of the system.

(g) *Precipitation crystallization*: supersaturation is achieved by adding individual reagents for the reaction to form a relatively insoluble product in the crystallization vessel. The reaction product forms rapidly at a concentration higher than its solubility.

(h) *A purge stream* may also be necessary to remove either a particular fraction of the crystalline content in order to improve the product size distribution, or a liquid stream to stop a particular impurity from concentrating.

(i) *a recycle stream* may be necessary for recycle of either the solution or the crystal phase.

2.3 Phase Equilibrium for Crystallization from Solution

The phase diagram represents the equilibria between the various phases of a system. It is very useful for crystallization operations since it suggests an operating condition (temperature, pressure, and concentration) for a desired product. If only one crystalline product is possible the phase diagram becomes a solubility diagram, as in Figure 2.2, where the solution concentration of the solute is plotted against temperature. Two lines divide the diagram into three major sections:

(I) The undersaturated liquid region where crystals would dissolve if present.

(II) The metastable region, which is above the line representing saturated liquid (C^*), but below the metastable limit line (C^{met}). Crystals may grow in this region, but nucleation will not occur from a particle free solution.

(III) The region of crystal growth and nucleation, where both processes are possible due to the larger driving force.
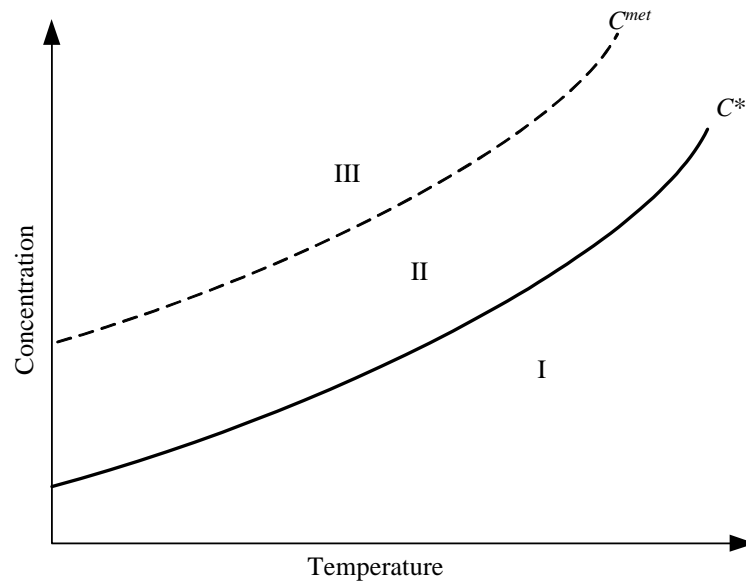
Figure 2.2 The generalized phase diagram for a single solute crystallized from solution.

The metastable region is not considered to be fixed since its position is dependent on both the time allowed for the nucleation to occur and the cooling rate that is used in the experiment: this means that it should not be considered a fundamental phase limit on the phase diagram, but a guide to operating points. The metastable region can be specified for the different types of nucleation, primary homogeneous, primary heterogeneous, or secondary nucleation. The widest region is for homogeneous nucleation. The heterogeneous primary nucleation metastable region is narrower than the homogeneous region, but wider than the secondary nucleation region. The diagram of these regions is shown in Chapter IV.

2.4 Solubility

The equilibrium for crystallization processes is the solubility of the crystallizing species in the solution it is being crystallized from. Figure 2.3 is the phase diagram of fructose and establishes the solubility curve of each crystalline form of fructose in aqueous solution (Young, Jones, and Lewis, 1952). This figure represents the four solids formed, i.e. ice, anhydrous **D**-fructose crystal, **D**-fructose hemihydrate crystal, and **D**-fructose dihydrate crystal, and one gel phase, present in the system in equilibrium with fructose solutions in the temperature range of –40 to 60°C.

The solubility curves for two different phases meet at the *transition point*, and a system may show more than one transition point (Mullin, 2001). For the fructose-water system, three forms of fructose are stable crystalline phases in aqueous solution at the different temperature ranges: **D**-fructose hemihydrate from a temperature of 19.9 up to 21.4°C, **D**-fructose dihydrate below 19.9°C, and anhydrous **D**-fructose, which is the stable phase at temperatures higher than 21.4°C. If the crystallization is below 0°C, ice is formed with some formation of fructose crystals (dependent on solution concentration). Young, Jones, and Lewis (1952) reported the presence of a gel, which forms spontaneously in concentrated **D**-fructose solutions. They also found this gel should change to hemihydrate above about 2°C (indicated by the point where the solubility of gel and hemihydrate cross, the transition point of these two forms).
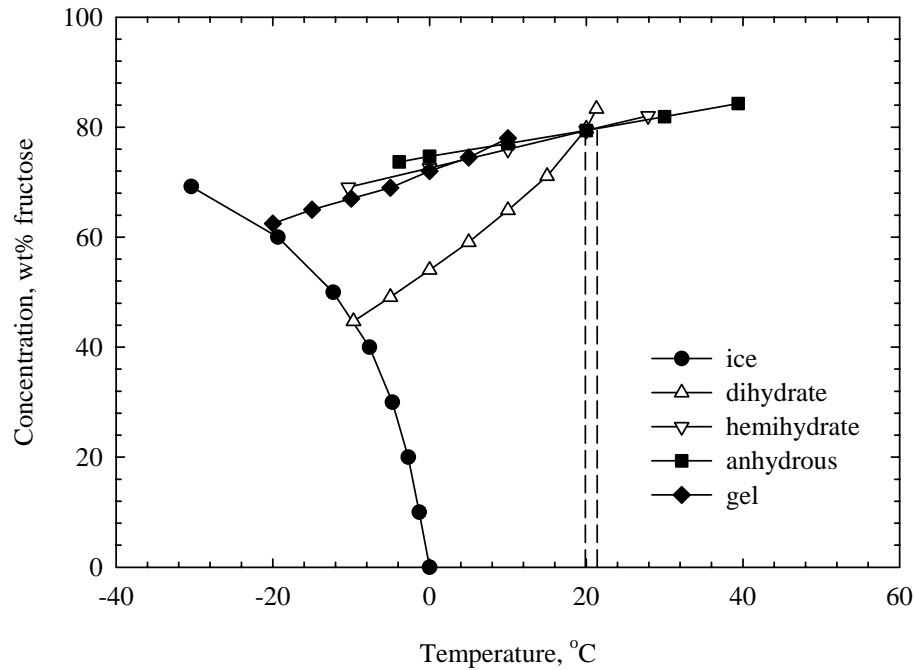
Figure 2.3 Phase diagram of fructose in water, which shows the temperature dependence of the fructose solubility in aqueous solution (Young, Jones, and Lewis, 1952). The two dashed lines represent two transition points.

The solubility of the particles is considered to be dependent on particle size (Mullin, 2001; Mersmann, 1995). The effect of size on particle solubility can be described using the Gibbs-Thomson (Ostwald - Freundlich) equation:

$$\ln \frac{c(r)}{c^*} = \frac{\beta V \sigma_s}{rkT} \tag{2.1}$$

where $c(r)$ is a solubility of a particle of radius r, c^* is an equilibrium solubility (or normal solubility), β is surface area shape factor, σ_s is the specific surface energy of the solid particle, V is molecular volume, k is a property dependent constant, and T is the absolute temperature.

Normal solubility (or equilibrium solubility) refers to the solubility of very large particles. The result of the particle size solubility effect is that solution compositions may exceed the normal equilibrium value, if the dispersed particles in the solution are very small, say less than 1 μm (Mullin, 2001; Mersmann, 1995).

2.5 Supersaturation

The driving force for both the nucleation and crystal growth process is supersaturation. Supersaturation is the magnitude of the difference between the actual state of the system and the equilibrium state, in the other words it shows how far above saturation (equilibrium) the process is. There are many techniques to achieve supersaturation for crystallization from solution, and the popular techniques are given in Figure 2.4. At point A in the figure, the solution is undersaturated with respect to the crystallizing species: following the line A-B is a cooling crystallization where the supersaturation is reached by removing heat from the solution. The line A-C is the technique to achieve supersaturation by evaporating off the solvent and leaving the solute in solution at a concentration in excess of the saturation point. The line A-D illustrates the technique called salting-out crystallization where addition of a non-solvent species in the solution is used to decrease the solubility.
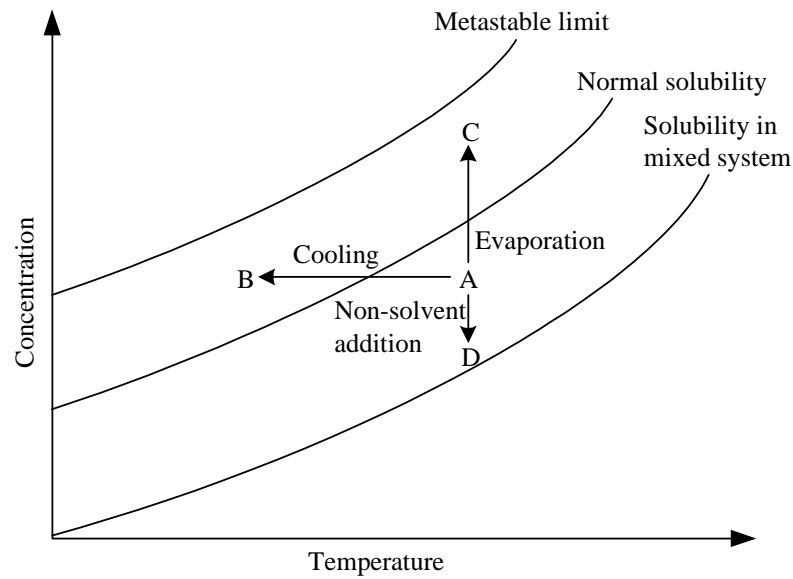
Figure 2.4 Techniques for achieving supersaturation in solution crystallizations.

The true driving force in crystallization from solution is the difference in the chemical potential of the crystallizing species in the solution phase, and in the crystal phase. Unfortunately the calculation of this driving force requires knowledge of the temperature and concentration dependence of the solute's activity coefficient in the solution, and it is very difficult to measure these dependencies or predict them from a *priori* models. Thus, this formal definition of supersaturation is very rarely used in practice. Supersaturation is usually given in terms of mass or molar concentrations, or mass or mole fractions, which assumes that the activity coefficient of the solute does not change significantly between the solution concentration and the solubility value. Even if the activity coefficients do vary over the compositions encountered, these definitions can be seen as practical definitions that are useful and convenient for industrial conditions.

Supersaturation is usually defined via one of the following three relationships:

$$\Delta C = C - C^* \tag{2.2}$$

$$S = \frac{C}{C^*} \tag{2.3}$$

$$\sigma = \frac{C - C^*}{C^*} = S - 1 \tag{2.4}$$

The definition used depends on which process is being modeled and what the mechanism is thought to control the process. Equation 2.2 is often used for crystal growth where the rate limiting step is mass transfer, Equation 2.3 is often used for nucleation models, and Equation 2.4 is often used for crystal growth where surface integration is rate limiting, however, there are many exceptions to these conventions. Table 2.1 summarizes the commonly used definitions of driving force in crystallizing systems and also shows the unit of the driving force used, whereas Table 2.2 shows the supersaturation used in precipitation or reaction crystallization.

Table 2.1 Driving forces using in crystallization of molecular species (Mersmann, 1995).

Kinetic parameter		Driving force
Growth	Diffusion controlled	ΔC [kmol/m^3] or Δc [kg/m^3]
	Surface integration controlled	$\sigma = \Delta c / c^*$ or $\Delta C / C^*$
Nucleation	Primary	$S = 1 + \sigma$
	Secondary	σ

Table 2.2 Definitions of supersaturation in crystallizing systems (Mersmann, 1995).

$$A_xB_y \; \overrightarrow{\longleftarrow} \; xA^{z+} + yB^{z-}$$

Solubility product

    With activity

$$K_a = \left(a_A^*\right)^x\left(a_B^*\right)^y = \left(\gamma_A y_A^*\right)^x\left(\gamma_B y_B^*\right)^y$$

    With concentration

$$K_c = \left(c_A^*\right)^x\left(c_B^*\right)^y$$

Solubility for binary electrolytes

$$c* = \left(\frac{K_c}{x^x y^y}\right)^{1/(x+y)} \text{ with } c_A^* = xc*, \; c_B^* = yc*$$

$$c* = \sqrt{K_c} \text{ with x = y = 1, } c_A^* = c_B^* = c*$$

Supersaturation

$$S_a = \left(\frac{\left(a_A\right)^x\left(a_B\right)^y}{K_a}\right)^{1/(x+y)}$$

$$S = \left(\frac{\left(c_A\right)^x\left(c_B\right)^y}{K_c}\right)^{1/(x+y)} \text{ with } x = y = \gamma_A = \gamma_B = 1$$

$$S = \frac{c}{c*} = \frac{\sqrt{c_A c_B}}{\sqrt{K_c}}$$

2.6 Nucleation Theory

Nucleation is the formation of new crystallites (nuclei) in suspensions. It is modeled as a rate of formation of new nuclei per solution volume (or crystallizer volume in some cases) per second, which assumes that it is a bulk phase process (mechanism) rather than a surface occurrence. Nucleation is generally classified into primary and secondary nucleation. Primary nucleation occurs when the nucleation mechanism does not depend on the presence of suspended solute crystals in the

solution. Secondary nucleation occurs when the nucleation mechanism requires suspended crystals. Primary nucleation is further divided into homogeneous mechanisms and heterogeneous mechanisms. Homogeneous nuclei occur spontaneously at very high supersaturations in clean solutions, while heterogeneous nucleation occurs when the presence of such foreign particles is required to obtain primary nuclei. Secondary nucleation is far more significant than primary nucleation in most industrial crystallization units because the vessel is run continuously containing solute crystals. The details of nucleation theory including the types of secondary nucleation mechanisms and the metastable zone are explained in Chapter IV.

The nucleation of crystals is similar, but not a perfect analogy, to the nucleation of liquid droplets. To understand how nucleation occurs, droplet formation theory is needed. For nucleation in industrial crystallizers, most nuclei are generated by contact with the crystallizer environment (Myerson and Ginde, 2002), and is most often modeled with the empirical models of the form:

$$B^0 = k_N \sigma^a T^b M_T^c \omega^d \tag{2.5}$$

Where B^0 is the nucleation rate [number of nuclei/m^{3}s], σ is supersaturation, T is temperature, M_T is suspension density [kg/m^3 solution], ω is an agitation speed, and k_N is an empirical constant obtained from the experimental measurements.

2.7 Crystal Growth Theory

Crystal growth is a multiple step process. Solute molecules, or clusters, must first diffuse to the surface of the growing crystal through a mass transfer mechanism, due to a concentration gradient near the adsorbed layer. The solute molecules then

adsorb to the surface of the crystal, where they can integrate into the crystal lattice if they find a suitable integration site via surface diffusion, or desorb and return to the solution phase. According to these steps, diffusion and surface integration play an important role in crystal growth (Mersmann, 1995). When the rate of mass transfer to the crystal surface is much slower than the rate of integration into the lattice, the growth is termed *diffusion controlled*, and the converse process is described as *surface integration controlled* growth. The process can be partly controlled by these two mechanisms in some cases. These two mechanisms can be easily understood by considering the concentration gradient of solute (species A) as in Figure 2.5.

crystal facial surface

driving force for mass transfer

$N_{A(0)}$

$N_{A(s)}$

driving force for integration

$N_{A(eq.)}$

concentration
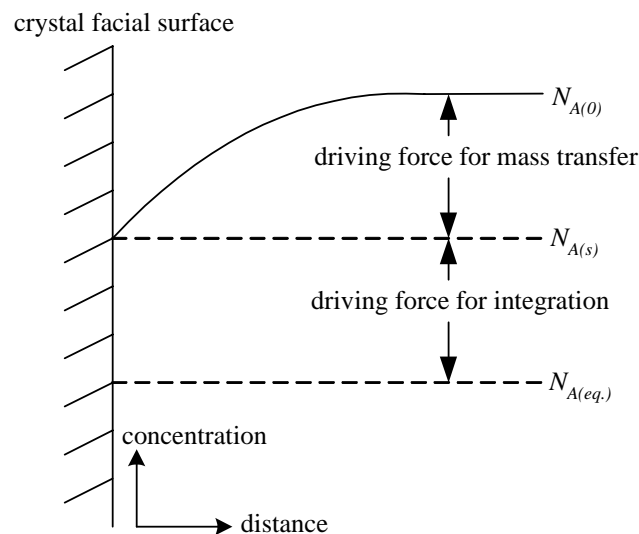
distance

Figure 2.5 The concentration of solute as a function of distance from the crystal face (adapted from Strickland-Constable, 1968).

There are three significant molecular concentrations, the bulk concentration, $N_{A(0)}$, the surface concentration, $N_{A(s)}$, and the concentration at equilibrium, $N_{A(eq.)}$. The

rate of mass transfer is equal to $K_m(N_{A(0)} - N_{A(s)})$ where K_m is the mass transfer coefficient. The mass transfer coefficient is usually assumed to be constant with respect to the driving force, but is a function of the degree of turbulence of the fluid phase. Normally the degree of turbulence is considered as a function of the stirring speed applied in the system. When the growth rate is plotted against the stirring rate, or other measures of turbulence, the curve usually rises as the stirring is increased, but may flatten out to give a constant growth rate for very high stirring rates. The later stage is where the growth rate becomes surface integration controlled.

The rate of the surface growth process will be some function of the supersaturation at the surface. These can be concluded in the following equations with $\mathfrak{I}_A$ being the net molecular-growth flux:

Mass transfer process:
$$\mathfrak{I}_A = K_m\left(N_{A(0)} - N_{A(s)}\right) \tag{2.6}$$

Surface reaction process:
$$\mathfrak{I}_A = f\left(N_{A(s)} - N_{A(eq.)}\right) \tag{2.7}$$

If the function in Equation 2.7 is assumed known and re-written in the form $k(N_{A(s)} - N_{A(eq.)})$ with k being a constant with respect to supersaturation, the surface growth process may be said to follow a linear growth law (Strickland-Constable, 1968). From this assumption, a combination of Equation 2.6 and the re-written Equation 2.7, can be combined as:

$$\mathfrak{I}_A = \frac{1}{\dfrac{1}{K_m} + \dfrac{1}{k}}\left(N_{A(0)} - N_{A(eq.)}\right) \tag{2.8}$$

Mass transfer controlled: when $K_m << k$, Equation 2.8 can be reduced to

$$\mathfrak{I}_A = K_m\left(N_{A(0)} - N_{A(eq.)}\right) \tag{2.9}$$

Surface integration controlled: when $k << K_m$, Equation 2.8 can be reduced to

$$\Im_A = k\left(N_{A(0)} - N_{A(eq.)}\right) \tag{2.10}$$

In actual systems, it is suggested that the growth law may be an order higher than linear. It may be empirically given by the following formula where n has a value greater than or equal to one, with a probable theoretical upper limit of 2 (Strickland-Constable, 1968):

$$\Im_A = k\left(N_{A(s)} - N_{A(eq.)}\right)^n \tag{2.11}$$

There are a number of theories used to explain growth phenomenon on the surface of the crystal; they can be roughly classified into the *two-dimensional growth theories*, the *Burton-Cabrera-Frank (BCF) model*, and the *diffusion layer model*. The first theory assumes the layer growth by surface nucleation, while the second theory predicts the continuous growth due to screw dislocations. The last one is a simple model that focuses on the diffusion of solute through the boundary layer near the surface of crystal which is the explanation of the propagation of steps on the crystal surface, either by the surface nucleation of the two-dimensional growth theory or by the screw dislocation of the BCF theory. The growth equations for these crystal growth theories are presented in Table 2.3.

Two-dimensional growth model

This is also called the layer growth model; the crystals grow with smooth facets even though the supersaturation is not uniform across the face of a crystal. Initially the surface nucleus is formed and diffuses to the growing surface: it then spreads over the surface to find a kink site, which is the most favorable site, in terms of energy, to attach in. This model can be separated into three sub-models that differ in how these surface nuclei spread over the surface to form a complete layer. The simplest crystal growth theory, which is called the *mononuclear model*, assumes that

the surface nuclei spread across the surface at an infinite velocity. Then, the surface must wait for the formation of other surface nuclei, and so surface nucleation is the rate limiting step for this model. If the surface nuclei is assumed to not spread at all when it forms (the spreading velocity is equal to zero), a layer would be formed by the formation of enough nuclei to cover the layer: this model is called the *polynuclear model*. Between the extremes of these two models is a model called the *birth and spread model*. The *birth and spread model* has the assumption that the nuclei can form at any location on the surface, allows the spreading of nuclei at a finite constant rate, and the spreading velocity is assumed independent of surface nuclei size.

The BCF model

The assumption for this model is that the surface nuclei cannot form on a smooth surface, but the steps are self-perpetuating by propagating using a dislocation in the crystal, known as a screw dislocation. These steps grow continuously and the surface becomes a spiral staircase. The key part of the mechanism is that for a screw dislocation, after a layer is complete, the dislocation is still present.

The diffusion layer model

This model focuses the diffusion of solute molecule through the boundary layer (the layer near the crystal surface in which concentration is changing). This idea can also be shown as the concentration gradient in the Figure 2.5.

Table 2.3 Summary of the growth equations of the crystal growth models. C_1, C_2, C_3,
C_4, C_5, K_1, and K_2 are constants that are related to the system parameters
(Ohara and Reid, 1973).

Model	Growth rate equation
Mononuclear	$G = C_1 hA[\ln(S)]^{1/2} \exp\left[-\dfrac{C_2}{T^2}\ln(S)\right]$
Polynuclear	$G = \left(\dfrac{C_3}{T^2}[\ln(S)]^{3/2}\right)\exp\left[-\dfrac{C_2}{T^2}\ln(S)\right]$
Birth and spread	$G = C_4(S-1)^{2/3}[\ln(S)]^{1/6}\exp\left[-\dfrac{C_5}{T^2}\ln(S)\right]$
BCF	$G = K_1 T(S-1)\ln(S)\tanh\left[\dfrac{K_2}{T}\ln(S)\right]$
Diffusion layer	$\dfrac{dm_c}{dt} = K_G A\Delta C^g$

Note: G is the growth rate perpendicular to the surface, h is the step height, A is
surface area, S is supersaturation, T is temperature, m_c is the mass of crystal,
K_G is constant, g is the order ranging from 1 to 2.

2.8 Particle Size Distributions

The particle size distribution (PSD, also known as crystal size distribution,
CSD, if the particles being modeled are mainly single crystals) is a very important
function to describe the product from crystallizers. The PSD is simply a function that
describes the amount of crystal (as a number, volume, or mass), relative to the size of
particle (for instance the diameter, or volume of a single particle). The two main
parameters given from the PSD are the mean particle size (the averaged size) and

range of particle sizes (the spread of the distribution). This is due to the fact that not all particles in a sample have the same size.

The particle size distribution for crystallization usually considers the number distribution of particles as a function of the linear particle size. The number distribution is chosen because of the great significance of nucleation to crystal size distributions; nucleation leads to an increase in the number of particles, but not any significant increase in the volume or mass of the solid material. Linear particle size (the diameter for instance) is usually preferred over particle volume for the abscissa, since it is then easier to relate the PSD to crystal growth rates, due to the McCabe law of crystal growth (Randolph and Larson, 1988). The particle size distribution may be determined either from models of the process (largely the population balance model that is to be discussed in Section 2.11) or from measurements of the particle size of a representative sample of the solid phase. The later technique is presented here, including the moments of a particle size distribution that are very useful mathematical formulations for calculating various properties of the distribution.

The particle size measurement needs to be performed over a representative sample of the entire population of discrete particles. A representative sample must consist of a random chosen sample of the population that is large enough to effectively represent what is usually a continuous distribution in the process. The measurement may be undertaken in a variety of ways, including instrumental techniques *in situ* or on suspension samples (light scattering, zone sensing, etc.) and physical techniques on a number of individual particles (size, volume, or weight measurements). The two accepted methods of representing the distribution

graphically are the cumulative distribution and the density distribution, both of which may be plotted as a continuous or a discrete function.

Experimental data is normally represented by discrete distributions, the definitions for which are:

Cumulative undersize distribution: Plot $\displaystyle\sum_{i=1}^{n}\Delta N_i$ versus $\displaystyle L_0 + \sum_{i=1}^{n}\Delta L_i$

Density distribution: Plot $\displaystyle\frac{\Delta N_i}{\Delta L_i}$ versus $\displaystyle L_0 + \sum_{i=1}^{n-1}\Delta L_i + \frac{1}{2}\Delta L_n$

Where L_0 is any size smaller than the smallest particle, ΔN_i is the number of particles in the size increment i, and ΔL_i is the width of the size increment i. When N is defined as the total number of particles in the sample (or the total number of particles considered in the distribution), the normalization of both distributions can be obtained by dividing the above distributions by N, equivalent to arbitrarily choosing the total number of particles to be considered to be equal to one.

Several sizing techniques, notably sieving and light scattering methods, give results based on volume or mass in a particular size range. In this case some auxiliary calculations to convert from mass or volume to number must be performed in order to calculate the number-based particle size distribution. These calculations are exact as the measured size intervals (ΔL_i) tend to zero, but may involve significant errors as the size intervals become large, particularly if there is a wide range of the particle sizes in the population.

In some systems the density distribution based on mass (mass density of crystals in a size range versus particle size) may be preferred, rather than the number density distribution, or the cumulative distribution for either parameter. The

distributions are relatively easy to transform between each other using the identities in Figure 2.6.
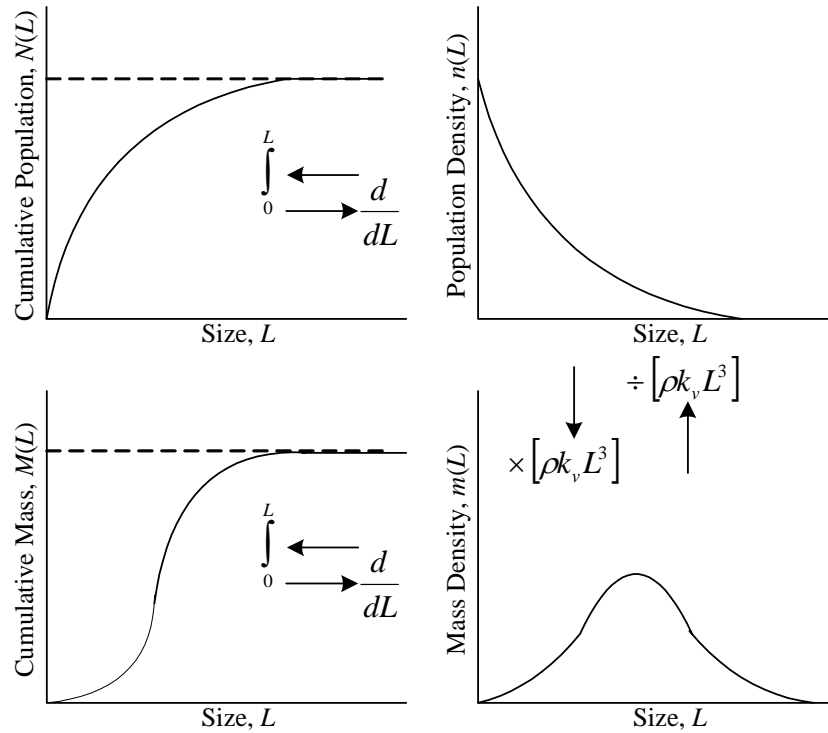
Figure 2.6 Method of conversion between types of the particle size distributions (Re-drawn from the plot in Randolph and Larson, 1988).

2.9 Moments of a Particle Size Distribution

The moments of the particle size distribution are mathematical formulations that simplify the characterization and interpretation of the distribution. The moments may be generically described by the following equation:

$$g_j \equiv \int_{-\infty}^{\infty} (L - L_g)^j f(L) dL \tag{2.12}$$

This equation represents the jth moment of the function $f(L)$ measured around the point L_g (which can be any value, but is usually either the origin or the mean of the distribution). Moments about the mean are described by the following equation with $\overline{L}$ being the mean of the distribution:

$$m_j \equiv \int_{-\infty}^{\infty} \left(L - \overline{L}\right)^j f(L) dL \tag{2.13}$$

Moments about the origin are described by:

$$\mu_j \equiv \int_{-\infty}^{\infty} L^j f(L) dL \tag{2.14}$$

Particle size distributions have an independent variable, the length, which cannot take on negative values, so the lower integration limit can be taken as zero in any practical application. In some cases the experimental data is expressed in grouped data and the moments in Equation 2.13 and 2.14 can be re-written as Equations 2.15 and 2.16.

Moments about the mean: $m_j \equiv \sum_g n_i \left(\overline{L_i} - \overline{L}\right)^j \Delta L_i$ \hfill (2.15)

Moments about the origin: $\mu_j \equiv \sum_g n_i \overline{L_i}^j \Delta L_i$ \hfill (2.16)

where n_i is number in size intervals ΔL_i and $\overline{L_i}$ is mean size of the size interval ΔL_i.

2.9.1 The Significance of the Moment Values

(a) μ_0 represents the total number of particles in the system.

(b) μ_1 represents the total linear length in the system.

(c) μ_1 / μ_0 is the number average particle size in the system.

(d) $k_a \mu_2 / \mu_0$ represents the number average surface area in the system, where k_a is an area shape factor.

(e) $k_v \mu_3 / \mu_0$ represents the number average volume in the system, where k_v is a volume shape factor.

(f) m_2 represents the variance of the distribution, which is the square of the standard deviation, σ. The standard deviation is also sometimes said to be the width of the distribution.

2.9.2   Other Importance Parameters for Particle Size Distribution

In some cases, only two main parameters, mean and standard deviation, are not enough to represent how particle size distributions look and sometimes may give the wrong interpretation of the data. Three other significant parameters are described here.

(a) The *coefficient of variation* is the relative width of the particle size distribution defined by CV = $\sigma / \overline{L}$. In other words, CV shows the spread of the particle size distribution relative to the mean size.

(b) *Skewness* = m_3/σ^3 is a measure of the non-symmetry of the distribution. It has a zero value for the normal distribution (which will be presented in the next section) and any other symmetric distribution, a positive value for distributions skewed to right, and a negative value for distributions skewed to left.

(c) *Kurtosis* = m_4/σ^4 - 3 is a measure of the shape of the distribution at the extremes (or shape of the tails of the distribution). It has a zero value for the normal distribution, a positive value for distributions with sharp peaks but broad tails, and a negative value for distributions with broad peaks but thin tails.

2.10 Fitting Particle Size Distribution with Empirical Functions

It is often necessary to fit discrete data to a continuous function for the distribution. There are a number of common distributions used, and the main ones are summarized in Table 2.4 and the plots that are shown in Figure 2.7.

The normal distribution is the simplest and the most well known distribution, but is not suitable to use for describing the particle size distribution since finite populations are predicted for negative values of size, which is not possible for real systems. The log-normal distribution is simply a normal distribution in terms of the logarithm of particle size (log L). This distribution is quite simple and very useful for fitting the particle size distribution, since in most real systems the particle size distribution is skewed to the right. The further advantage is that this distribution predicts only positive values of size. The density function for the gamma distribution also satisfies the requirement for only positive values of particle size and is also suitable for fitting of particle size distributions because of the right skewed distribution (having a positive value of the skewness).

Table 2.4 Definition and properties of some useful empirical distribution functions (Randolph and Larson, 1988).

Parameter	Normal	Log-normal	Gamma
Density distribution	$f(L) = \left[(2\pi)^{1/2}\sigma\right]^{-1}$ $\times \exp\left[-0.5\left(\dfrac{L-\bar{L}}{\sigma}\right)^2\right]$	$f(\log L) = \left[(2\pi)^{1/2}\log\sigma'\right]^{-1}$ $\times\exp\left[-0.5\left(\dfrac{\log\left(L/\bar{L}'\right)}{\log\sigma'}\right)^2\right]$	$f(L) = \left[\Gamma\left((a+1)\right)(b/a)^{a+1}\right]^{-1}$ $\times L^a\exp(-aL/b)$

Table 2.4 (Continued)

Parameter	Normal	Log-normal	Gamma
Range	L in $(-\infty, \infty)$	L in $(0, \infty)$	L in $(0, \infty)$
Mean size	$\overline{L}$	$\overline{L}^{/} [\exp(0.5)\log^2 \sigma^{\prime}]$	$b(a+1)/a$
Mode size	$\overline{L}$	$\overline{L}^{/}$	b
Median size	$\overline{L}$	$\overline{L}^{/}$	$f(a)$
Coefficient of variation	$\sigma/\overline{L}$	$[\exp(\log^2 \sigma^{\prime})-1]^{1/2}$	$1/(a+1)^{1/2}$
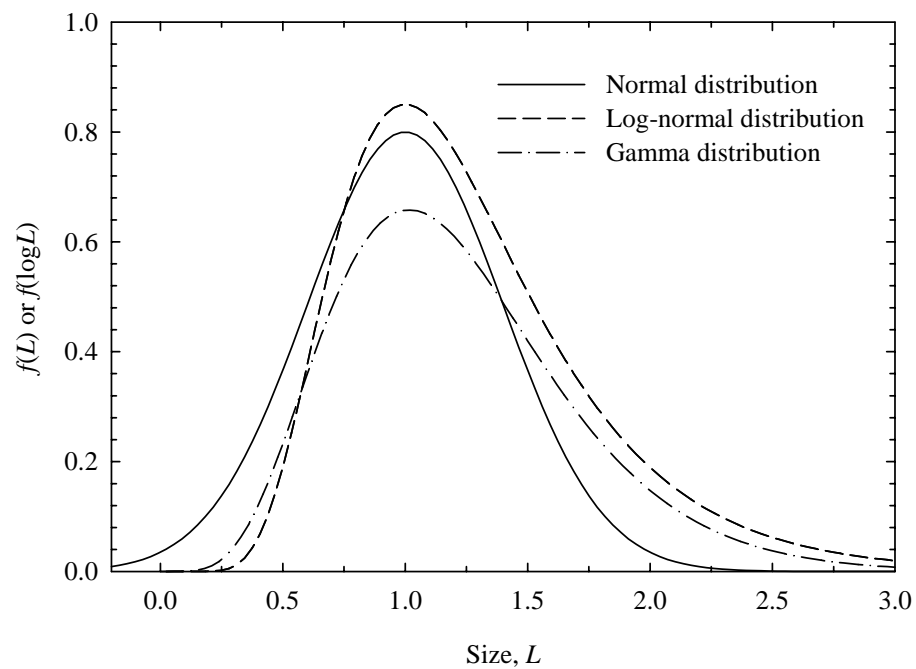
Figure 2.7 Plots of the density functions from the normal, log-normal, and gamma distributions having identical modes (equal to one) and standard deviations (Re-plotted from Randolph and Larson, 1988).

2.11 The Population Balance

The population balance is an equation of continuity for discrete entities having a particular characteristic. In crystallization, the population consists of the particles or crystals within the crystallization unit (or a particular subsection of the unit) and the characteristic of most significance is the particle size based on a particular linear dimension. The full form of the spatially independent population balance is:

$$\frac{\partial n}{\partial t} + \frac{\partial (Gn)}{\partial L} - B + D + \sum_{i=1}^{k} \frac{Q_k n_k}{V} + n\frac{d(\log V)}{dt} = 0 \qquad (2.17)$$

Where n is number density distribution, G is crystal growth rate, B is birth term, D is death term, Q_k is the flow rate for stream k, and V is the crystallizer volume. A spatially dependent form of the population balanced is also sometimes required, particularly for cases where there is a clear change in properties along some spatial axis: a plug-flow cooling crystallizer is a particular example. The population balances for the crystallization systems are shown below.

2.11.1. The Ideal, Steady-state, Mixed Suspension - Mixed Product Removal (MSMPR) Crystallizer

This type of crystallizer is similar to the CSTR (Continuous-Stirred Tank Reactor). There are several assumptions for this type of crystallizer:

(a) The vessel is perfectly mixed with respect to both the liquid phase (no spatial variation in concentration, temperature, or driving force) and the solid phase (no spatial variation in the population density function).

(b) The suspension in the product stream is identical to the suspension in the crystallizer vessel.

(c) There are no crystals or particles in the feed stream.

(d) There is no agglomeration or breakage of the particles in the crystallizer.

(e) Nucleation occurs at zero size. This allows the nucleation rate to be considered via a boundary condition (n^0) rather than as a birth term.

(f) The growth rate is size independent ($G \neq f(L)$).

The population balance may be simplified to the following equation with τ defined as the residence time (V/Q):

$$\frac{dn}{dL} + \frac{n}{G\tau} = 0 \tag{2.18}$$

with the boundary condition $n(0) = n^0 = B^0/G$, where n^0 is the number density distribution of nuclei, the solution is

$$n = n^0 \exp\left(\frac{-L}{G\tau}\right) \tag{2.19}$$

2.11.2. Batch Crystallizer

The assumptions for this crystallizer are that it is well mixed with respect to both liquid and solid phases. The assumption of steady state cannot be made for the batch crystallizer since the particle size distribution changes over time. Moreover, the initial conditions are important because both seeds used and initial nucleation affect the particle size distribution and become part of the product. For a batch system, or unseeded semi-batch system, there are no crystals in the inflow and outflow streams, no birth and death considered in the system, and the growth rate is size independent, the population balance becomes:

$$\frac{\partial n}{\partial t} + G\frac{\partial n}{\partial L} + n\frac{d(\log V)}{dt} = 0 \tag{2.20}$$

2.12 References

Mersmann, A. (1995). **Crystallization Technology Handbook**. New York: Mercel
     Dekker.

Mullin, J. W. (2001). **Crystallization** (4th ed.). Oxford: Butterworth-Heinemann.

Myerson, A. S. and Ginde, R. (2002). Crystal, Crystal Growth, and Nucleation. In A.
     S., Myerson (ed.). **Handbook of Industrial Crystallization** (2nd ed.,
     pp.121-176). Boston: Butterworth-Heinemann.

Ohara, M. and Reid, R. C. (1973). **Modeling Crystal Growth Rates from Solution**.
     New Jersey: Prentice-Hall.

Randolph, A. D. and Larson, M. A. (1988). **Theory of Particulate Processes** (2nd
     ed.). New York: Academic Press.

Strickland-Constable, R. F. (1968). **Kinetics and Mechanism of Crystallization**.
     London: Academic Press.

Young, F.E., Jones, F. T., and Lewis, H. J. (1952). D-Fructose-Water Phase Diagram.
     J. Phys. Chem. 56: 1093-1096.

CHAPTER III

Mutarotation Reactions of Simple Carbohydrates

3.1 Abstract

Crystallization is a very important separation and purification process. Sugars are usually crystallized from solutions in industrial operations. It has been shown that the mutarotation reaction of reducing sugars plays a significant role in determining the crystallization rate of these sugars, and it is beneficial to be able to model and predict mutarotation rates for common sugars. The mutarotation rate and equilibrium of simple carbohydrates: D-glucose, D-galactose, D-cellobiose, D-maltose, and D-turanose, in aqueous solutions were measured between 7 and 35ºC, using ^{13}C-NMR. The effects of sugar concentration and temperature on the rate of mutarotation and mutarotation equilibrium were observed. It has been found that the rate of mutarotation slightly decreases as the sugar concentration increases. This observation suggests that the reaction is not true first order, which would not display concentration dependence in the rate constant. The rate constant of the studied sugars follows an Arrhenius relationship with respect to temperature. There are no clear correlations between the equilibrium constant and the sugar concentration or the temperature but neither parameter affects the equilibrium constant strongly. The equilibrium composition is difficult to correlate in terms of the sugar type (i.e. ketose and aldose) because the steric and solvent effects vary strongly even among the individual aldose and ketoses sugars. Finally, it is quite clear that the mutarotation

rate of ketose sugars is higher than the mutarotation rate of aldose sugars, and the number of rings in the structure (i.e. monosaccharide and disaccharide) does not have a significant effect on the rate of mutarotation.

3.2 Introduction

Carbohydrates occur in all plants and animals and are the main source of energy supply in most cells. They are a very large family of compounds comprising sugars, starches, cellulose, and many other compounds found in living organisms. In their most basic form, carbohydrates are simple sugars or monosaccharides, which cannot hydrolyze further to smaller constituent units. The general formula of the monosaccharides is $(CH_2O)_n$ or $C_n(H_2O)_n$ with n commonly ranging from 3 to 7: this is why these compounds are called carbohydrates (hydrates of carbon). For $n = 2$ the molecule is not a carbohydrate, while linear or cyclic monosaccharides with $n = 8$ are very unstable, and therefore unlikely to exist in any significant amount. Monosaccharides are also divided into aldoses or ketoses according to whether their acyclic form possesses an aldehyde (aldoses) or ketone group (ketoses). 2-Ketoses (with the ketone group on the second carbon) are easily the most common ketose sugars. Examples of monosaccharide aldoses and 2-ketoses in the open chain form appear in Table 3.1 and Table 3.2, respectively. In these tables, monosaccharides are also classified according to the number of carbon atoms present. Carbohydrates are referred to as trioses, tetroses, pentoses, and hexoses when they contain 3, 4, 5, and 6 carbon atoms, respectively. There are only two trioses, glyceraldehyde and dihydroxyacetone, that are the simplest aldose and ketose, respectively. Other aldoses and ketoses can be derived from these two forms by adding carbon atoms, each with a

hydroxyl group (Hart, Craine, and Hart, 1999). Monosaccharides can combine with each other to form more complex carbohydrates.

Oligosaccharides are compounds in which monosaccharides are joined by glycosidic linkages. They are also named disaccharides, trisaccharides, and so on, after the saccharidic lengths; for instance, disaccharides and trisaccharides are composed of two and three monosaccharide units, respectively. The most abundant oligosaccharides are disaccharides, examples of which in the ring form are shown in Table 3.3. The borderline between oligo- and polysaccharides cannot strictly specified; however, the term "oligosaccharide" is commonly used to refer to well-defined structures as opposed to the term "polysaccharide" which is referred to a polymer of unspecified length and composition (Boons, 1998). Polysaccharides are possibly linear or branched polymers of the same monomeric unit (simple polysaccharides or homopolysaccharides) or different monomeric units (complex polysaccharides or heteropolysaccharides). The most important polysaccharides are starch, cellulose, and glycogen. Starch is an important constituent of human diet and contains about 20% amylose, a linear glucose polymer, and amylopectin (the only other component of starch), a branched glucose polymer (Beyer and Walter, 1996). Cellulose is a linear polymer of glucose and is the main plant structural material, while glycogen is a branched glucose polymer and known as an animal starch.

Table 3.1 Examples of common aldose monosaccharides.

Number of Carbon	Monosaccharide	Acyclic Form
3 (Aldotriose)	**D**-Glyceraldehye	
4 (Aldotetrose)	**D**-Erythrose	
	D-Threose	
5 (Aldopentose)	**D**-Ribose	
	D-Arabinose	
	D-Xylose	
6 (Aldohexose)	**D**-Allose	

Table 3.1 (Continued)

Number of Carbon	Monosaccharide	Acyclic Form
6 (Aldohexose)	**D**-Altrose	H–C=O, HO–C–H, H–C–OH, H–C–OH, H–C–OH, CH₂OH
	D-Glucose	H–C=O, H–C–OH, HO–C–H, H–C–OH, H–C–OH, CH₂OH
	D-Mannose	H–C=O, HO–C–H, HO–C–H, H–C–OH, H–C–OH, CH₂OH
	D-Gulose	H–C=O, H–C–OH, H–C–OH, HO–C–H, H–C–OH, CH₂OH
	D-Idose	H–C=O, HO–C–H, H–C–OH, HO–C–H, H–C–OH, CH₂OH

Table 3.1 (Continued)

Number of Carbon	Monosaccharide	Acyclic Form
6 (Aldohexose)	**D**-Galactose	
	D-Talose	

Table 3.2 Examples of 2-ketose monosaccharides.

Number of Carbon	Monosaccharide	Acyclic Form
3 (Ketotriose)	Dihydroacetone	
4 (Ketotetrose)	**D**-Erythrulose	
5 (Ketopentose)	**D**-Ribulose	
	D-Xylulose	

Table 3.2 (Continued)

Number of Carbon	Monosaccharide	Acyclic Form
6 (Ketohexose)	**D**-Psicose	
	D-Fructose	
	L-Sorbose	
	D-Tagatose	

Table 3.3 Examples of disaccharides.

Disaccharide	Description	Full name [a]	Cyclic Form (main)
Sucrose [b]	common table sugar	α-**D**-glucopyranosyl- β- **D**-fructofuranoside	
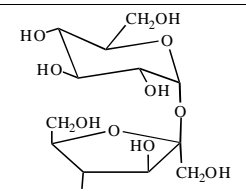
Table 3.3 (Continued)

Disaccharide	Description	Full name [a]	Cyclic Form (main)
Lactose	main sugar in milk	4-*O*-β-**D**-galactopyranosyl-**D**-glucose	
Maltose	product of starch hydrolysis	4-*O*-α-**D**-glucopyranosyl -**D**-glucose	
Cellobiose	product of cellulose hydrolysis	4-*O*-β-**D**-glucopyranosyl-**D**-glucose	
Turanose	rare sugar	3-*O*-α-**D**-glucopyranosyl-**D**-fructose	
Trehalose [b]	found in fungi	α-**D**-glucopyranosyl-α-**D**-glucopyranoside	
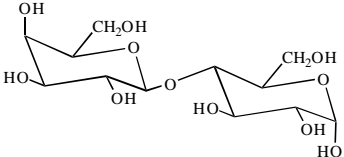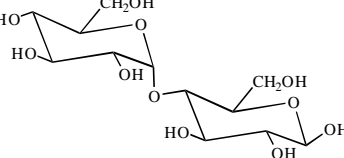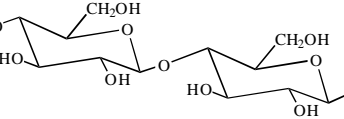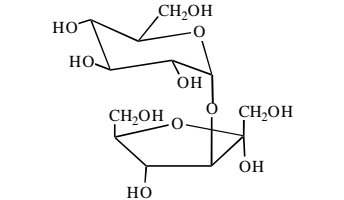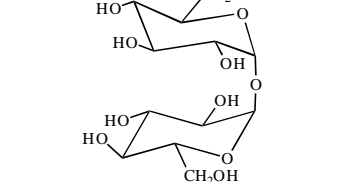
[a] The last part of the name (i.e. **D**-glucose, **D**-fructose) suggests the reducing ring: it can be in α- or β-forms and can be furanose (a five-membered ring) or pyranose (a six-membered ring). The definition of these terms is described in Section 3.2.1.

[b] Non-reducing sugars

3.2.1 The Mutarotation Reaction

The linear form of sugars (i.e. glucose) is normally energetically unfavorable relative to a cyclic hemiacetal form (Boons, 1998), so in various media

(i.e. aqueous solution) sugars with four or more carbons tend to be cyclized to form ring structures. A six-membered cyclic form of most hexoses is the preferred structure for this type of sugar (Hart, Craine, and Hart, 1999). This structure is called a "pyranose" form and it is formed by reaction of the hydroxyl group at C5 with the carbonyl group. In some sugars, the hydroxyl group at C4 reacts instead, and in this case the cyclic that is formed has a five-membered ring; this type of cyclic monosaccharide is called a "furanose". The ring formation can occur because of the "intramolecular" bonds between the carbonyl (C=O) and hydroxyl (OH) group in the same sugar molecule (Beyer and Walter, 1996; Hart et al.). This force bends a straight form of the sugar and allows the ring to be formed.

The ring-closing mechanism is not deeply described here, however, it starts with the carbonyl oxygen being protonated by an acid catalyst, after which the alcohol oxygen attacks the carbonyl carbon, and finally a proton is lost from the resulting positively charged oxygen (Hart et al.). Each step is reversible. During these processes, bonds between carbon atoms are rotated and cause the different ring structures that can be formed (pyranose, furanose, α, and β). If the bond between C4 and C5 rotates, the pyranose form is expected, and the furanose form is obtained if the bond between C3 and C4 is rotated. The rotation around the C1 and C2 bond causes two different forms, the α- and β-forms. In the α-anomer, the hydroxyl group of the anomeric carbon is pointing almost perpendicular to the plane of the molecule, and this is called the axial orientation. The hydroxyl group of the anomeric carbon of the β-anomer is pointing out along the plane of the molecule, and this is called the equatorial orientation. An example of this is shown in Figure 3.1, which shows α-glucopyranose and β-glucopyranose in the chair structure, and also shows the

mutarotation mechanism that is described below. These forms are in equilibrium with each other in solution.

Sugars undergo interconversion between the anomeric (or tautomeric) forms (pyranose, furanose, and open-chain form) in solution. The interconversion is particularly important in aqueous solution, because the sugars appear in aqueous solutions in biological systems, and most processing of the sugar is also performed in aqueous solution. This interconversion causes changes in the optical rotation of the solutions, and thus it is called the mutarotation reaction (muta = change).

The interconversion between the different ring forms of the sugars must pass through the straight chain (aldehyde or keto) form of the sugar via ring opening and ring closing reactions, and this is shown using **D**-glucose as an example in Figure 3.1. These reactions are acid/base catalyzed, and at approximately pH 4 the reaction rate is minimized; the reactions are faster at extremes of pH (Isbell and Pigman, 1969; Nelson and Beegle, 1919). The effects of pH on the mutarotation rate of glucose and fructose are shown in Figure A-1 and A-2, respectively. The apparent first order reaction is catalyzed by substances that can act simultaneously as proton donors and acceptors e.g. polar solvents, and also follows an Arrhenius relationship with respect to temperature (Flood, Johns, and White, 1996; Kraus and Nývlt, 1994).

Many research studies have investigated the mutarotation rate and mutarotation equilibrium of simple carbohydrates in aqueous solutions. In the first period of research in this field (circa 1900-1940), the observation of the optical rotation change was a popular technique. More recently GLC, FTIR, and NMR have been used since they are more powerful techniques.
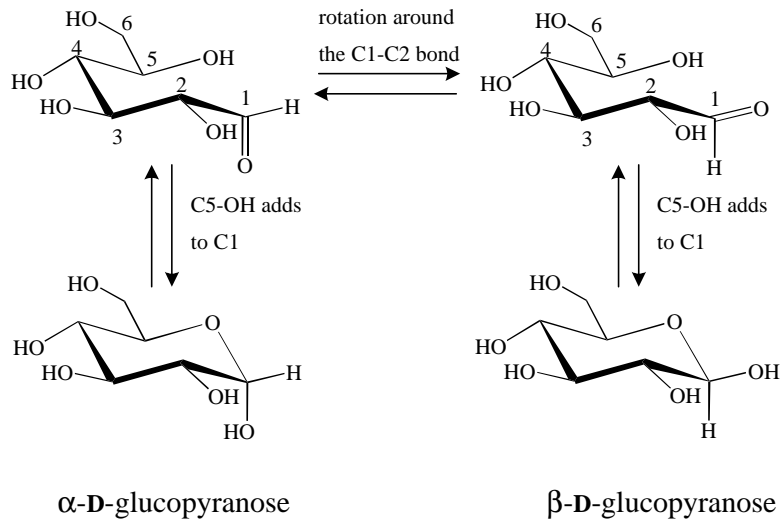
Figure 3.1 Mutarotation reaction schemes of **D**-glucose.

3.2.2   Objectives of the Study

The aim of this work was to describe the mutarotation reaction of simple carbohydrates, and especially glucose. A number of different sugars were studied in order to investigate the effect of certain parameters on the rate and equilibrium of the mutarotation reaction. The two main sugar dependent parameters were whether the sugar is an aldose (having an aldehyde group in the straight-chain form) or a ketose sugar (having a ketone group in the straight-chain form of the sugar), and whether the sugar is a monosaccharide sugar (containing only a single ring, and having a molecular weight of 180.16 for a true hexose sugar) or a disaccharide sugar (composed of two monosaccharide rings bonded through a single dehydration step, having a molecular weight of 342.29 for disaccharides composed of 2 hexose monosaccharides). Glucose was chosen as a common monosaccharide aldose sugar that has been studied previously and thus useful to judge the accuracy of

the technique. Galactose is a second example of a monosaccharide aldose, used to determine whether similar sugars displayed similar mutarotation behavior. Cellobiose and maltose are common disaccharide aldose sugars. Turanose is a common disaccharide ketose. Monosaccharide ketoses were not used in the current study, because the mutarotation behavior of the two common sugars of this type (**D**-fructose and **L**-sorbose) has already been determined.

The mutarotation reaction was investigated to produce a model that can predict the mutarotation reaction parameters of various sugars without the need to perform additional experiments. The result will be further used to verify if the mutarotation reaction has a significant effect on the overall crystallization rates.

3.3 Materials and Methods

3.3.1 Materials

Sugar solutions used in the mutarotation experiments were prepared from AR grade sugars, HPLC grade water, and deuterium oxide (D_2O). The supplying details of all sugars are as follows: α-**D**-Glucose anhydrous, Carlo Elba; β-**D**-Glucose, Sigma; **D**-Galactose, Sigma; **D**-Maltose monohydrate, Sigma; **D**-Cellobiose, Sigma; and **D**-Turanose, Acros. All chemicals were used without further purification.

D_2O was used in this experiment as a reference for the chemical shift assignment. However, previous work (Isbell and Pigman, 1969) has shown it has an effect on the mutarotation rate. In this work, the composition of D_2O (v/v) in solute-free solvent was varied to also observe this effect. The prepared solution volume should not be more than 700 μL due to the requirement of NMR.

3.3.2   Experimental Procedure

The solution was prepared by introducing known amounts of sugar and solvent into a 2 ml vial. The solution was vigorously shaken until the solids dissolved completely. The solution was transferred to a 5 mm NMR tube using a pipette, and the experiment was immediately started. The delay times between the initial dissolution and the start of the experiment were controlled within 2-3 minutes, except in high concentration experiments, where delay times were found to be within 4-5 minutes due to slow dissolution. Typically these time delays were not a serious impediment to accurate results because the time constants for the mutarotation reaction are usually around one to two orders of magnitude larger than this.

^{13}C-NMR was performed on a Varian Unity Inova 300 spectrometer at 75.42 MHz. A switchable broadband (SW/BB) and Fourier transform technique was used. Chemical shift (expressed as parts per million downfield from TMS) were calculated by using the deuterium signal of D_2O as a reference. A 90º pulse (9.2 μs, at a power of 52 dB) was applied to acquire maximum peak intensity. A 5.0 s time delay before every pulse was chosen to obtain quantitative results having a peak as large as possible, while minimizing the time delay between data points in the kinetic experiments. Kinetic experiments were performed using 16 scans per data point in order to obtain suitable peak heights, while minimizing data collection time to obtain the maximum number of data points. Each experiment was stopped when the mutarotation mechanisms reached their equilibrium (1.5-7.0 hr).

NMR spectroscopy is based on the property of nuclear spin. When a molecule is placed in a magnetic field, the nuclear spin can align and lead to a different energy level. The NMR spectrum obtained from such a measurement

contains information on the chemical environment of atoms (chemical shift), the molecular geometry (spin-spin coupling), and the number of atoms giving rise to the signal (integral).

3.4 Results and Discussion

Typical ^{13}C-NMR spectrums obtained almost immediately after dissolution and at the equilibrium of monosaccharide sugars are shown in Figure 3.2 and 3.3 respectively, while Figure 3.4 and 3.5 are the spectrums for disaccharide sugars. For the first spectra after the dissolution (Figure 3.2 and 3.4), only the carbon chemical shifts of the dissolved form, and very small peaks of the other forms are present. At equilibrium (Figure 3.3 and 3.5), almost all carbon peaks of anomers were present, except where some peaks coincided with others. The coincident chemical shifts were not used in the composition calculations. Peaks were assigned based on literature data (Bock and Pedersen, 1983; Bock, Pedersen, and Pedersen, 1983). The anomeric compositions were calculated from the chemical peak height.
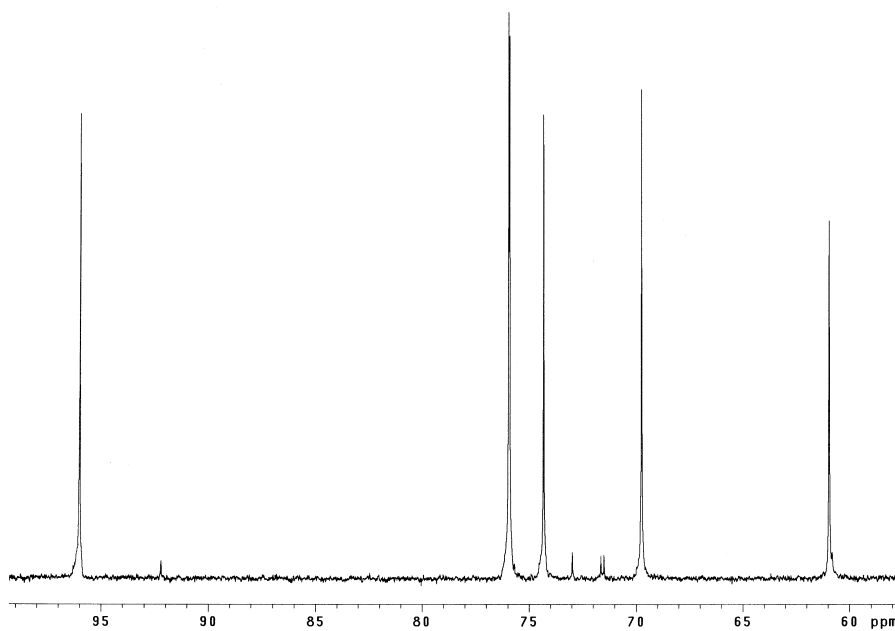
Figure 3.2 Typical ^{13}C-NMR spectrums after dissolution of 33% β-glucopyranose in

aqueous solution at 24°C.
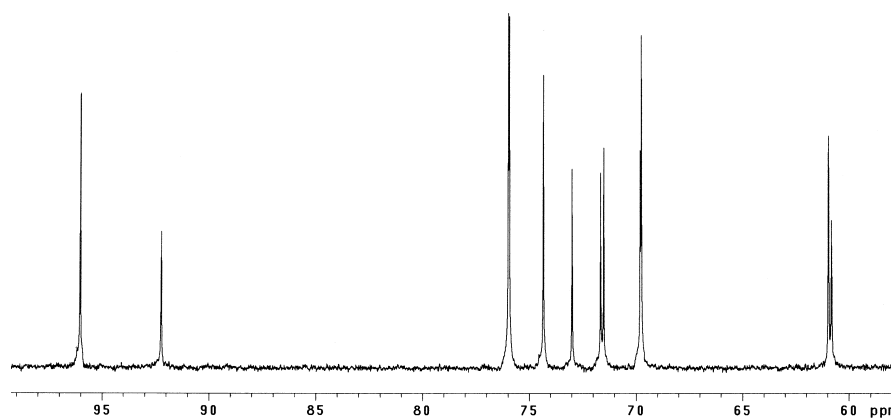
Figure 3.3 Typical ^{13}C-NMR spectrums at equilibrium of 33% β-glucopyranose in

aqueous solution at 24°C.
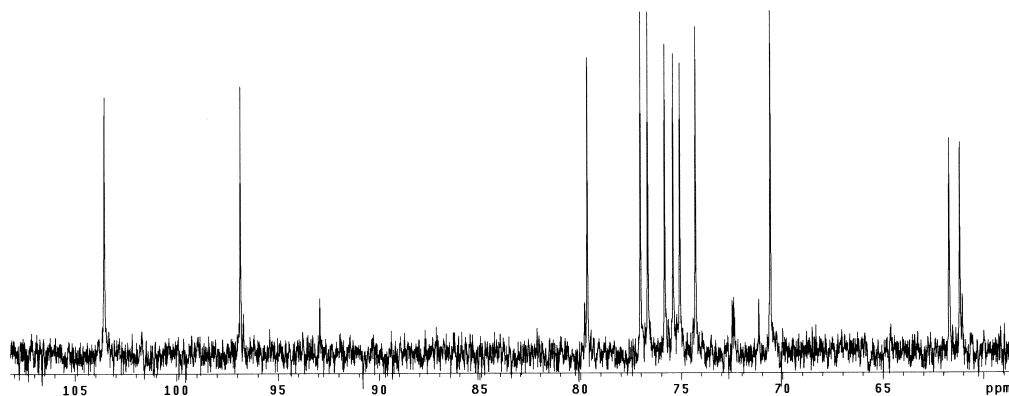
Figure 3.4 Typical ^{13}C-NMR spectrums after dissolution of 8% cellobiose in aqueous
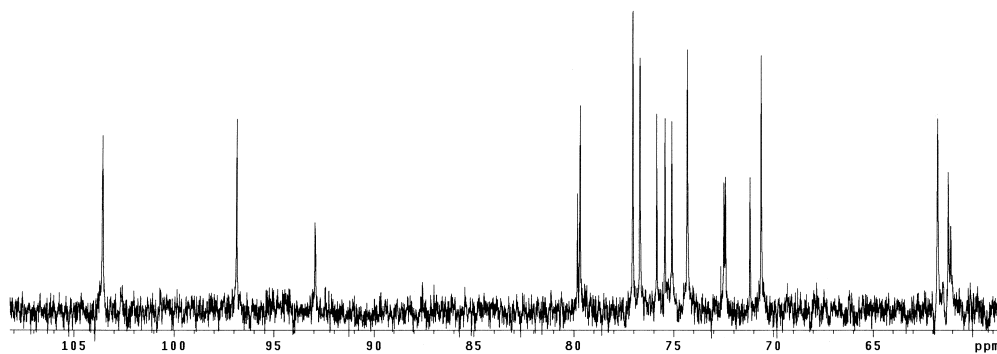
solution at 25ºC.

Figure 3.5 Typical ^{13}C-NMR spectrums at equilibrium of 8% cellobiose in aqueous

solution at 25ºC.

In the time dependent experiments, only the α-aldopyranose and β-aldopyranose forms of the aldose sugars, and β-ketopyranose, α-ketofuranose, and β-ketofuranose of the ketose sugars, are evident because of the low number of scans per data point in these experiments, and the other forms are present at very low

concentrations. A small number of scans per data point were necessary in order to follow the time dependence of the mutarotation accurately. The composition fraction of each form can be calculated from the relative chemical peak height of that carbon (assuming the dissolved form is 100% at the zero time). The typical plots between the fractions (or percent compositions) based on all existing carbons with time showing the mutarotation behavior (time course) of that sugar are shown in Figure 3.6. The results show that while the content of the dissolved form is decreased, the other form replaces it, and the total composition is constant over the time course of reaction. Please note that β-glucose was chosen to be the starting material in the mutarotation study of glucose since it has a higher solubility value at the experimental temperatures (7-35°C). This property produces accurate parameters obtained from the fitting, since dissolution was quicker. Crystalline α-glucose was used in some cases to check if there is some effect of the form on mutarotation rate; no effect was seen (see Figure 3.8). However, in the experiments where α-glucose crystalline is used, there were some difficulties in dissolving the crystals at high concentrations.

The mutarotation kinetics and equilibrium of monosaccharide aldose sugars were determined based on the relative fractions of α-pyranose and β-pyranose calculated from the C2 carbon atom only, as it was found well separated downfield from the other resonances (Gray, 1976). The mutarotation parameters of disaccharide aldoses were determined based on relative fractions calculated using C2 carbons of the anomer-determining ring (the ring which determines whether the sugar is in the α- or β- form) only. The anomeric carbon (C1) was not used because it always gives much smaller peaks than the other carbons. The C3 and C5 were not used due to the β-anomer peaks of these carbons were not well separated, especially where high

sugar concentrations were used. The α-C4 and β-C4 peaks were not used since they were not separated in the initial period of the experiment.
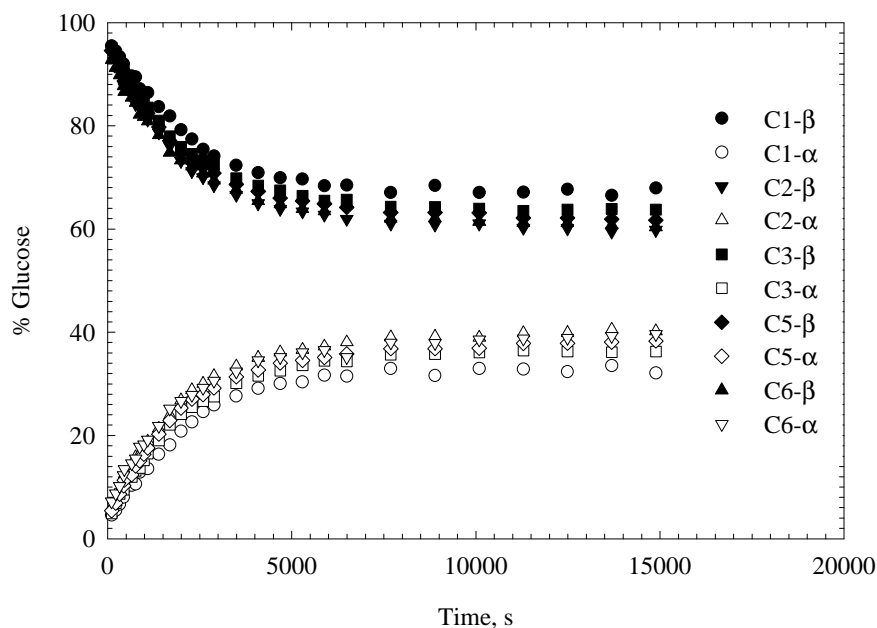
Figure 3.6 The mutarotation behavior of glucose in aqueous solution at 24ºC. Note that zero time corresponds to the starting of the NMR measurement, not to the initial mixing time.

The relative fractions of pyranose and furanose (α-furanose + β-furanose) forms of ketose calculated using C2, C3, and C5 of the anomer-determining ring were used in the mutarotation kinetic and equilibrium calculation; C1, C4, and C6 were not used due to these peaks not being well separated in some cases. The mutarotation rates and equilibrium compositions were determined by fitting the relative fractions and time with a first order equation (Equation 3.1 and 3.2). The delay time, overall

reaction rate, and equilibrium composition were used as the fitted parameters. A time delay was used since slow dissolution made the exact time the mutarotation reaction began uncertain.

First order exponential decay for the dissolved form:

$$f_{or} = b - a(1 - exp[-k(t-t_d)]) \tag{3.1}$$

First order exponential growth for the muta- form:

$$f_{ot} = a(1 - exp[-k(t-t_d)]) \tag{3.2}$$

where f_{or} and f_{ot} are the composition fractions of dissolved form and other form, a and b are constants, k is the overall first order mutarotation rate constant, and t and t_d are the experimental time and delay time, respectively. The experimental data (rates and equilibrium) are shown in Appendix A. The literature mutarotation rate and equilibrium values of simple carbohydrates are also included in Appendix A.

3.4.1 Temperature Effect on the Mutarotation Rate and Mutarotation Equilibrium

Figure 3.7 shows the mutarotation behavior of glucose in aqueous solution, where only C2 is used in the plot, to investigate the effect of temperature on its behavior. This graph shows qualitatively the temperature effect on the mutarotation rates and mutarotational equilibrium. The rate is higher at higher temperature, shown by the steeper slope of the fraction changes in the plot, and that the equilibrium values are similar for different temperatures.
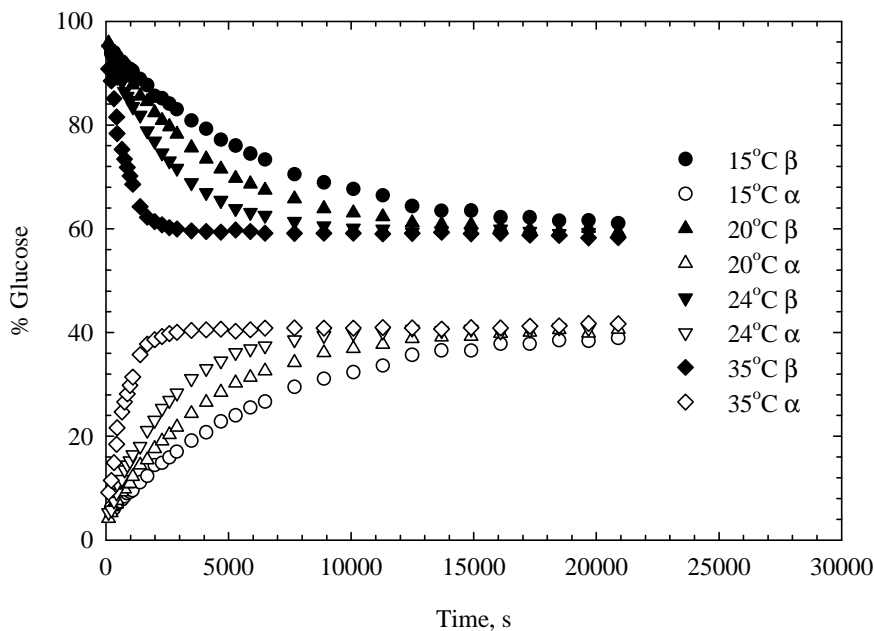
Figure 3.7 The mutarotation behavior of glucose in aqueous solution for several experimental temperatures. Note that zero time corresponds to the starting of the NMR measurement, not to the initial mixing time.

Figure 3.8 shows an Arrhenius plot of glucose in aqueous solution with varying glucose content. In this figure, two main conclusions can be seen; first the mutarotation of glucose follows an Arrhenius relationship with respect to temperature very well, and second the mutarotation rate is not a function of sugar content since only one line can be fitted through all the data. However, the effect of concentration on the mutarotation kinetics is considered in Section 3.4.2.
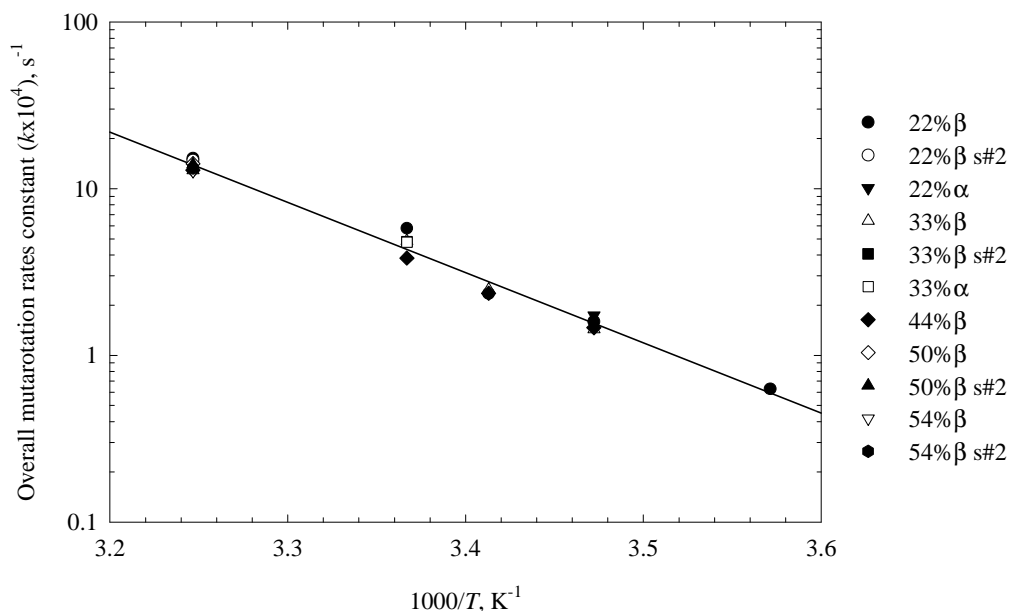
Figure 3.8 Arrhenius plot of glucose showing the temperature dependence of the mutarotation rates. The line is an Arrhenius regression. The symbol α and β represent dissolved forms and s#2 represents sample no. 2 (duplicated sample).

An Arrhenius plot of mutarotation rates with respect to the reaction temperature of all sugars investigated in the current study is shown in Figure 3.9. Data at any particular temperature is the averaged value from different concentrations since the concentration does not have a significant effect on the rates (details are in Section 3.4.2). It is quite clear that the rates of all studied sugars are temperature dependent, with higher rates occurring at higher temperatures, and also follow an Arrhenius relationship. A true first order reaction must follow an Arrhenius relationship. Although the current system is only pseudo-first order (the reaction

scheme involves intermediates and other products), it closely follows first order kinetics. Most other reactions also approximately follow an Arrhenius relationship with respect to temperature. The activation energy of each sugar is calculated from the slope of this plot and is shown in Table A-2 (in Appendix A). The equilibrium composition of the most abundant form of each studied sugar is also shown in Table A-2 while Table A-9 is presented the equilibrium compositions of simple carbohydrates. The aldose sugars only contain large quantities of the pyranose anomers, whilst the ketose sugars often contain significant amounts of the furanose tautomers also. This suggests that the pyranose anomers are significantly more stable than the furanose anomers for aldose sugars, while the relative free energies of the pyranose and furanose forms are more similar for ketose sugars. It is more difficult to make firm conclusions about the effect of sugar type on the anomeric equilibrium of the pyranose forms; however it is very likely that steric effects will have a significant effect on the stability of each anomer. Therefore the positions of the hydroxyl groups near the anomeric carbon may have a very significant effect.
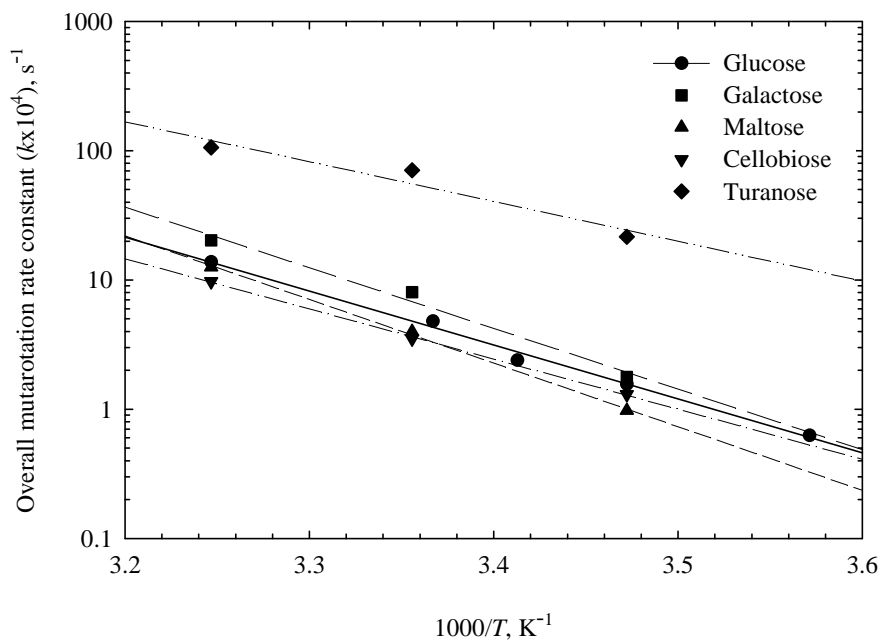
Figure 3.9 Arrhenius plot of studied sugars shows the temperature dependence mutarotation rates. Lines are the Arrhenius regressions for each sugar.

3.4.2 Concentration Effect on the Mutarotation Rate and Mutarotation Equilibrium

Currently there is no clear conclusion to whether there is a concentration effect on the mutarotation rate or equilibrium of sugars (Barc'H, Grossel, Looten, and Mathlouthi, 2001; Hudson and Dale, 1917; Hudson and Sawyer, 1917; Lowry and Smith, 1929). This is an important point in a study of the mutarotation reaction because if the mutarotation rate or equilibrium depends on the sugar content, the reaction cannot be a true first order reaction. To study this effect, the concentration of glucose was varied from 22% by weight to close to the solubility value at a particular temperature. The study in supersaturated solutions is difficult due

to the difficulty of dissolution into supersaturated solutions. The experimental results are shown in Figure 3.10. This figure shows that the rate is not affected by the sugar content at low temperature (i.e. up to 20ºC), but at higher temperature the rates seem to be slightly dependent on the glucose concentration. The dependence shows that at higher glucose concentration the mutarotation rate is lower. Due to the very weak dependence of concentration on the mutarotation rate, the averaged value of the rates at each temperature was used.

Figure 3.11 shows a slight increase in α-glucose content at equilibrium when glucose concentration is increased. This result is consistent with the previous result of Barc'H, Grossel, Looten, and Mathlouthi (2001). The equilibrium α-glucose point at 7ºC appears to be an outlier. This inconsistency may be due to the nature of the NMR equipment; at low temperature the chemical peaks are not well separated, or may be due to the experimental data not being sufficient to fit it with an accurate time course making an uncertainty in the equilibrium composition (i.e. no experimental data at a later time where the mutarotation reaches its equilibrium). However, the α-glucose at equilibrium can be concluded to be 40.0 ± 3.0 % (neglecting the value at 7ºC) which is the same range as Barc'H et al.'s work. This value suggests an equilibrium constant K (the ratio of the β-glucose and α-glucose at equilibrium) of 1.50 ± 0.2. Kraus and Nývlt (1994) used 1.72 for the equilibrium constant with no dependence on temperature.
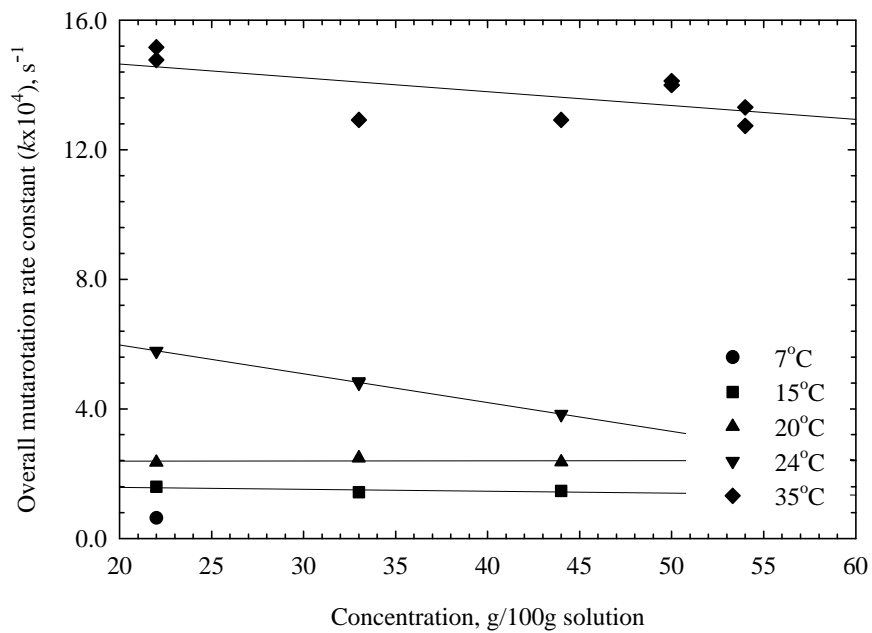
Figure 3.10 Glucose mutarotation rate as a function of concentration in solution.
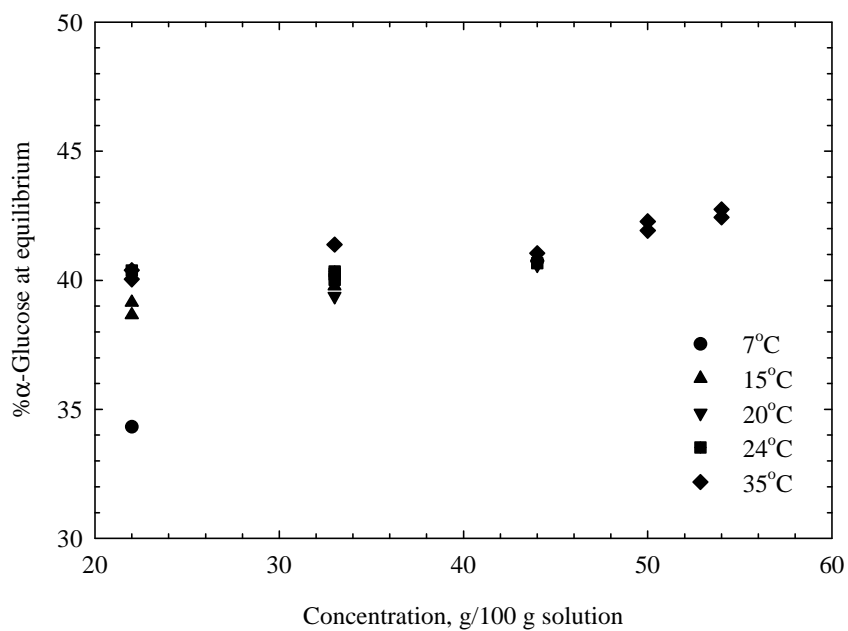
Figure 3.11 The effect of glucose concentration on the α-glucose at equilibrium.

3.4.3 The Solvent Effect on the Mutarotation Rate and Mutarotation Equilibrium

Deuterium oxide (D_2O) was chosen to observe this effect since it was necessary to use this solvent as a reference for the chemical peak assignment in the NMR equipment. A preliminary study on the effect of D_2O on the mutarotation rate and equilibrium of D-glucose was performed. Seven experiments were carried out at 24°C with a glucose concentration of 33% by weight. The amount of D_2O used (on a solute-free basis) was varied from 0% to 100%. The overall mutarotation rate with respect to the D_2O composition is shown in Figure 3.12, while the equilibrium composition of α-glucose with respect to the D_2O composition is demonstrated in Figure 3.13.

Figure 3.12 shows the mutarotation rate is a significant function of D_2O composition in the solvent, as a relationship: $k \times 10^4 = 5.9376 - 0.037 \times \%D_2O$, where k is an overall mutarotation rate constant (in s^{-1}). This relationship suggests that the rate decreases $0.037 \times 10^{-4} \pm 0.006 \times 10^{-4}$ (95% confidence interval) s^{-1} for every 1% increases in D_2O. The result expresses the isotope effect as a k_H/k_D ratio, the ratio of the rate in normal water over the rate in heavy water, of 2.65, while Isbell and Pigman (1969) shows this ratio of 3.87 and 3.80 for the mutarotation of α-glucopyranose at 20°C and 25°C, respectively. The results from Pacsu's work at 18°C and 20°C seem to show the same range of the isotope effect as Isbell and Pigman's. The results from the current work demonstrate that the isotope effect is less significant than previously thought, and show that adding a small amount (10% for instance) of D_2O to achieve improved NMR resolution will not change the mutarotation rate and equilibrium data significantly.
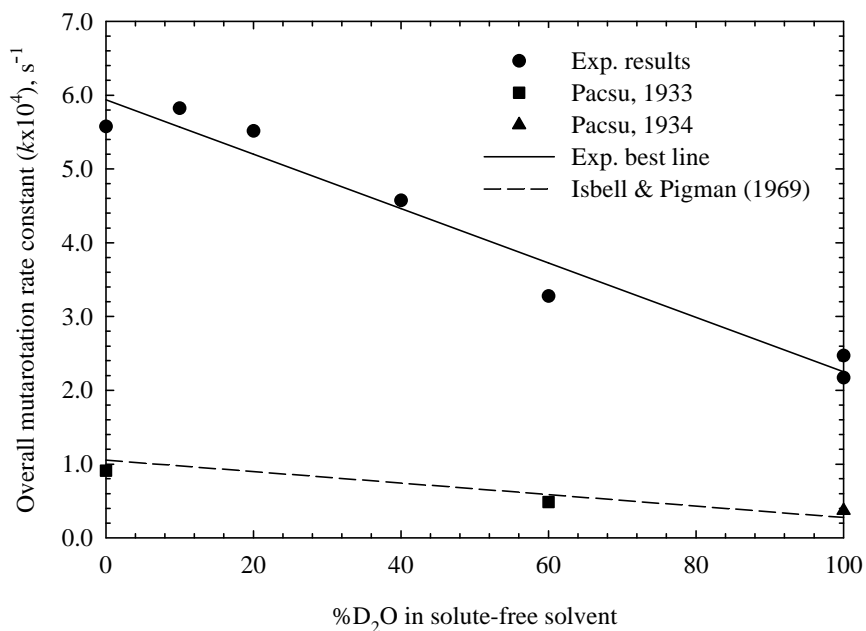
Figure 3.12 The overall mutarotation rate of glucose as a function of an amount of D$_2$O. Experimental temperature, this work: 24ºC, Pacsu (1933): 18ºC, Pacsu (1934): 20ºC, and Isbell and Pigman (1969): 20ºC.

Figure 3.13 shows the effect of D$_2$O content on the equilibrium compositions of α-glucopyranose. Equilibrium α-glucose composition increases by 0.023 ± 0.009% (95% confidence interval) for every 1% increase in D$_2$O in the solvent. This increasing is small but significant, based on a statistical analysis. The D$_2$O shifts the mutarotation equilibrium of glucose up, but in very small amount, say 1-2% α-glucose. This effect can be neglected when the accuracy of the equipment is considered.
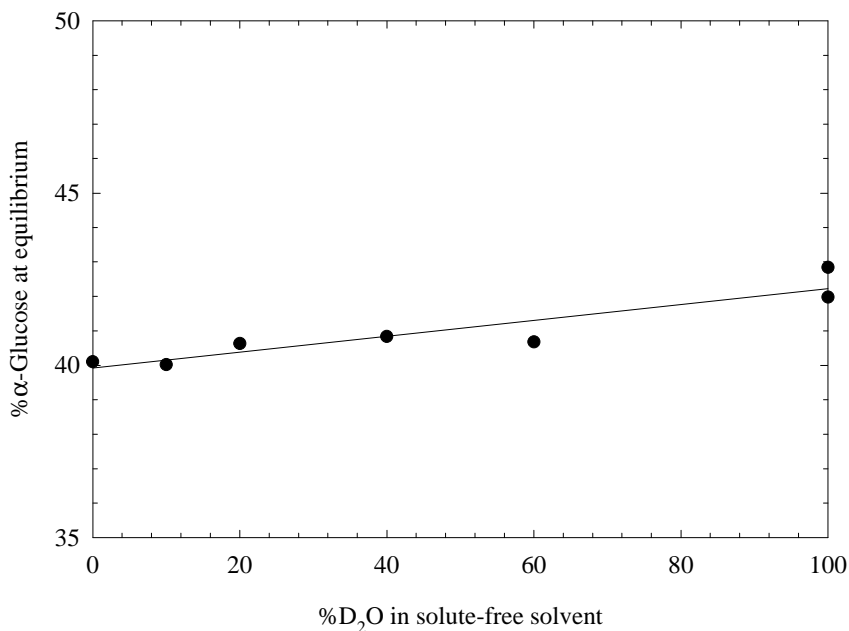
Figure 3.13 Percent α-glucose as a function of an amount of D$_2$O in the system. Line

is a linear regression.

3.4.4 Effect of Ring Structure on the Mutarotation Rate and Mutarotation Equilibrium (Aldoses versus Ketoses)

The mutarotation rates of the sugars in the current study are compared to the mutarotation rate of the monosaccharide ketoses **D**-fructose (Nelson and Beegle, 1919) and **L**-sorbose (Pigman and Isbell, 1968), and the monosaccharide **D**-mannose (Pigman and Isbell; Lee, Acree, and Shallenberger, 1969) in Figure 3.14. Extra data for **D**-glucose was taken from many previous studies (Barc'H, Grossel, Looten, and Mathlouthi, 2001; Hudson and Dale, 1917; Kraus and Nývlt, 1994; Lee et al.; Nelson and Beegle; Nelson and Johnson, 1976; Pigman and Isbell), and all these results were used in the calculation. The galactose rates of mutarotation were

also taken from various studies (Nelson and Johnson; Pigman and Isbell; Wertz, Garver, and Anderson, 1981) and were treated in the same way as for glucose. This plot shows whether there is a relationship between the type of sugar (aldose and ketose), and the size of the sugar (monosaccharide or disaccharide) and the mutarotation rate. The overall mutarotation rates of the ketose sugars (turanose, fructose, and sorbose) fall in a band that is significantly higher than that of all the aldose sugars. The aldose sugars (glucose, mannose, galactose, maltose, and cellobiose) have mutarotation rates in a narrow range; with the fastest rate (that of mannose) being only approximately double that of the slowest rate (that of glucose).
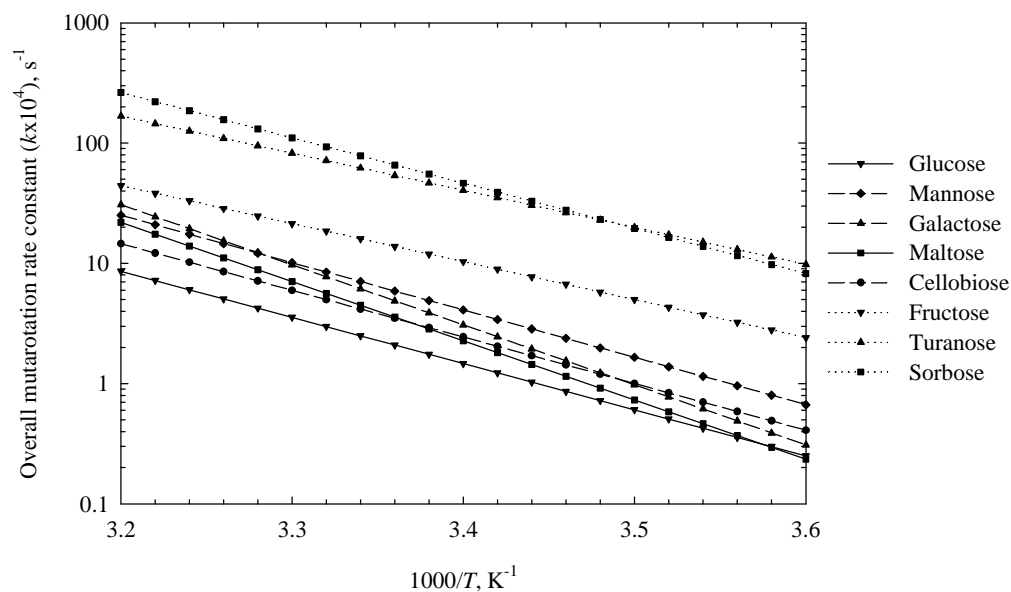
Figure 3.14 Arrhenius plots for the overall mutarotation rates of common sugars. Symbols are from the Arrhenius model, and used to distinguish curves for different sugars only.

3.4.5 Effect of the Number of Rings on the Mutarotation Rate and Mutarotation Equilibrium (Mono- versus Disaccharide)

Figure 3.15 is the Arrhenius plot of aldose sugars studied in this work. There appears to be no strong correlation between the number of rings of the sugar and the mutarotation rate; disaccharides appear to have a rate very similar to that of the mutarotating monosaccharide in their structure. This result suggests that the chemistry of the non-mutarotating ring of a disaccharide does not have a significant effect on the reaction at the anomeric carbon of the mutarotating ring. Thus the mutarotation rate of a disaccharide may be reasonably well predicted as the rate of the monosaccharide in the anomer-determining ring.
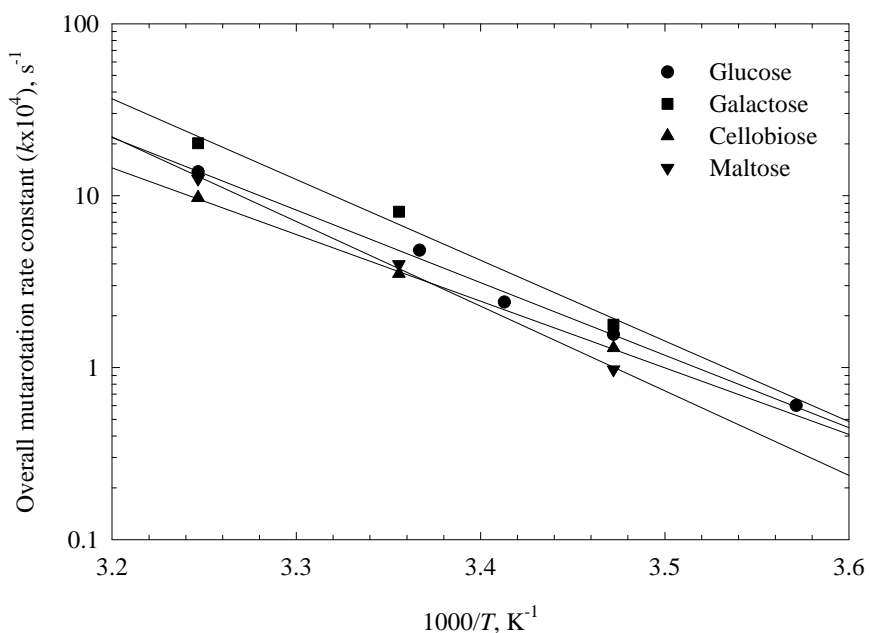
Figure 3.15 Arrhenius plots for the overall mutarotation rate constants of aldoses.

3.5 Conclusion

The overall mutarotation rate of the simple sugars is contained in narrow bands on an Arrhenius plot, depending on whether they are aldose or ketose sugars. Ketose sugars are significantly faster mutarotating in aqueous solutions than aldose sugars. The rate of mutarotation of disaccharides is similar to the rate of the constituent monosaccharide determining the anomeric form. There is a strong effect of temperature on the overall mutarotation rate, and this dependence is easily modeled by the Arrhenius relationship. There appears to be a small reduction in overall mutarotation rate as the sugar concentration is increased; however, this dependence is small enough that it can probably be neglected for modeling of industrial processes. The mutarotational equilibrium is more difficult to predict but is probably related to the steric effects between hydroxyl groups on the anomeric carbon and hydroxyl groups on adjacent carbons. A study of whether hydroxyl groups are axial or equatorial at the anomeric carbon may help to explain the different anomeric compositions of the various sugars.

Because the rate of the mutarotation of ketose sugars in aqueous solutions is very rapid, the mutarotation reaction will not be the rate controlling step in aqueous crystallizations of these sugars. Based on the results of the current study, the crystallization of aldose sugars may be mutarotation rate controlled, depending on crystallization conditions.

3.6 References

Barc'H, N. L., Grossel, J. M., Looten, P., and Mathlouthi, M. (2001). Kinetic study of the mutarotation of D-glucose in concentrated aqueous solution by gas-liquid chromatography. **Food Chem.** 74: 19-124.

Beyer, H. and Walter, W. (1996). **Handbook of Organic Chemistry**. London: Prentice Hall.

Bock, K. and Pedersen, C. (1983). Carbon-13 nuclear magnetic resonance data of monosaccharides. **Adv. Carbohydr. Chem. Biochem.** 41: 27-65.

Bock, K., Pedersen, C., and Pedersen, H. (1983). Carbon-13 nuclear magnetic resonance data for oligosaccharides. **Adv. Carbohydr. Chem. Biochem.** 42: 193-225.

Boons, G.-J. (1998). Mono- and oligosaccharides: structure, configuration and conformation. In G.-J. Boons (ed.). **Carbohydrate Chemistry** (pp 1-20). London: Blackie Acadamic & Professional.

Flood, A. E., Johns, M. R., and White, E. T. (1996). Mutarotation of D-fructose in aqueous-ethanolic solutions and its influence on crystallization. **Carbohydr. Res.** 288: 45-56.

Gray, G. R. (1976). Solution structures of the keto sugars and their biologically important phosphate esters. **Acc. Chem. Res.** 9: 418-424.

Hart, H., Craine, L. E., and Hart, D. J. (1999). **Organic Chemistry: A Short Course** (10th ed.), Boston: Houghton Mifflin.

Hudson, C. S. and Dale, J. K. (1917). Studied on the forms of D-glucose and their mutarotation. **J. Am. Chem. Soc.** 39: 320-328.

Hudson, C. S. and Sawyer, H. L. (1917). The preparation of pure crystalline mannose and a study of its mutarotation. **J. Am. Chem. Soc.** 39(3): 470-478.

Isbell, H. S. and Pigman, W. (1969). Mutarotation of sugars in solution. II Catalytic processes, isotope effects, reaction mechanism, and biochemical aspects. **Adv. Carbohydr. Chem. Biochem.** 24: 13-65.

Kraus, J. and Nývlt, J. (1994). Crystallization of anhydrous glucose I. Mutarotation rate and solid-liquid phase equilibria. **Zuckerind**. 119(1): 24-29.

Lee, C. Y., Acree, T. E., and Shallenberger, R. S. (1969). Mutarotation of D-glucose and D-mannose in aqueous solution. **Carbohydr. Res.** 9: 356-360.

Lowry, T. M. and Smith, G. F. (1929). The mutarotation of galactose. **J. Am. Chem. Soc.** 33(1): 9-21.

Nelson, J. M. and Beegle, F. M. (1919). Mutarotation of glucose and fructose. **J. Am. Chem. Soc.** 41: 559-575.

Nelson, R. G. and Johnson, W. C. Jr. (1976). Optical Properties of Sugar. 3. Circular Dichroism of Aldo-and Ketopyranose Anomers. **J. Am. Chem. Soc.** 98(14): 4290-4295.

Pigman, W. and Isbell, H. S. (1968). Mutarotation of sugars in solution. I History, basic kinetics, and composition of sugar solutions. **Adv. Carbohydr. Chem.** 23: 11-57.

Que, L. Jr. and Gray, G. R. (1974). 13C nuclear magnetic resonance spectra and the tautomeric equilibria of ketohexoses in solution. **Biochem.** 13(1): 146-153.

Sweeley, C. C., Bentley, R., Makita, M., and Wells, W. W. (1963). Gas-liquid chromatography of trimethylsilyl derivatives of sugars and related substances. **J. Am. Chem. Soc.** 85(16): 2497-2507.

Wertz, P. W., Garver, J. C., and Anderson, L. (1981). Anatomy of a complex mutarotation. Kinetics of tautomerization of α-**D**-galactopyranose and ß-**D**-galactopyranose in water. **J. Am. Chem. Soc.** 103: 3916-3922.

Wilbur, D. J., Williams, C., and Allerhand, A. (1977). Detection of the furanose anomers of **D**-mannose in aqueous solution. Application of carbon-13 nuclear magnetic resonance spectroscopy at 68 MHz. **J. Am. Chem. Soc.** 99(16): 5450-5452.

CHAPTER IV

Secondary Nucleation Thresholds of Glucose Monohydrate

in Aqueous Solutions

4.1 Abstract

Secondary nucleation is the main source of nucleation occurring in the majority of industrial crystallizers. Nucleation is typically avoided or minimized in crystallization processes involving molecular species since it is difficult to control and introduces undesired variability in the product size distribution. For this reason, the secondary nucleation thresholds of glucose monohydrate in aqueous solutions were determined in an agitated batch system prior the crystal growth experiment to ensure no nucleation would take place in the crystallizer. Over the experimental temperature range, the widths of the secondary nucleation thresholds decreased as the induction time increased and were found to be temperature independent when supersaturation was based on the absolute concentration driving force. These data were used to determine the time dependent concentration limits in the batch crystallization experiments discussed in Chapter V.

4.2 Introduction

As mentioned in Chapter II, crystallization is considered to be a two-step process, namely nucleation followed by crystal growth. Nucleation is the formation of

new crystals suspended in the solution. Crystal growth is the growth of these crystals to larger sizes through deposition of solute from the solution. Both nucleation and crystal growth require a supersaturated environment in order to occur. This phenomenon can be explained in terms of thermodynamics; the supersaturated solution is not at equilibrium and the system moves toward the equilibrium state (in this case the solubility) by crystallizing out. When the crystallization starts, the supersaturation can be reduced by a combination of nucleation and crystal growth processes. Controlling the degree of nucleation and crystal growth during the operation can control the product crystal size and size distribution.

Supersaturated solutions exhibit a metastable zone, where crystals can grow without significant birth of new crystals (nuclei). Further increases in the supersaturation will cause the solution to reach a value where secondary nucleation in the presence of prior crystals occurs; this limit is known as the metastable limit for secondary nucleation. Nucleation is necessarily avoided or minimized in crystallization processes since it is difficult to control and gives a bad product size distribution. In batch processes, operation is usually undertaken in the metastable zone, if possible, and crystallization is initiated through the addition of seed crystals, thus avoiding large amounts of nucleation. Fortunately, the secondary nucleation threshold of sugars is usually quite large (Johns, Judge, and White, 1990; Kraus and Nývlt, 1994; Nývlt and Kraus, 1993).

4.2.1   The Glucose-Water Phase Diagram

In order to study the crystallization of glucose in aqueous solution, the phase diagram of this system is required. Figure 4.1 is the phase diagram of glucose (Young, 1957) and establishes the solubility curve of each of the crystalline forms of

glucose in aqueous solution. This figure represents the four solids formed, i.e. ice, α-glucose monohydrate crystal, α-glucose anhydrous crystal, and β-glucose anhydrous crystal, present in the system in the temperature range of –22 to 120°C. For the glucose-water system, three forms of glucose may be deposited from aqueous solution depending upon the temperature: α-monohydrate from approximately –5 up to 55°C, α-anhydrous from 55 up to 91°C, and β-anhydrous above approximately 91°C. If the crystallization is below 0°C, ice is formed with some formation of crystalline glucose (depending on solution concentration). Please note that the transition points presented in this figure are determined from the extrapolation of Young's data only, while other works present a more accurate transition points for glucose-water system, particularly at the higher temperatures (Goldberg and Tewari, 1989; Kraus and Nývlt, 1994; Lloyd and Nelson, 1984; Schenck, 1989). However, the α-glucose monohydrate solubility line is most significant in the study of secondary nucleation threshold without operation near the transition points to avoid the formation of metastable crystalline forms.
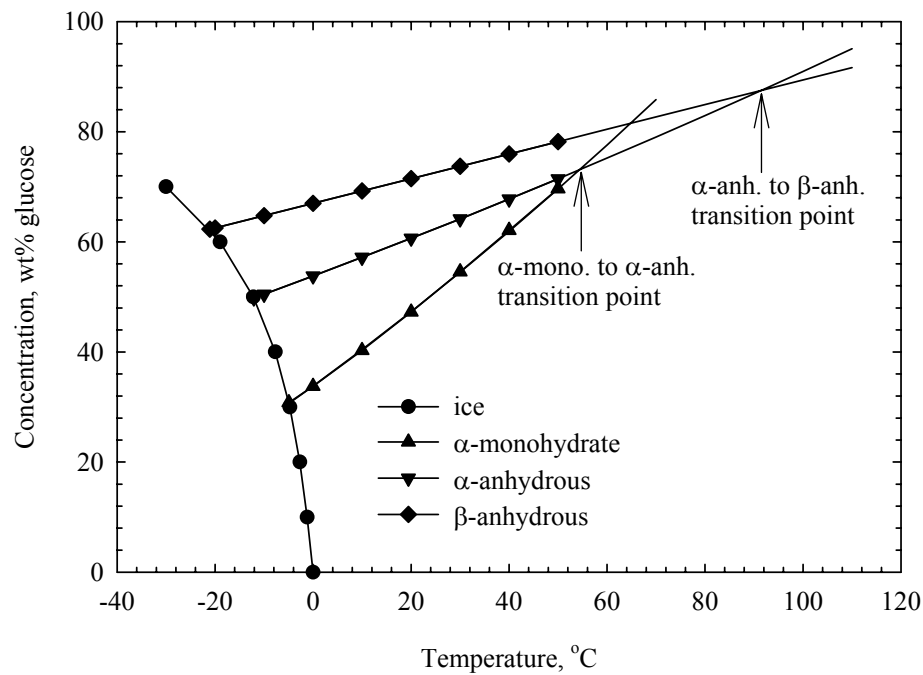
Figure 4.1 Phase diagram of glucose in water, showing the temperature dependence

of the glucose solubility in aqueous solution (Young, 1957).

4.2.2 Theory in Nucleation

Nucleation from solution can occur by either primary or secondary mechanisms. Figure 4.2 shows that primary nuclei can appear spontaneously in homogeneous systems or be enhanced by the presence of suspended dust particles or apparatus surfaces: the latter case is called heterogeneous nucleation. Secondary nucleation describes a range of mechanisms relating to the presence of suspended solute crystals. Secondary nucleation can be separated into several mechanisms as shown in Figure 4.3. In this figure, secondary nucleation can be divided into nucleation by contact, shear, fracture, attrition, and needle breeding. Randolph and Larson (1988) also propose an initial breeding nucleation mechanism, which is an

important source of nuclei in seeded systems. Myerson and Ginde (2002) explain that the initial breeding or dust breeding nuclei are formed by tiny crystals or dust on the surface of dry particles that are directly introduced into the solution in the start-up of the batch operation. This dust is swept off and acts as nucleation sites.

```
                    ┌──────────────┐
                    │  Nucleation  │
                    └──────┬───────┘
              ┌────────────┴────────────┐
         ┌─────────┐              ┌───────────┐
         │ Primary │              │ Secondary │
         └────┬────┘              └───────────┘
       ┌──────┴──────┐          (induced by crystals)
┌─────────────┐ ┌───────────────┐
│ Homogeneous │ │ Heterogeneous │
└─────────────┘ └───────────────┘
(spontaneous)   (induced by foreign particles)
```
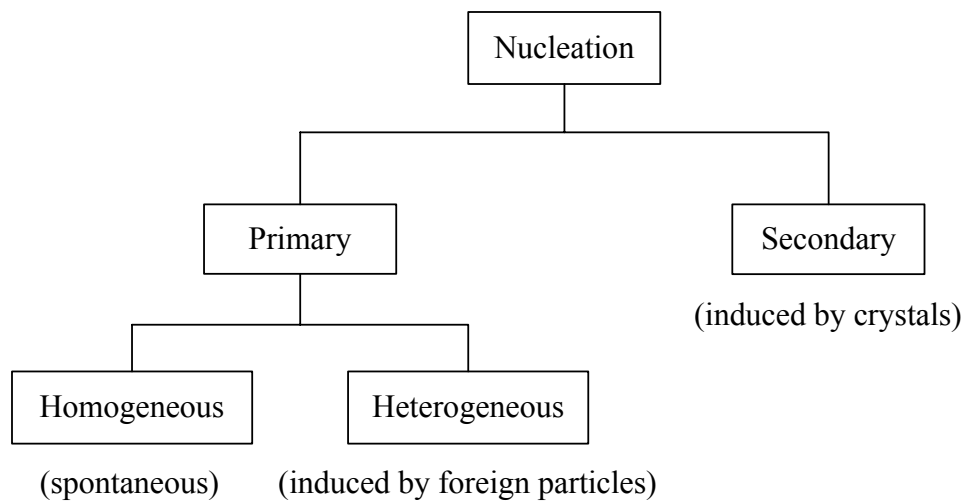
Figure 4.2 Categorization of nucleation mechanisms (Mullin, 2001).
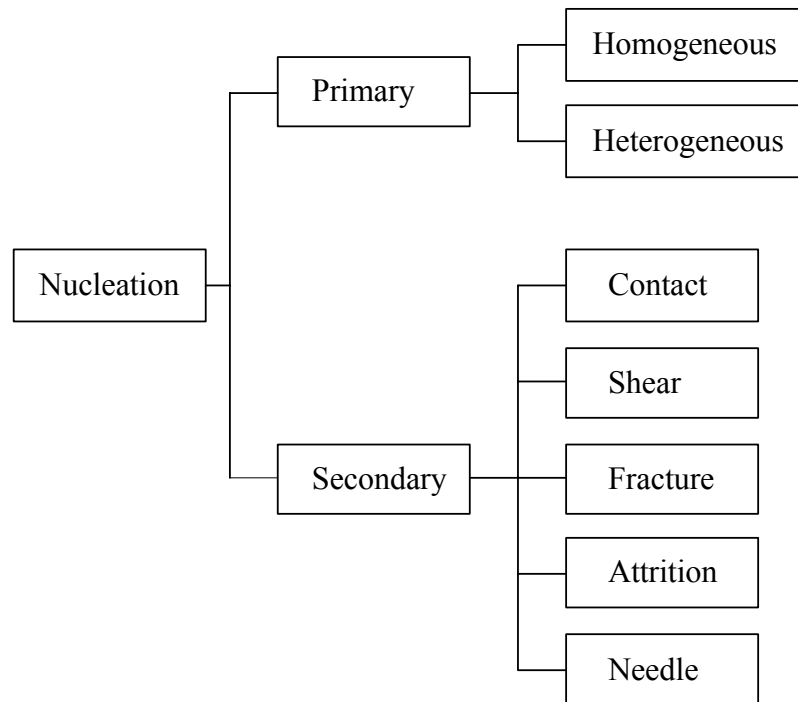
Figure 4.3 Nucleation mechanisms (Randolph and Larson, 1988).

The secondary nucleation mechanisms can be clearly explained using diagram of a growing crystal in Figure 4.4. This diagram can be separated into three parts, the parent crystal, the absorbed layer containing solute molecules, and the solute molecules in the supersaturated bulk solution. Fracture and attrition concern the breakage of the parent crystal, while the other mechanisms concern the absorbed layer. When fragile particles suspended in a dense suspension are subjected to violent agitation or high velocity pumping, the damage is usually done by crystal-crystal interaction or crystal-apparatus contact. Attrition is merely fracture but the fragments are very much smaller than the parent and the visible damage is usually less than for fracture. Needle breeding occurs because of dendritic growth on the parent crystal. These dendrites are very easy to break especially under violent conditions. Nucleation

by fluid shear results when the fluid velocity relative to the crystal velocity is large and some of the absorbed layer is removed. If there is enough energy these absorbed molecules may agglomerate together and form nuclei; else they will disappear. The most important source of nuclei in industrial crystallization is contact nuclei that result from the contact between the particles and stirrer, pump, flow-lines or other crystals. The products of the contact may be attrition, fracture, or contact nuclei, but the last differs from the others because it concerns the absorbed layer, not the parent crystal.
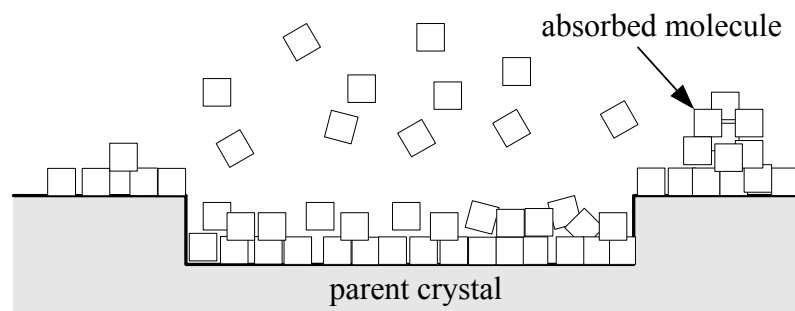
Figure 4.4 Absorbed layers of solutes on the surface of growing crystal (adapted from Randolph and Larson, 1988).

Heterogeneous primary nucleation and secondary nucleation are the most important sources of new crystals formation in industrial crystallization (Randolph and Larson, 1988). Homogeneous nucleation is considered to be an insignificant phenomenon in crystallizers since it is nearly impossible to produce a system with an absence of dust and dirt in the original solution, and because it requires very high supersaturations to produce significant nuclei. The best method for

inducing crystallization is to seed a supersaturated solution with small particles of the material to be crystallized (Mullin, 2001), which is also the reason that homogeneous nucleation can be neglected in industrial crystallizers.

4.2.3   Metastable Zone and Secondary Nucleation Threshold

The phase diagram is a necessary tool for solution crystallization. The crystallization diagram allows us to determine whether a solution will crystallize at a given condition, i.e. at a particular temperature and pressure, and if so, what species will crystallize: it is a map for the crystallization operation. The condition of supersaturation with respect to temperature alone is not sufficient for a system to begin to crystallize (Mullin, 2001; Randolph and Larson, 1988). Accurate information on the metastable zone is necessary for the optimum crystallizer operation. Since this study concerns secondary nucleation only, the time dependent secondary nucleation threshold (SNT) is specified. This section shows details on the metastable zone for different nucleation mechanisms and the time dependent SNT, while details concerning the kinetics of crystal growth will be discussed in Chapter V.

Supersaturated solutions exhibit a metastable zone as shown in Figure 4.5 where the widths of the zone for different nucleation mechanisms are drawn. The lowest solid line is the solubility curve where solid and liquid are in equilibrium with each other. In this state, the solute deposition rate and the solute removal from the crystal occur at the same magnitude. Thus, the induction time, t_{ind}, defined as the time where the nuclei appear, for nucleation (both primary and secondary) is infinite at this condition. Further increases in the supersaturation from the solubility will cause the solution to reach a value where secondary nucleation, heterogeneous primary nucleation, and homogeneous primary nucleation, occur progressively. The limit of

each mechanism is known as the metastable limit or nucleation threshold for the particular mechanism. The zone boundaries are all time dependent, i.e. they depend on the induction time.
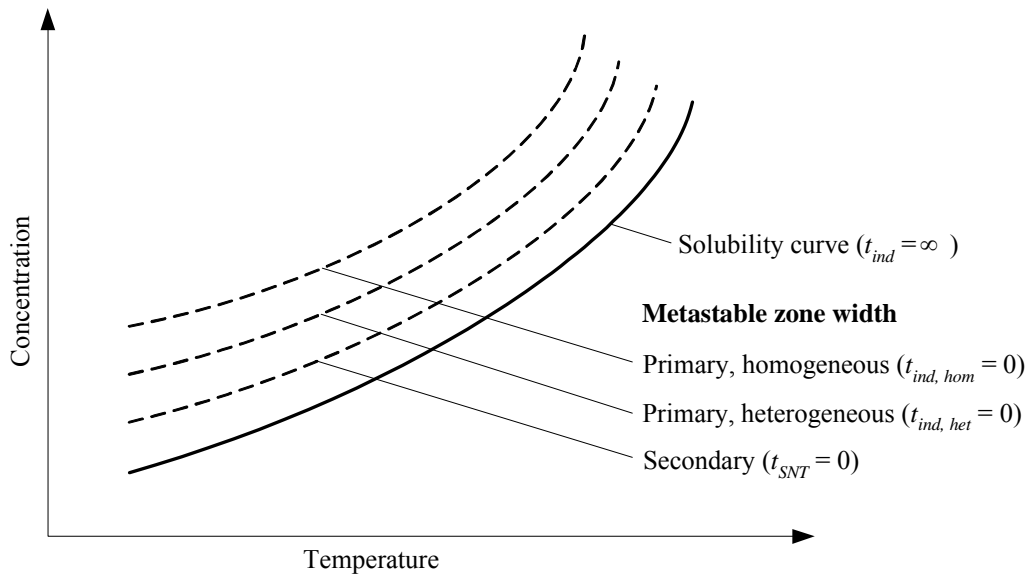
Figure 4.5 Metastable zone widths for different nucleation mechanisms (Mersmann, 1995). The variables t_{SNT}, $t_{ind,\ het}$, and $t_{ind,\ hom}$, are the induction time for secondary nucleation, heterogeneous, and homogeneous nucleation, respectively.

The secondary nucleation zone in Figure 4.5 is expanded in Figure 4.6. The upper dashed line in this figure is the instantaneous secondary nucleation threshold (metastable limit, $t_{SNT} = 0$). Between this line and the solubility curve, which is called secondary nucleation zone, the time dependent secondary nucleation thresholds are drawn. It is noted that the time necessary to induce secondary nuclei varies from zero (at the metastable limit for secondary nucleation) to infinite (at

solubility curve). This can be explained through the fact that the smaller the supersaturation the greater the time required to induce nucleation to occur in the presence of the solute crystals in the system.
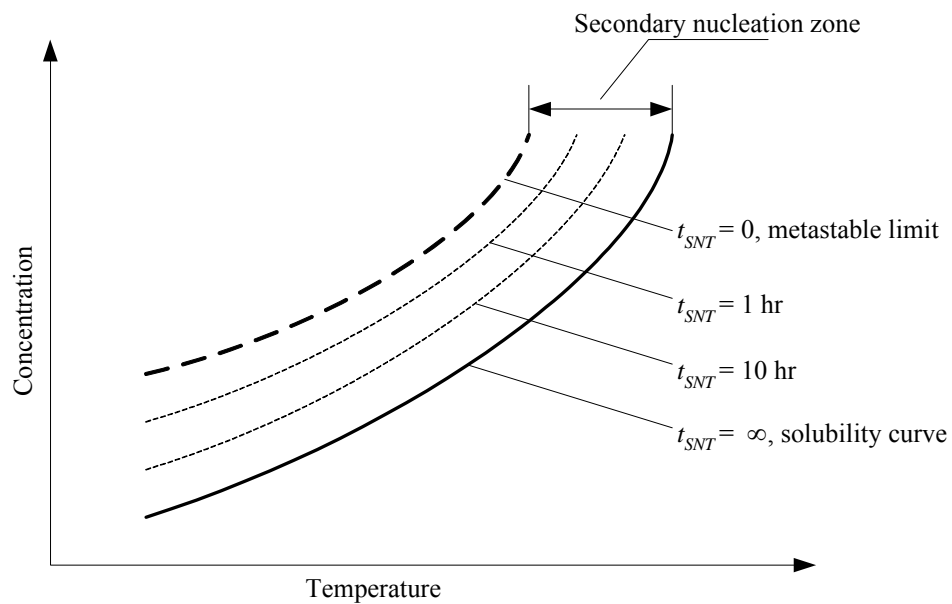
Figure 4.6 A diagrammatic representation of the secondary nucleation thresholds of solution crystallization.

4.2.4 Objectives of the Study

The time dependent SNT of glucose monohydrate in aqueous solutions was determined before the crystal growth study started to ensure the system is operated within the region where nucleation does not occur. This study produces important information for the non-nucleating batch bulk crystallization of α-glucose monohydrate in aqueous solution.

4.3 Materials and Methods

4.3.1 Materials

All glucose solutions used in the secondary nucleation experiments were prepared from analytical reagent (AR) grade anhydrous D-glucose supplied by Chem-Supply Pty. Ltd., Australia, and water treated by reverse osmosis (RO). The anhydrous D-glucose was confirmed to contain less than 2% moisture using the vacuum evaporation (dry substance method) explained in Section 4.3.4. The solution was made from known amounts of glucose and water dissolved in a microwave oven, for which the power was set at the medium level to avoid chemical degradation. Seed crystals were prepared from D-glucose monohydrate supplied by Asia Pacific Specially Chemical Limited (APS), Australia. A seed size larger than 180 μm (dry-sieved) was used since it made it easy to distinguish between the seed added and the nuclei formed.

4.3.2 Apparatus

The 50 ml stirred bottles shown in Figure 4.7 (schematic drawing) were used as agitated batch crystallizers for the secondary nucleation threshold experiments. The research group of Prof. E. T. White of the Particle and System Design Centre (PSDC), Division of Chemical Engineering, the University of Queensland, Australia, designed this secondary nucleation threshold apparatus. The attrition and breakage of the particles caused by contact with the stirrer and the bottom of vessel is minimized by use of a stirrer bar supported some distance above the base of the bottle using an axle mounted on a hub in the bottom of the bottle. A multi-point (15 points) submerged stirring plate set at 200 rpm drove the stirrer bars.

This stirrer speed was chosen since it was the stirring speed where the particles were just suspended, and the stirrer caused no significant breakage of the particles.

The stirred bottles and the submerged stirrer plate were placed in a constant temperature water bath, where the experimental temperature was controlled within ± 0.5°C. A cooling unit was required at low experimental temperatures (i.e. at 10°C).
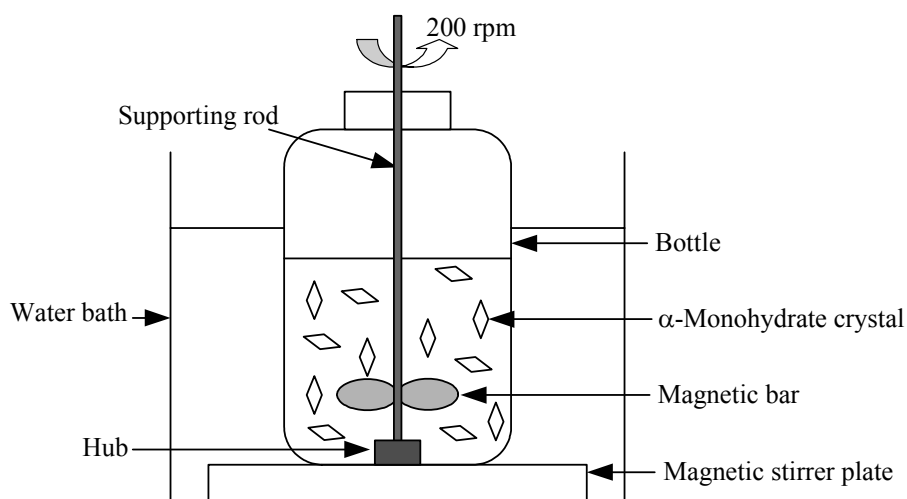
Figure 4.7 Secondary nucleation experimental setup drawing (not to scale).

4.3.3 Experimental Procedure

Secondary nucleation experiments were performed at 10, 25, and 40°C. Each secondary nucleation run involved observation of the nucleation of a number of supersaturated solutions containing α-glucose monohydrate crystals. A series of supersaturated solution was prepared and heated to 20°C above the experimental temperature for 20 minutes to ensure that no ghost nuclei remained in

the solution. These nuclei may appear during the storage of the solution overnight, especially in cases of high supersaturation. Approximately 1 mg of α-glucose monohydrate crystals was added to each solution to induce secondary nucleation. Nucleation was determined visually at many time intervals, with nucleation being indicated by precipitation or clouding by amounts of very fine nuclei. Concentrations of the highest concentrated solution that had not nucleated and the lowest that had were recorded; concentrations being those of the initial concentration prior to nucleation. The experiments were duplicated (at 25ºC) or replicated (at 10 and 40ºC) to check reproducibility.

4.3.4 Dry Substance Method

The dry substance method is a very accurate technique to measure the sugar concentration in solution. However, this technique is time consuming and it is not convenient to use in the kinetics measurement, so it was not used for concentration measurement in this research. The method was used to monitor the amount of water (percent moisture) in the glucose anhydrous and glucose monohydrate crystals to ensure that the storage of the crystals is sufficiently good to keep the crystals dry without water absorption from their surrounding.

Special apparatus

1. Glass weighing bottles approximately 10 ml in volume with ground glass stoppers.

2. Strips of filter paper 60 × 4.5 cm, rolled in loose coils and placed inside the bottles.

Procedure

1. Pre-dry the bottle and filter paper in a vacuum oven at 63°C overnight.

2. Stopper immediately after removal from the oven and cool in a desiccator for 30 minutes.

3. Weigh the sealed bottle plus paper; this is assigned to be equal to W_1.

4. Remove the paper and then weigh the bottle (W_2).

5. Introduce approximately 2 g of glucose crystals and weigh (W_3).

6. Add approximately 2 ml of distilled water, and then mix by swirling.

7. Insert the paper coil and allow standing for 30 minutes before the drying process.

8. Dry the sample at 63°C for 16 hours under a vacuum of 26 to 29 in. Hg.

9. Close the stopper and cool for 30 minutes before weighing (W_4).

The dry substance is calculated from the relationship:

$$\text{Dry substabce} = \frac{(W_4 - W_1)}{(W_3 - W_2)} \tag{4.1}$$

Percent moisture is calculated from (1.00 - Dry substance)×100%.

4.4 Results and Discussion

4.4.1 Effect of Observation Time and Temperature on SNT

An example of the observation time on the measured secondary nucleation is shown in Table 4.1 for the first replicate experiment at 25°C. The rest of the results are presented in Appendix B. In this table, the border between the nucleated and non-nucleated regions can be easily seen. The effect of observation time on the measured SNT at three different temperatures is shown in Figure 4.8. In this figure, each data value consists of two data points joined by a vertical line: the upper point represents the lowest absolute supersaturation that nucleated (the data at the tick symbol in Table 4.1), and the lower point represents the highest absolute supersaturation that did not nucleate (the data at the cross symbol in Table 4.1). The

true value of the SNT must lie between these two points. The mean value of these two points is used to represent the experimental data at that experimental time.

Table 4.1 Secondary nucleation experimental results at 25°C, replicate number 1.

Concentration [g/100g soln.]	Inspection time, hr											
	0.5	1.5	2	4	6	8	21	24	31	33	34	48
52.30	×	×	×	×	×	×	×	×	×	×	×	×
54.97	×	×	×	×	×	×	×	×	×	×	×	√
57.55	×	×	×	×	×	×	×	×	?	√	√	√
60.00	×	×	×	×	?	×	?	?	√	√	√	√
62.57	×	×	×	×	?	?	√	√	√	√	√	√
64.97	×	×	×	√	√	√	√	√	√	√	√	√
67.35	?	√	√	√	√	√	√	√	√	√	√	√
70.00	√	√	√	√	√	√	√	√	√	√	√	√
72.46	√	√	√	√	√	√	√	√	√	√	√	√
74.00	√	√	√	√	√	√	√	√	√	√	√	√

Note: The tick symbol indicates that secondary nuclei were observed, the cross symbol indicates the lack of secondary nuclei, and the question mark represents cases where the result could not be clearly determined.

An exponential decay function is fitted through the data (the mean value as described above), and this line is represented as the best fit SNT. The 95% confidence intervals (2 standard errors) and one standard error intervals of the SNT (in the other word, the confidence intervals of best fit SNT) are included in this

figure. The figure shows the time dependence of the SNT, with the SNT decreasing as the observation time (or induction time) increases. An instantaneous (or initial) secondary nucleation zone width (SNZW) in absolute supersaturation is about 16g/100g solution. At large induction time (i.e. 48 hours) the SNZW is about 5g/100g solution. Even after two days some of the low supersaturated solutions had not nucleated.
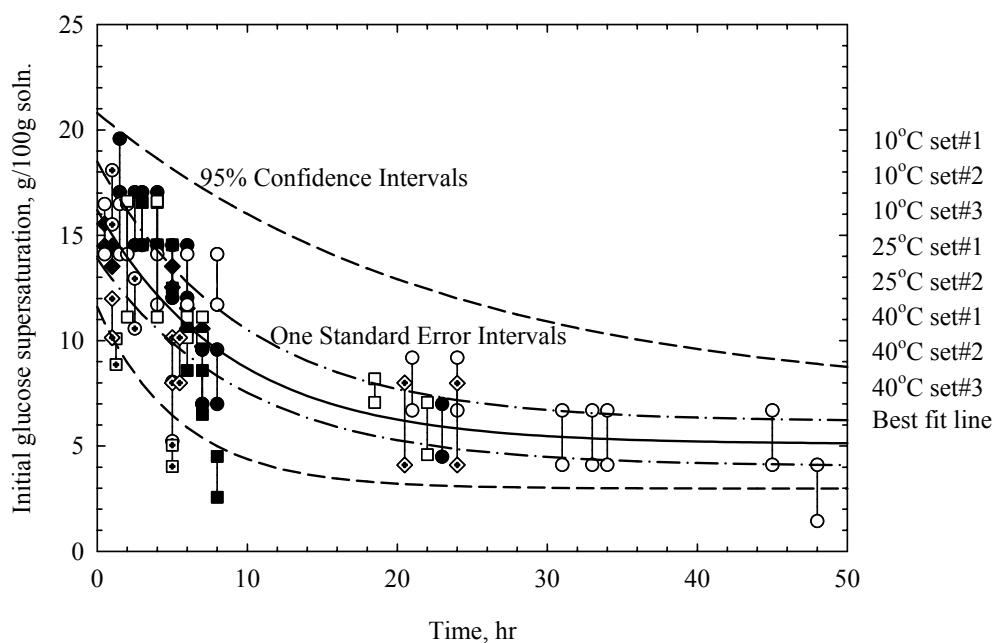
Figure 4.8 The time dependence of the secondary nucleation zone width.

The SNT at 10, 25, and 40°C overlap when plotted in terms of the absolute value of the supersaturation, as in Figure 4.8, and allows a single line to represent the zone width for the three temperatures studied. This result implies that temperature does not have a significant effect on SNT over the range of temperatures where glucose monohydrate is likely to be crystallized. Because the solubility of

glucose is a strong function of temperature, this does not result if the data is plotted with respect to relative supersaturation (in this case, there is a particular SNT for a particular temperature), which is the more common measure of the driving force for crystal growth. In a limited number of the SNT experiments (8 experiments) in some cases, both points are below, or both points are above the line of best fit. This is thought to be due to the stochastic nature of the nucleation process. While a large number of experiments could have been done to locate the mean of the stochastic distribution with high accuracy, this was not considered worthwhile as the secondary nucleation experiments are very time consuming and the results are of acceptable accuracy for further use.

The line of best fit to the data is an exponential decay with three parameters (Equation 4.2), where C represents the total glucose concentration in g glucose/100g solution, C^* is the solubility, and t is the observation time in hour.

SNZW: $\qquad C - C^* = 5.093 + 11.11\exp(-0.1129t)$ $\qquad\qquad\qquad\qquad$ (4.2)

The 95% confidence intervals of the coefficients in Equation 4.2 obtained from the fitting are as follows: 5.1 ± 2.1, 11.1 ± 2.5, and 0.113 ± 0.069. This suggests that the instantaneous SNZW (based on the 95% confidence interval) is in the range of $11.6 - 20.8$ g glucose/100 g solution.

In the fundamental limits, all supersaturated solution should nucleate eventually, i.e. $C - C^*$ should reaches zero as the induction time reaches infinity. Equation 4.2 does not agree with this fundamental limit due to the small number of the experimental data as well as the limitation in the experimental setup. The maximum supersaturated solutions observed were 15 samples (15 points on the magnetic stirrer plate) and the maximum observation time was 48 hours, which is a

reasonable time for industrial crystallization of glucose monohydrate. The observation of SNT at times greater than 48 hours is pointless. However, the results are acceptable for further use especially when the confidence intervals are considered.

Accurate solubility data for glucose monohydrate in water has already been published (Young, 1957). The solubility data in the temperature range of 0 to 50°C was fitted using a quadratic polynomial equation, with the result shown in Equation 4.3 where T represents the experimental temperature in degree Celsius.

Solubility: $C^* = 33.82 + 0.6484\,T + 0.00135\,T^2$ (for 0°C < T < 50°C)   (4.3)

Substitution of Equation 4.3 into Equation 4.2 gives the SNT concentration as a function of time, as shown in Equation 4.4. Because the SNT is not a significant function of temperature, and glucose monohydrate is stable between –5 to 50°C it is likely that this equation is reasonably accurate representation of the SNT concentration over the entire range of conditions where glucose monohydrate crystallizes.

SNT: $C = 38.91 + 0.6484\,T + 0.00135\,T^2 + 11.11\exp(-0.1129t)$ (4.4)

4.4.2   Use of SNT in the Non-nucleating Batch Bulk Crystallization

Figure 4.9 displays the induction time dependent secondary nucleation thresholds of glucose monohydrate in aqueous solutions (each line is drawn from the data calculated using Equation 4.4). This graph is very important in non-nucleating batch crystallizations because it shows limitations on either the operating concentration or the batch time to ensure that nuclei are not formed, so that the system can be easily controlled. For instance, when crystallization occurs at 30°C and the operating time is within 24 hour, the initial concentration that can be used without a significant birth of new crystals is up to approximately 60 g glucose/100 g solution.

This initial concentration may be higher if the concentration decrease is rapid enough to ensure that the combination of concentration and time always puts the mother liquor at a point below the SNT.
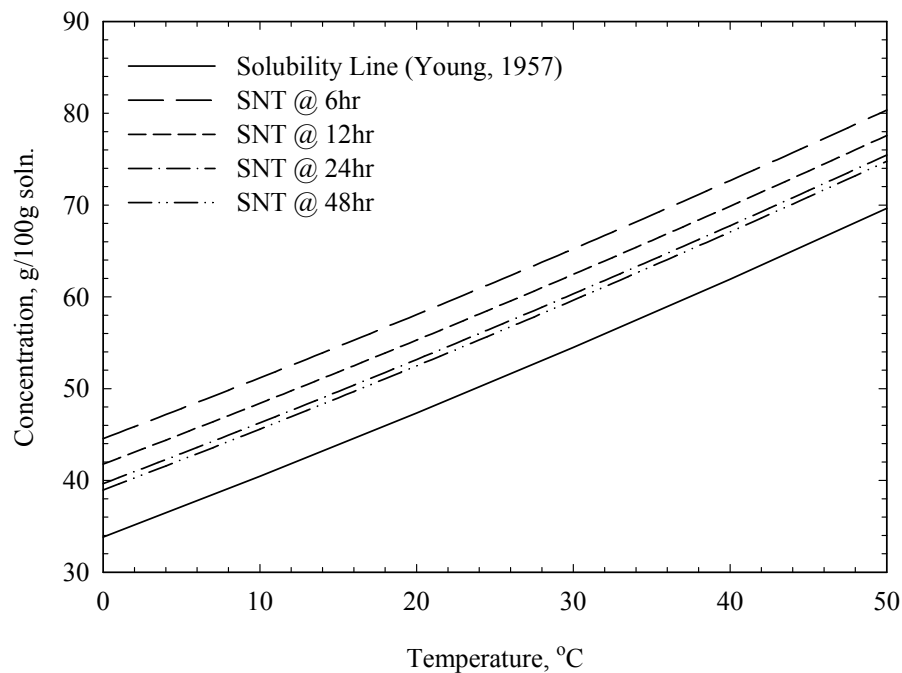
Figure 4.9 Secondary nucleation thresholds for α-glucose monohydrate at the operating time of 6, 12, 24, and 48 hr.

Figure 4.10 is the phase diagram of glucose-water system where the metastable zone for secondary nucleation of α-glucose monohydrate is specified. The dashed line in the plot is the SNT at 48 hours, which is assumed to be equal to the SNT at infinite time (as indicated from Figure 4.9 and Equation 4.4). This region is assumed valid over the crystallizing temperature range of α-glucose monohydrate (about -5.5 to 55°C), however, the operation near the transition points (-5.5°C and

55°C) needs to be minimized to avoid the formation of the metastable phase. For instance, in seeded batch operations over approximately 42°C, and at solution concentration higher than approximately 68.5% glucose, nucleation of α-glucose monohydrate may occur together with the formation of α-glucose anhydrous crystals. Several researchers have found this phenomenon, either with glucose or other common sugars, such as galactose (Beckmann, Boje, Rössling, and Arlt, 1996; Boje, Beckmann, Arlt, and Rössling, 1997; Mulvihill, 1992; Young, 1957; Young, Jones, and Lewis, 1952).
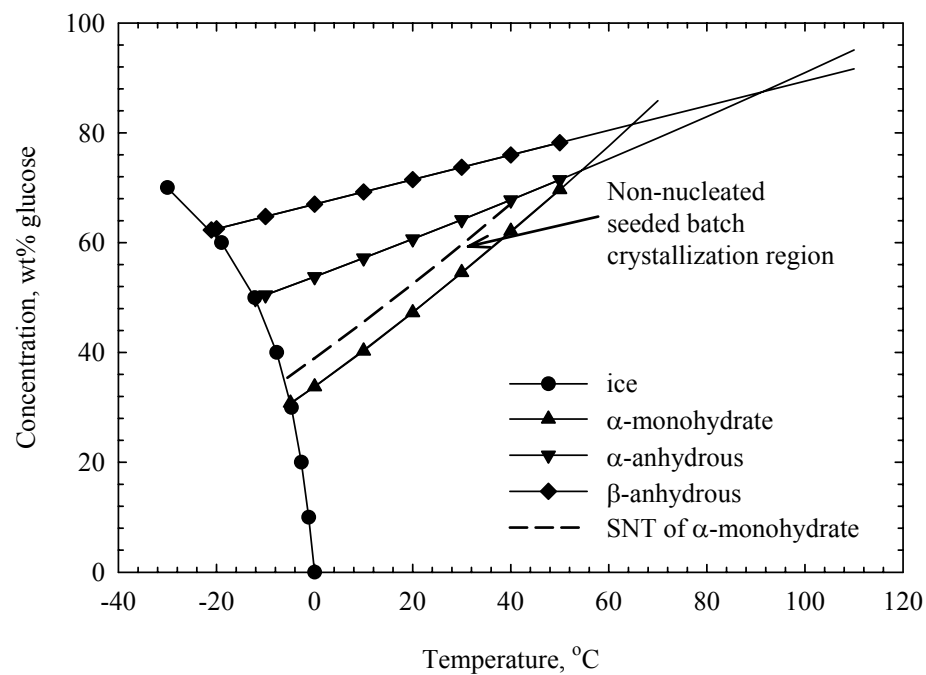
Figure 4.10 Phase diagram of the glucose-water system with the large time metastable region for secondary nucleation of α-glucose monohydrate specified.

4.5 Conclusion

The secondary nucleation threshold (SNT) of α-glucose monohydrate in aqueous solutions is large but decreases with increasing induction time. The instantaneous secondary nucleation threshold (the SNT immediately after the addition of parent crystals) is approximately 16 g glucose/100 g solution for all temperatures studied. Temperature does not have any effect on the width of the SNT. The operating condition where crystals can grow without nucleation is specified by this relation and the phase diagram, as shown above. The results obtained will be further used to determine suitable conditions for crystal growth experiments.

4.6 References

Beckmann, W., Boje, G., Rössling, G. and Arlt, W. (1996). Crystallization of Galactose from Aqueous Solutions: Influence of the α- and β-Anomers. In B. Biscans, and J. Garside (eds.). **Proceeding of 13th Symp. on Industrial Crystallization** (pp 497-502). LGC-CNRS: Toulouse, France.

Boje, G., Beckmann, W., Arlt, W., and Rössling, G. (1997). A Model for the Batch Cooling Crystallization of α- and β-**D**-Pyrano-Galactoses from Aqueous Solutions. In J. Ulrich (ed.). **Proceeding of Fourth Int. Workshop on Crystal Growth of Organic Materials** (pp 342-349). Shaker Verlag: Aachen, Germany.

John, M.R., Judge, R.A., and White, E.T. (1990). Kinetics of Ethanolic Crystallization of Fructose. In A.S., Myerson and K., Toyokura (eds.). **Crystallization as a Separation Process** (pp 198 – 209). Washington DC: ACS.

Kraus, J. and Nývlt, J. (1994). Crystallization of anhydrous glucose IV. Batch Crystallization and Secondary Nucleation. **Zuckerind**. 119(5): 407-413.

Mersmann, A. (1995). **Crystallization Technology Handbook**. New York: Mercel Dekker.

Mullin, J. W. (2001). **Crystallization** (4th ed.). Oxford: Butterworth-Heinemann.

Mulvihill, P. J. (1992). Crystalline and Liquid Dextrose Products: Production, Properties, and Applications. In F. W., Schenck and R. E., Hebeda (eds.). **Starch Hydrolysis Products: worldwide technology production and applications** (pp 121-176). New York: VCH.

Myerson, A. S. and Ginde, R. (2002). Crystal, Crystal Growth, and Nucleation. In A. S., Myerson (ed.), **Handbook of Industrial Crystallization** (2nd ed., pp 121-176). Boston: Butterworth-Heinemann.

Nývlt, J. and Kraus, J. (1993). Crystallization of anhydrous glucose II. Metastable Zone-width and Nucleation Rate. **Zuckerind**. 118(3): 219-222.

Randolph, A. D. and Larson, M. A. (1988). **Theory of Particulate Processes** (2nd ed.). New York: Academic Press.

Young, F.E. (1957). D-Glucose-Water Phase Diagram. **J. Phys. Chem.** 61(5): 616-619.

Young, F.E., Jones, F. T., and Lewis, H. J. (1952). D-Fructose-Water Phase Diagram. **J. Phys. Chem.** 56: 1093-1096.

CHAPTER V

Crystal Growth Kinetics of α-Glucose Monohydrate

in Aqueous Solutions

5.1 Abstract

There is no significant crystal growth kinetics data in the literature for the crystallization of α-glucose monohydrate from aqueous solutions. This study has the aim to determine the crystal growth kinetics of this sugar in aqueous solution in the region where nucleation does not play any role in the system. The bulk crystallization experiments were performed in an isothermal and agitated batch crystallizer. The growth of particles was initiated by adding pretreated α-glucose monohydrate crystals into prepared glucose solutions. Mother liquor and crystal samples were taken at various time intervals to measure the solution concentration and the particle size distribution. The results showed that glucose monohydrate crystals had an abnormally fast growth rate during the first period of the experiment and then the growth rate remained constant at constant supersaturation. The growth rate constant followed an Arrhenius relationship with respect to temperature, and the activation energy of surface integration controlled crystal growth of glucose monohydrate was calculated from this dependence. The results from this study can be used together with mutarotation kinetics and equilibrium data to model the industrial crystallization of this sugar considering the effect of mutarotation.

5.2 Introduction

5.2.1   Introduction

Crystallization is one of the main separation and purification processes used in the production of a wide range of materials. It is used in many industries to remove a valuable substance from an impure mixture, glucose monohydrate from hydrolyzed starch, for example. Industrial crystallization processes in the chemical, pharmaceutical, and food industries mostly involve crystallization from solution. The crystallizing form can be anhydrous or hydrated depending on the operating conditions; however, usually only one crystal form is stable at a particular condition. **D**-glucose, for example, can be crystallized from aqueous solution in three different forms: α-**D**-glucose monohydrate, anhydrous α-**D**-glucose, and anhydrous β-**D**-glucose. The first two forms are produced commercially while the last one is available as a specialty chemical. In aqueous solutions, from the eutectic point at approximately -5°C up to approximately 50°C, the solution is in equilibrium with α-**D**-glucose monohydrate. Between 50°C and approximately 115°C, anhydrous α-**D**-glucose is the solid phase in equilibrium, whereas at temperatures above 115°C the stable phase is anhydrous β-**D**-glucose (Young, 1957). At conditions near the transformation points (approximately 50°C and 115°C), the two most stable forms can exist simultaneously. Away from these points, the less stable phase is transformed to the more stable one. At just below approximately 50°C, the hydrate- to-anhydrous transformation point, both hydrate and α-**D**-glucose anhydrous can be crystallized out (Mulvihill, 1992). This phenomenon occurs when the crystallizer is operated at a high supersaturation, well above the solubility of the anhydrous α-**D**-glucose form.

However the unstable anhydrous crystals dissolve later in the crystallization process to form the hydrate form, as the solubility concentration of the anhydrous form is above the solubility of the hydrate. In the same way, the phase transition of the anhydrous β form may occur near 115°C, which is the α-anhydrous-to-β-anhydrous transformation point. Note the transition points quoted are a little different from different sources, but mainly range from 50 to 55°C for the α-monohydrate-to-α-anhydrous transition point, and 90 to 115°C for the α-anhydrous-to-β-anhydrous transition point (Goldberg and Tewari, 1989; Kraus and Nývlt, 1994; Lloyd and Nelson, 1984; Schenck, 1989; Young). The words transformation and transition are used with the same meaning here.

The crystallization of **D**-glucose also involves mutarotation (Kraus and Nývlt, 1994). In solution, both α-**D**-glucose and β-**D**-glucose anomers exist simultaneously and undergo reversible mutarotation along with crystallization by the scheme shown in Figure 5.1 (a). If a part of the α-anomer is crystallized out, part of the β-anomer slowly converts into the α-anomer and, if necessary, vice versa. If the rates of the mutarotation reactions are slower than the rates of crystallization, the crystallizing anomer will be depleted such that it is below the anomeric equilibrium in solution, leading to a decrease in the driving force for crystallization. Thus mutarotation could have an important effect on the kinetics of crystallization of **D**-glucose in aqueous solution, by having an effect on the supersaturation (Kraus and Nývlt, 1994). This behavior has also been reported for fructose crystallized from aqueous ethanol solutions, where the mutarotation kinetics is particularly slow due to the less polar nature of the solvent (Flood, Johns, and White, 1996). Consequently, the authors reported the crystal growth rate with respect to the concentration of the

crystallizing form (β-fructopyranose, in this case) instead of the total fructose in the system. The group of Arlt and Beckmann noted similar behavior for galactose, including initial nucleation of the unstable crystalline form, followed by a solution mediated (mutarotation controlled) phase transition to the stable crystalline phase (Beckmann, Boje, Rössling, and Arlt, 1996; Boje, Beckmann, Arlt, and Rössling, 1997). They also defined the crystallization driving force with respect to the α-anomer, which is the stable crystalline form. The crystallization scheme including the mutarotation and an unstable phase transformation of galactose is shown in Figure 5.1 (b).
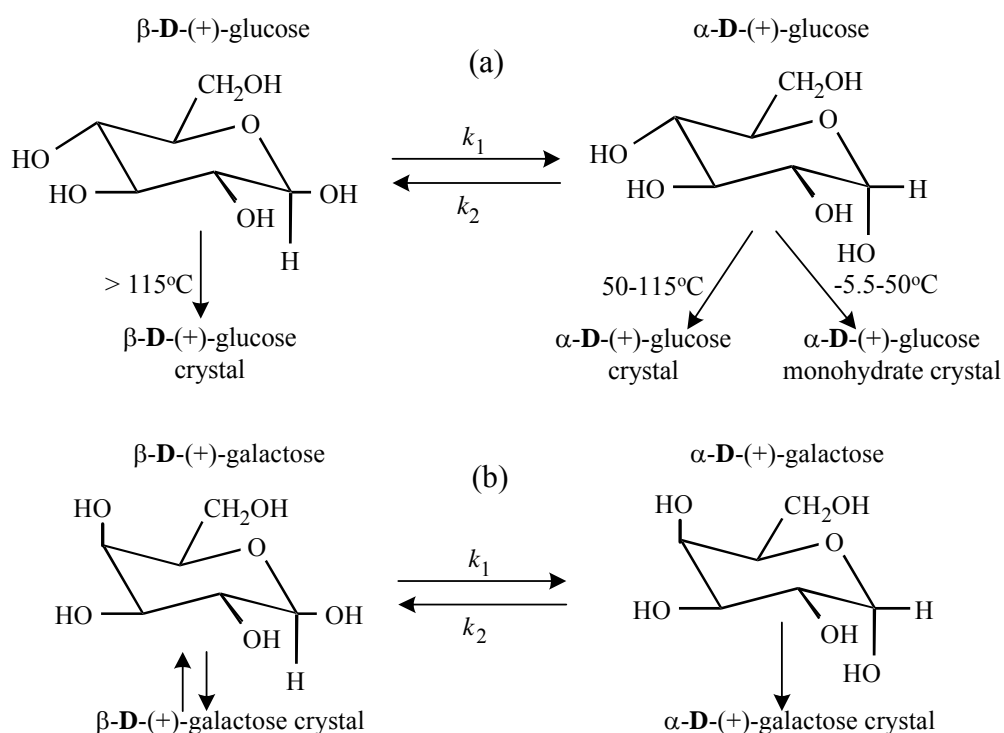
Figure 5.1   Reaction schemes for the crystallization including the mutarotation reaction of (a) **D**-glucose and (b) **D**-galactose (Boje, Beckmann, Arlt, and Rössling, 1997).

Mutarotation may be the rate-limiting step in the crystallization of glucose monohydrate, depending on the relative rate constants of the mutarotation and crystallization kinetics. The crystallization kinetics also depend on nucleation, but the secondary nucleation thresholds of industrial sugar crystallizations are large, so operation is mostly seeded and non-nucleating. In seeded batch crystallizations, the kinetics depends on the initial suspension density, which in industrial crystallization of glucose monohydrate is about 3 to 15% by volume (Mueller, 1970). However, in order to study the crystallization kinetics where the mutarotation effect is to be neglected, the depletion of the crystallizing anomer due to the crystal growth needs to be significantly slower than the generation via mutarotation. This can be achieved using batches containing small numbers of seed crystals operating within the metastable zone (operation with no nucleation).

5.2.2 Growth Rate Dispersion (GRD)

Growth rate dispersion (GRD) is the phenomenon where apparently identical crystals of the same size grown under the same environment have different growth rates (Butler, 1998; Randolph and Larson, 1988). In other words, GRD is the distribution of growth rates evident in a homogeneous sample of crystals growing in a uniform environment (Liang, Hartel, and Berglund, 1989). The large spread of product size distribution in batch crystallizers without nucleation is due to GRD (Flood, Johns, and White, 2000; Liang, Hartel, and Berglund, 1987; Liang, Hartel, and Berglund, 1989). Contact nuclei grown in nucleation cells show evidence of GRD of crystal populations (Elankovan and Berglund, 1987; Jones and Larson, 1999; Shanks and Berglund, 1985; Shiau and Berglund, 1987). In continuous crystallizers, the major cause of the spread in product size distribution is due to the distribution of

residence times of crystals, but GRD still causes a significant spread in sizes (Randolph and White, 1977). For the MSMPR crystallizer, GRD causes an extra curvature in the number population density plot (Shi, Liang, and Hartel, 1990).

GRD is not fully understood, however it thought to occur due to different densities of screw dislocations on the crystal surfaces; a greater density of dislocations should result in higher growth rates (Randolph and Larson, 1988). Some works also showed that the presence of some impurities causes increases in the GRD of crystal populations (Liang, Hartel, and Berglund, 1987; Randolph and Larson, 1988).

5.2.3   Common History (CH) Seed

Common History (CH) seed is a crystal population where crystals of the same size have the same growth rate, and the growth rate is proportional to the size. The assumptions for CH seed when used for a batch crystallizer are as follows (Butler, 1998).

1. Each crystal has its own growth rate which is constant over the period of growth.

2. No further nucleation occurs during growth.

3. No breakage or agglomeration occurs during growth.

These assumptions cause the growth rate distribution of CH seed to be directly proportional to the particle size distribution (PSD); growth rates of crystals between nucleation and seeding could be directly calculated from the size divided by the growth time. Over the growing period, the PSDs of CH seed on a linear scale are increasingly stretched along the size scale, while on a log scale the shape of the PSDs remains constant but the mean shifts along the size scale. The constant shape on the log size scale is due to the constant relative growth rate of the seed crystals (Butler,

1998). This makes the distributions fall onto one curve when divided by a reference size (with the reference size usually being the mean size at that particular time).

5.2.4   Objectives of the Study

The aim of this study is to determine the crystal growth kinetics of glucose monohydrate in aqueous solutions. Here, the effects of temperature and supersaturation on the crystal growth were investigated. Pure aqueous solutions were crystallized in isothermal batch crystallizers in order to simplify the system studied. Due to the very slow crystal growth of this sugar, and the small amount of seed added, the glucose concentration in the crystallizer was essentially constant during the crystallization. And due to the small amount of seed used, the crystal growth data is crystallization rate controlled, without data artifacts due to the mutarotation reaction in the glucose system.

5.3 Materials and Methods

5.3.1   Materials

The glucose solutions used in both the secondary nucleation and crystal growth experiments were prepared similarly and the method was shown previously in Section 4.3.1. The prepared solution was kept overnight at 10°C above the experimental temperature to ensure the establishment of the mutarotation equilibrium and to ensure that no nuclei were formed. Seed crystals were prepared from α-glucose monohydrate supplied by Asia Pacific Specially Chemical Limited (APS), Australia, and a pretreatment stage was found to be necessary to minimize nucleation due to the presence of surface nuclei and particle dust. The procedure is presented in the following section.

5.3.2   Seed Slurry Preparation

Due to the possible formation of tiny crystals on the surface of the α-glucose monohydrate crystals, and also dust on the surface of the particles, a pre-treatment process was performed before the seeds were introduced into the crystallizer. The pretreatment minimized dust-breeding secondary nucleation, which is a serious problem in industrial batch operation (Myerson and Ginde, 2002). Seed crystals were prepared using a technique that initially sieved the commercial glucose monohydrate crystals through a set of sieves ranging from 45 to 250 μm. Sieving was performed to produce seed crystals with a narrow size distribution, in order to reduce difficulties in sizing wide particle size distributions, and to avoid the larger crystals growing out of size range measurable using Malvern Mastersizer/E. The 63 to 90 μm dry-sieved fraction of commercial α-glucose monohydrate crystals was wet sieved in denatured ethanol using a 63-μm sieve in order to remove fine crystals and dust from the particles. The wet-sieved product was then washed in 50% (by weight) aqueous glucose solution in water, which is undersaturated by a small amount at room temperature (approximately 25ºC), to remove the dust or surface nuclei from the surface of the particles. Observation of the crystals under a microscope showed that the appearance of the crystals was good and no significant amount of nuclei in the seed particles or on the crystal surface was seen. Two samples of this slurry were taken to measure the particle size distribution (PSD) using the Malvern Mastersizer/E before each experiment, and these results noted as the seed size. Two batches of seed crystals were produced, as the initial batch prepared, used for the 25°C experiments, was insufficient to complete the experiments at 10 and 40°C. The particle size distributions of the two batches of seed crystals prepared were slightly different, with

the seed prepared for the 25°C experiments having the same volume mean size (approximately), but a slightly larger coefficient of variation. Examples of the seed PSDs for the experiments at 10, 25, and 40°C are shown in Figure 5.2. It was also confirmed that there was no difference between the seed size measured before, and immediately after, addition to the crystallizer.
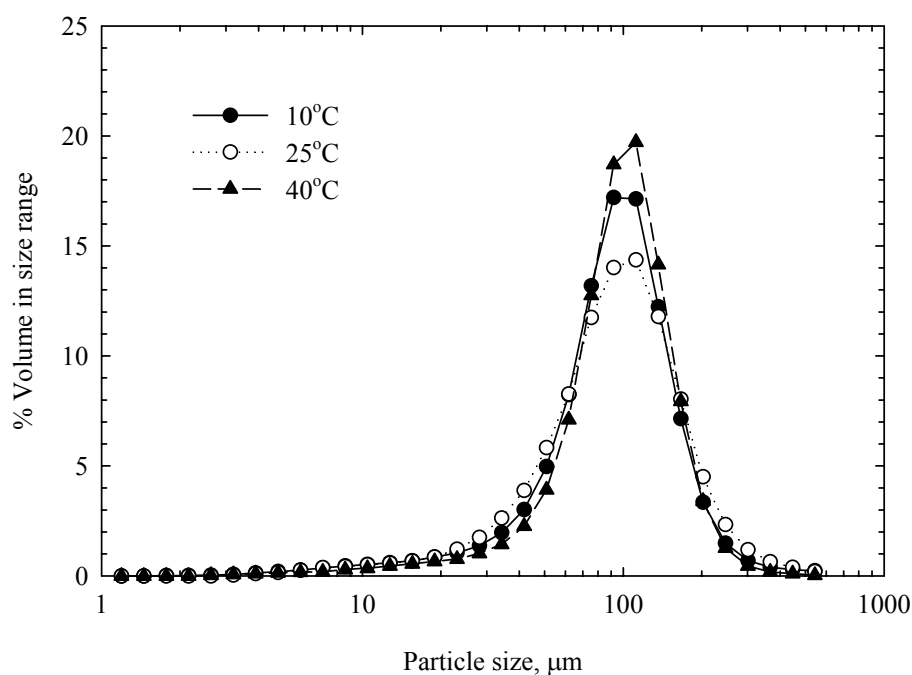
Figure 5.2 Averaged volume based particle size distributions for seed crystals used in experiments at 10, 25, and 40°C.

5.3.3   Dispersant Preparation

A supporting medium, which is also called the dispersant, is required to disperse the sugar crystals inside the sample cell during the particle size distribution (PSD) measurements using the Malvern Mastersizer/E. The rules for

choosing this dispersant are that the medium must be transparent to the laser wavelength, and have a different refractive index than the crystals. The particles must not dissolve, flocculate, or react chemically with the supporting media. The suspension medium used for the PSD measurement in this work was prepared from anhydrous ethanol (CSR Ltd., Sydney) and water treated by reverse osmosis (RO). Ethanol was chosen since there is no significant dissolution of glucose crystals in it, and water was added to prevent the dehydration of water from the hydrate crystals.

An amount of anhydrous α-glucose in excess of the solubility, i.e. more than 2.8% by weight (Peres and Macedo, 1997), was added to the 10% water in ethanol solution, and the solution was agitated using a magnetic stirrer at 40°C overnight. A tight capping of the bottle is necessary to prevent evaporation of ethanol from the bottle. This solution was then kept under stagnant conditions until the solution temperature decreased to room temperature and the remaining glucose crystals settled. Only clear solutions were pipetted for use in the size measurement. There was no point to filter this solution since the filtrate was still suspended with a large amount of fine particles (even in case of using the 0.22 μm membrane filter). α-Glucose monohydrate crystals did not dissolve in this solution since there was no significant change in the PSD of α-glucose monohydrate crystals resulting from Malvern Mastersizer/E over time, indicating no growth or dissolution.

5.3.4 Experimental Apparatus

The apparatus comprises of two 1-litre glass crystallizers, each with a 4-blade agitator and overhead stirrer. This experimental setup was placed inside a constant temperature water bath, where the temperature was controlled within ±

0.5°C. A schematic drawing of the experimental setup is illustrated in Figure 5.3.

Two batch crystallizations were performed simultaneously to check reproducibility.
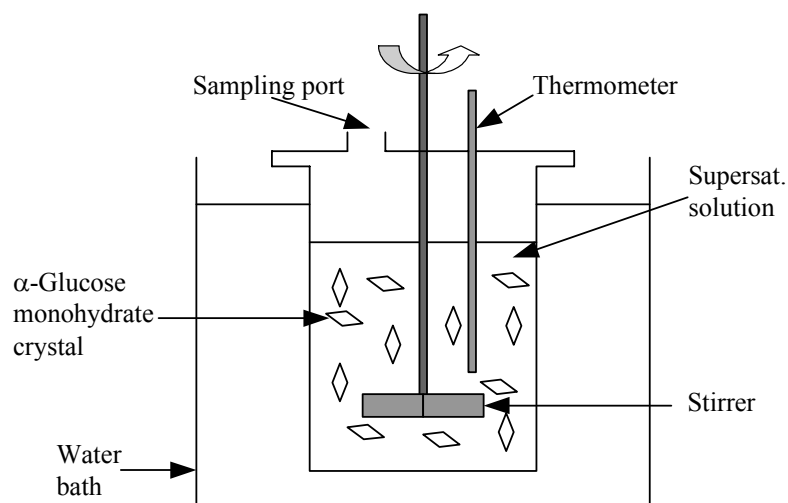
Figure 5.3 Experimental setup schematic (not to scale).

5.3.5 Experimental Procedure

Preliminary work was performed to check what agitation rate is required for the crystal growth mechanism to be controlled by the surface integration step. The experiments were carried out isothermally at 25°C with stirring speeds of 400, 500, and 550 rpm. The experimental conditions, such as solution concentration, seeding amount, experimental time, were controlled at the same values for all experiments.

The crystallization of α-glucose monohydrate was performed isothermally at 10, 25, and 40°C. Initial crystallization experiments at varying agitation rates demonstrated that the crystallization was surface integration controlled

at least at, and above, 450 rpm. It was important to achieve negligible attrition and/or breakage of seed crystals, so 500 rpm was chosen as the agitation speed for the crystallization experiments. A certain amount of a prepared solution was introduced to each crystallizer before addition of seed. The experiment was duplicated in a parallel crystallizer.

Batches were initiated by the addition of 10 ml of seed slurry. Before the addition of the seed to the crystallizer, and during the batch run, duplicate samples were taken at various time intervals to measure the PSD. The total experimental time depended on how quickly the crystals grew under the given conditions, but was chosen to be less than that for the secondary nucleation limit at the initial supersaturation to avoid undesired nucleation. Observation of samples under a microscope indicated that nucleation did not occur. The refractive index of the clear liquor was periodically monitored during the experimental run to ensure the concentration was essentially constant during crystallization. A digital refractometer (RFM 340, Bellingham & Stanley Limited, UK) was used and the discrimination of the refractive index (RI) value for this instrument is within $\pm$ 0.00001 RI units. A calibration curve of known concentration solutions was used to determine total glucose concentrations from the RI measurements. The low amount of seed added to the batch, and slow growth kinetics ensured that the batches were at constant composition within the accuracy of the measurements.

5.3.6   Particle Size Measurement

The PSD and volume concentrations were measured using the Malvern Mastersizer/E. The Malvern details and the measuring procedure are described here.

5.3.6.1 The Malvern Mastersizer/E

The Malvern Mastersizer/E uses a laser light scattering sizing technique. In general, it is used to measure the size of any one material phase in another. In this study it measured the particle size of α-glucose monohydrate crystals in 90% saturated ethanol solution, produced via the method shown in Section 5.3.3. All particles size analysis used a 300 mm focal length lens with the small sample cell having a beam length of 14.3 mm. This focal length measures the crystal sizes between 1.2 and 600 μm. Crystals are suspended in the path of a helium-neon laser beam (wavelength 633 nm) and scatter the laser beam as it passes through the sample. The scattered laser pattern passes through a focus lens and the laser light is focused onto a detector. A PC that is attached to the Malvern records the scattering pattern and the size distribution of the sample is calculated from this pattern. The basic principle of the Malvern is shown in Figure 5.4. An example of the data re-plotted from the raw data of the Malvern output is shown in Figure 5.5. The relative error in the volume median size obtained from Malvern is estimated at 2% (Malvern manual).
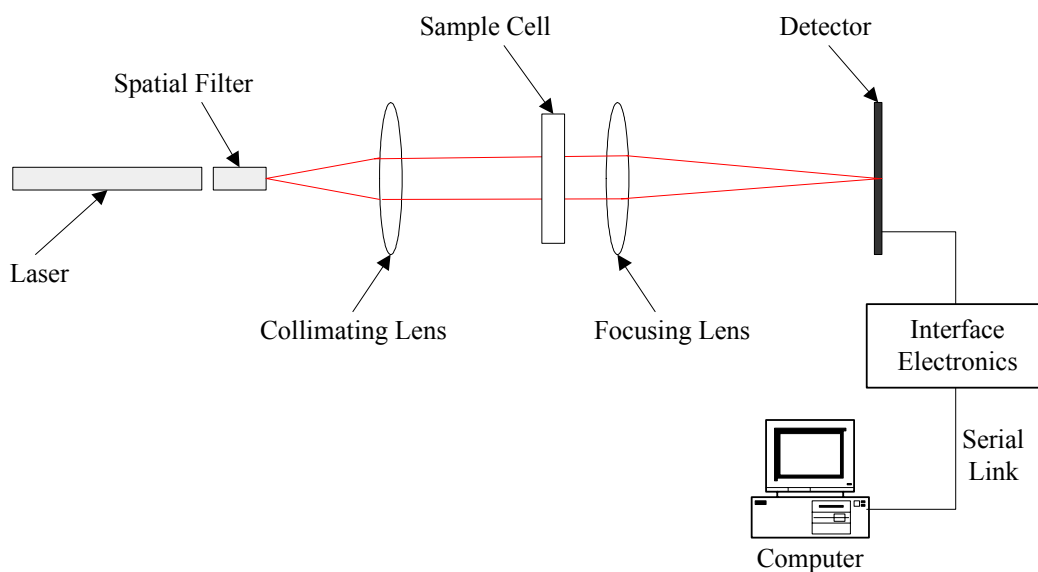
Figure 5.4 The Malvern Mastersizer basic principle (redrawn from the Malvern manual).
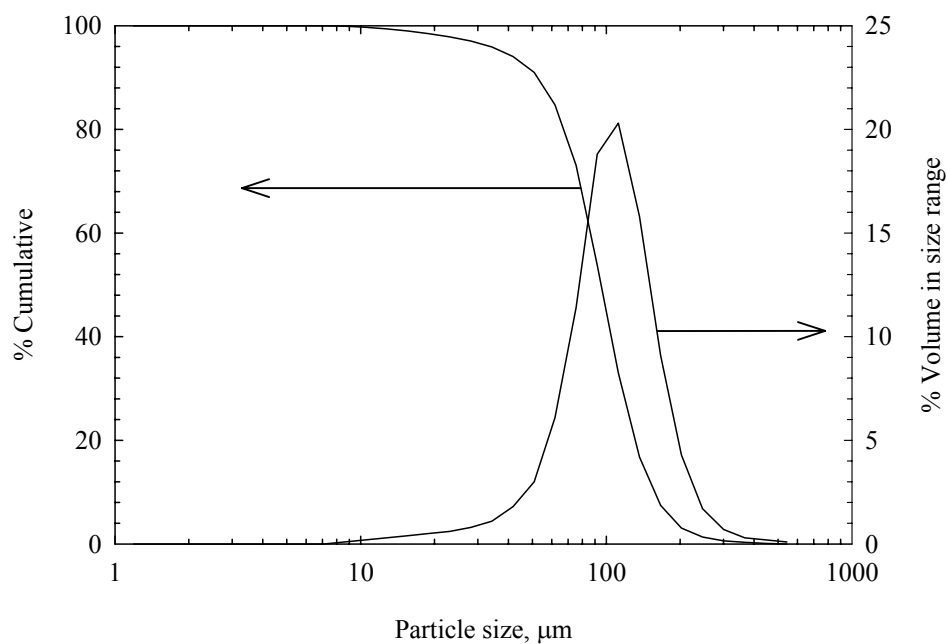
Figure 5.5 The Malvern Mastersizer/E output (re-plotted) for the seed at 40°C.

5.3.6.2 Particle Size Measurement Procedure

Approximately 16 ml of the dispersant was placed in the stirred Malvern cell and the top opening of the cell was immediately covered with a plastic strip to prevent ethanol evaporation. The stirring level of magnetic star stirrer was set at the medium level (i.e. at 7), which is enough to suspend the crystals in the dispersant and not sufficiently fast to break the crystals by contacts with the bead. A beam alignment and background measurement, respectively, were taken prior to the addition of α-glucose monohydrate slurry. An alignment of the beam light is needed to check whether the system is ready for the measurement or not; if the Malvern fails this step the sample cell glass or lens are not clean enough. The background measurement must be subtracted from the sample measurement to get the actual scattering from the sample particles alone.

The volume of glucose slurry added was adjusted case-by-case to make the measured obscurations at approximately 0.2 since this value is the ideal value for the measurement. The obscuration is the fractional loss of energy from the laser beam caused by scattering from the particles. If the sample concentration is too high then light will be scattered by multiple particles, giving an incorrect angular reading. If the sample concentration is too low, the obscuration is low, leading to an insufficient sample count (compared to the background) for an accurate reading. More dispersant was added in cases where a high obscuration value was obtained, and, if the obscuration was too low (less than 0.15) more glucose monohydrate slurry sample was added to the sample cell. The results were read about a minute after adding the sample.

5.3.6.3 Crystal Content Calculation

For each measurement, the percent volume concentration was noted. This value is the predicted percent crystal content (by volume) in the sample cell. The crystal content in the crystallizer is calculated from the equation:

$$\text{weight \% crystal} = \frac{\text{volume \% from Malvern} \times (V_d + V_s) \times \rho_x}{V_s \times \rho_s} \tag{5.1}$$

where V_d is the volume of dispersant, V_s is the volume of slurry, ρ_x is the crystal density, and ρ_s is the density slurry. Crystal content (in the unit of kg particles per kg suspensions) can be determined from:

$$\text{crystal content} = \frac{\text{volume \% from Malvern} \times (V_d + V_s) \times \rho_x \times V_B}{100 \times V_s \times M_B} \tag{5.2}$$

Where V_B is the crystallizer volume and M_B is the mass of crystallizer suspension. The crystal contents for some experimental runs are presented in Appendix C. The results in crystal contents were consistent with the increase in particle size due to crystal growth (increases in crystal content were of the same order of magnitude as increases in crystal mass (as calculated from changes in crystal size) under constant driving force conditions) and also confirm that no nucleation occurred inside the crystallizer.

5.4 Results and Discussion

Figure 5.6 shows an example of the PSDs from a batch run at 25°C plotted on a scaled log size basis. For the Common History (CH) seed, where the relative growth rate of a crystal is proportional to its size, growth will not change the shape of the size distribution plotted on a log scale (Butler, 1998). Thus, Figure 5.6 shows that the seed crystals are indeed CH seed. The particle sizes have been scaled relative to the

volume median size for each PSD to illustrate the constant shape of the distribution. The results show two PSD duplicated for each time. The PSD results appear to be approximately normally distributed on a log size scale, except occasionally where there is a tail at the same size ranges.
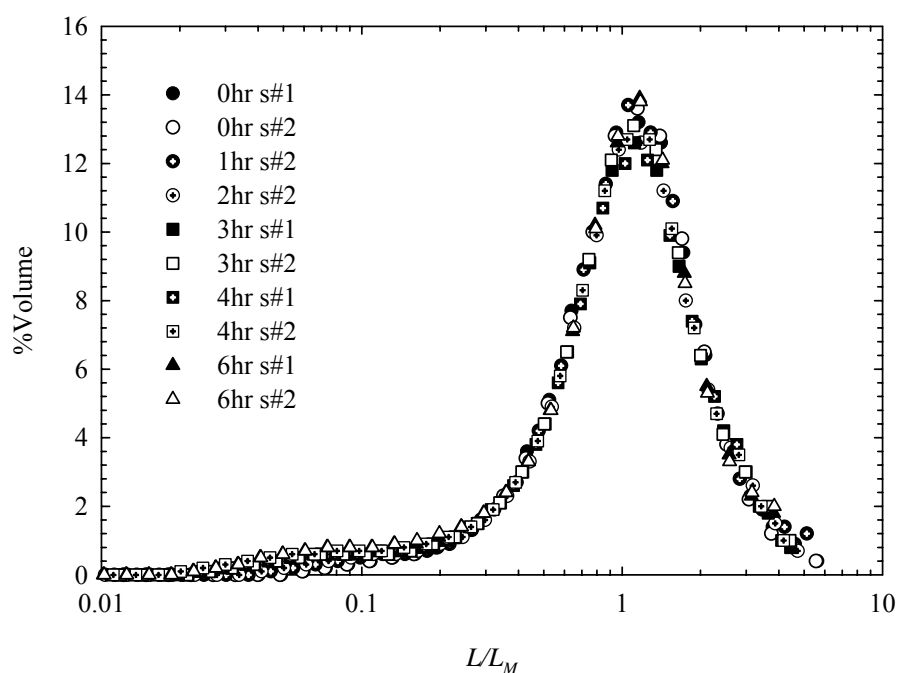
Figure 5.6 Scaled particle size distributions from a batch run at 25°C, with duplicated samples represented by filled and open symbol. s#1 and s#2 are sample 1 and 2, respectively.

Particles from the crystallizer were visually inspected under a microscope at intervals during the crystallization, and no evidence of the nucleation (as evident from particles smaller than the seed crystals) was noticed, so it is likely that the tail is an artifact of the sizing technique. Distributions appearing normal on a log size plot will

follow a log-normal distribution for linear size. A photomicrograph of crystals taken from one run of batch crystallization is shown in Figure 5.7 which shows good shape for α-glucose monohydrate crystals and no evidence of nucleation. Figure 5.8 shows SEM pictures from one of the experimental run at 10°C. Figure 5.8 (a) is the seed crystals, and shows very good uniformity of the seed crystals used in the experiment, however, the shape may not be perfect because of the breakage during the sieve process. Figure 5.8 (b), taken at 2 hours after seeding, shows a good shape for this sugar under the operating condition. Please note that due to the sample used for the SEM should be a dry sample, it is very difficult to avoid surface nucleation when the solvent is evaporated.
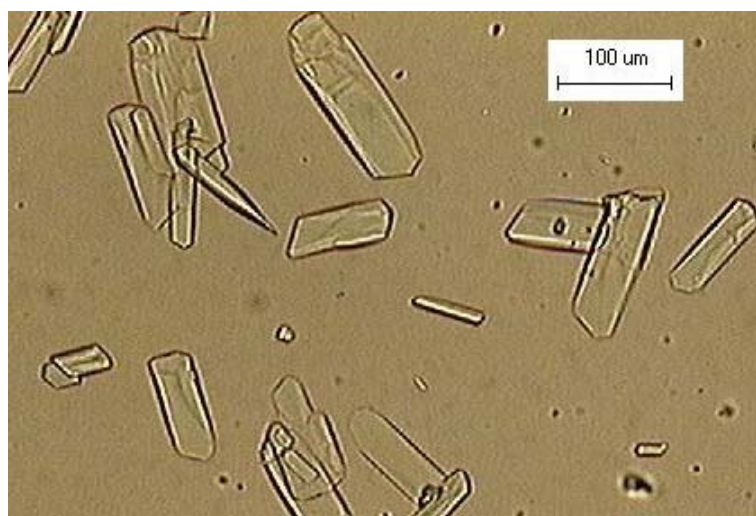
Figure 5.7   Photomicrograph of crystals taken from the isothermal batch crystallization 8 hours after seeding. The conditions for the crystallization were 25°C, agitation at 500 rpm, and the initial relative supersaturation was 0.027.

(a)   (b)
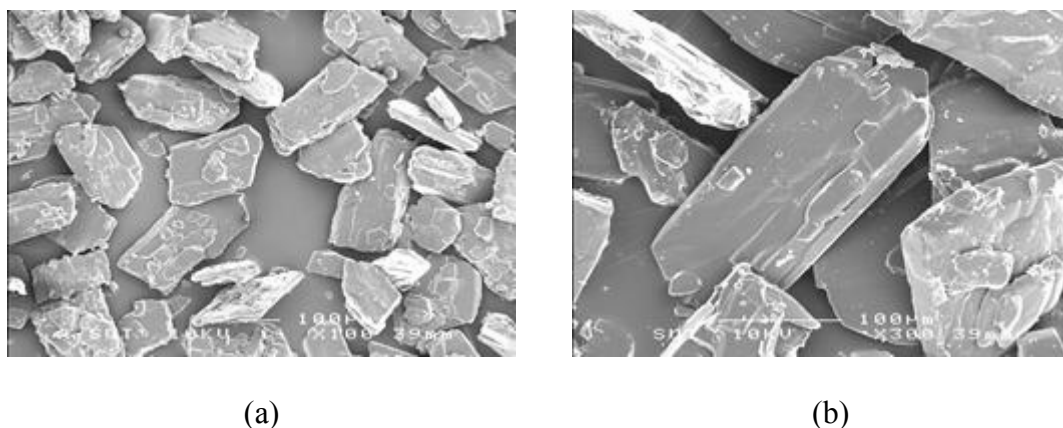
Figure 5.8 SEM pictures of (a) seed crystals and (b) crystals after 2 hours growth in
the batch crystallizer.

5.4.1   Effect of Stirring Speed on Crystal Growth

Crystallization experiments of glucose monohydrate with varying
stirring speed were performed to determine what stirring speed is required for the
crystal growth mechanism to be surface integration controlled crystal growth. The
result is shown in Figure 5.9 where the volume median size is plotted against the
experimental time. The slopes of this plot in time ranging from 1 hour to 6 hour were
determined and noted as the volume based growth rates. There are two groups of
results for each stirring speed; 400 rpm and 550 rpm, and 500 rpm. This is due to the
different seeds used. The seed used for the experiment at 500 rpm was the same as
used for all the experiments at 25°C, while the experiments at 400 and 550 rpm used
the same seed as the experiments at 10 and 40°C. The difference in these two groups
of the seed is shown in Section 5.4.3. However, there is no significant difference
between the growth rates calculated from these two groups of data, as can seen from

them having almost the same of slopes between volume median size with respect to time (Figure 5.9) and also directly from the growth rate values with respect to stirring speed as Figure 5.10. This figure shows the volume growth rates over this stirring range are within 0.07 to 0.16 μm/min with an average value of 0.125 μm/min. It is also concluded that the growth rate of glucose monohydrate in this region (400 to 550 rpm) is surface integration controlled. A stirring speed of 500 rpm was chosen to for the other crystallization experiments in order that they determine integration controlled growth kinetics.
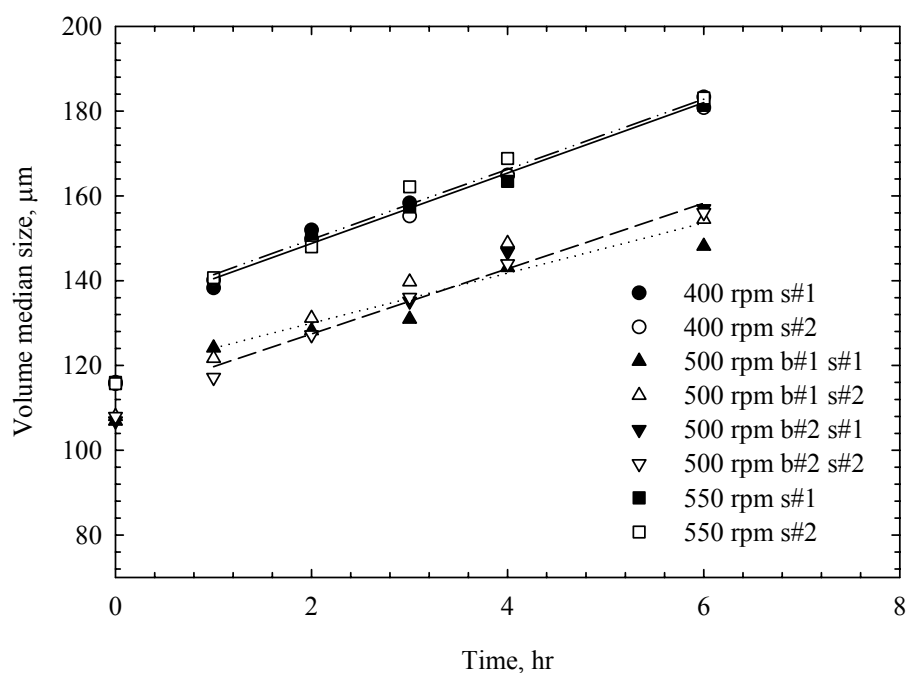
Figure 5.9 Volume median sizes as a function of time at the operating conditions of 25°C, averaged solution concentration of 57.62%, and averaged seeding rate of 0.0024 kg glucose monohydrate/kg solution. b#1, b#2, s#1, and s#2 are batch 1, batch 2, sample 1, and sample 2, respectively.
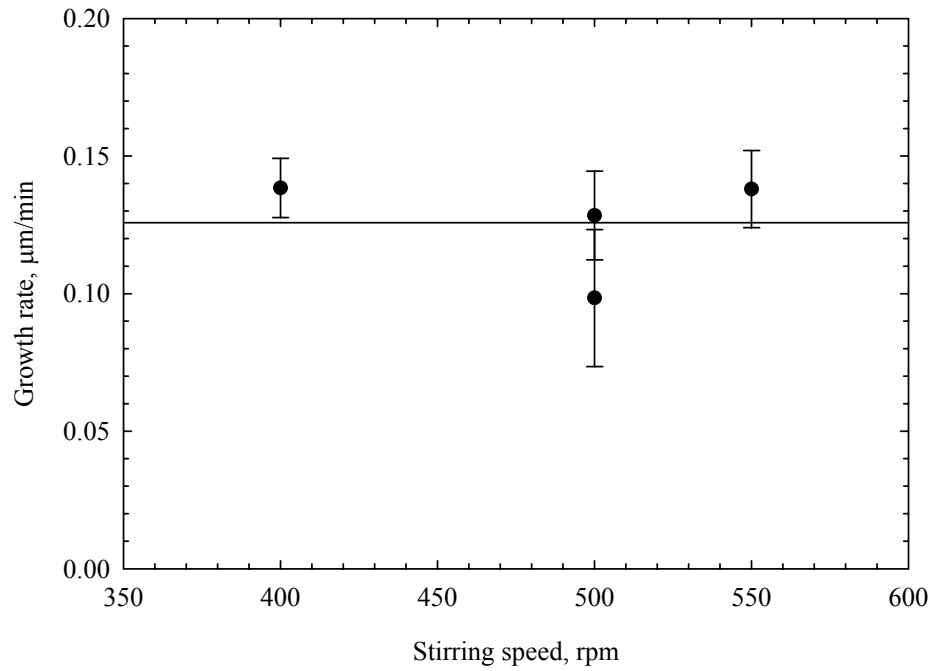
Figure 5.10 Volume growth rates as a function of stirring speed.

5.4.2   Crystallization Kinetics

If the volume distribution (or mass distribution) is log-normal, the number distribution is also log-normal with the same geometric standard deviation (Allen, 1997). The number mean size may then be calculated from the relationship:

$$\ln x_{NL} = \ln x_{gV} - 2.5 \ln^2 \sigma_g \tag{5.3}$$

where x_{NL} is the mean particle size, x_{gV} is the median of the volume distribution, and σ_g is the geometric standard deviation of the volume distribution. These results were confirmed by discretizing the volume density distribution into small elements (of 1 μm width) and calculating the number of particles in each element, and from that, the number mean particle size. The geometric standard deviation of the volume distribution was essentially constant over the time period of the experiment,

confirming there was growth rate dispersion and that the seeds were CH seed. The growth kinetics were determined based on the number mean particle size.

Due to the constant solution concentration during the crystallization process, the mean growth rate was calculated directly from the slope of the plot between the number mean crystal size and time. The growth rate of α-glucose monohydrate from aqueous solution was found to be unusually high in the first period of the experiments (i.e. the first hour) and then followed an expected linear relationship, as illustrated in Figure 5.11. An unusual accelerated rate of crystal growth at the initial stage of batch crystallization may be due to repair of the crystal surface (Addai-Mensah, 1992), poisoning from unidentified impurities (Flood, Johns, and White, 2000), or a roughening transition (Pantaraks and Flood, 2005). The growth rates shown here were calculated based on the linear rates evident after the first hour of growth.

Duplicated crystallizations were performed simultaneously for almost all experiments. The results at 40°C (Figure 5.11) showed that at the same conditions, the number sizes were essentially the same for all four measurements (two batches with two measurements each), and the same mean crystal growth rates were obtained. Thus, the reproducibility was good and within the estimated measures of uncertainty. The experimental data are presented in Appendix C.
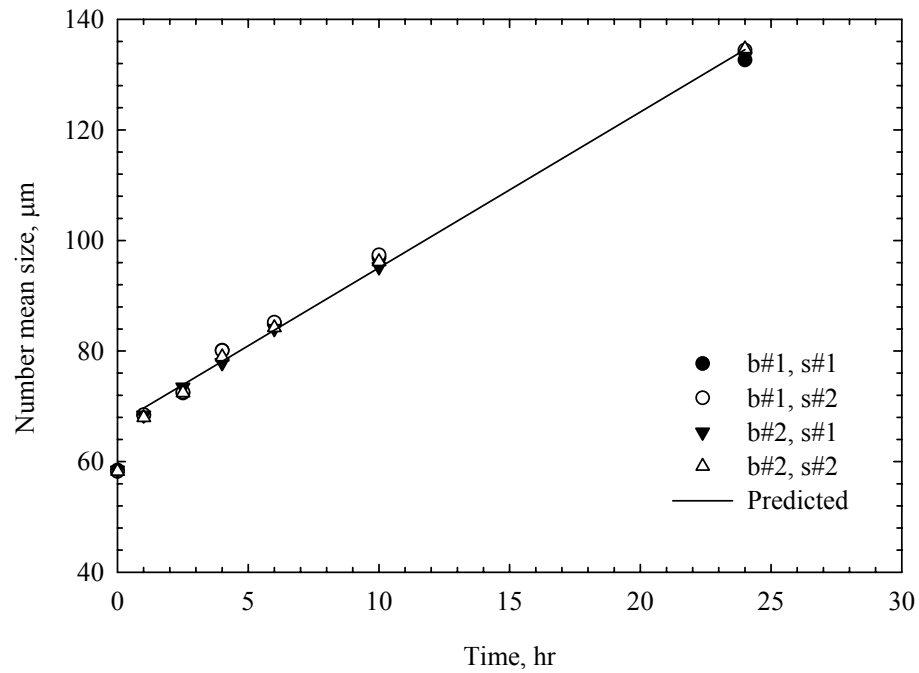
Figure 5.11 Number mean sizes of α-glucose monohydrate as a function of time at 40°C, operating concentration of 65.81 ± 0.25%. b#1, b#2, s#1, and s#2 are batch 1, batch 2, sample 1, and sample 2, respectively.

The plot between the mean crystal growth rates and relative supersaturation (Figure 5.12) for the three temperatures gives the growth rate constants for the experimental temperatures. The relative supersaturation is defined as Equation 2.4, and the growth rate (G) is defined as the product of the growth rate constant (k_g) and n order of relative supersaturation following equation:

$$G = k_g \sigma^n \tag{5.4}$$

It is clear that a growth rate order (n) of 1 fits the data acceptably. The growth rate constant increases significantly with increasing temperature. The growth rate constant was modeled by an Arrhenius relationship (Figure 5.13), as the

relationship $\ln k_g = 19.2 - 6010/T$, indicating an activation energy of 50 ± 2 kJ/mol.

This value is typical for the crystallization of simple sugars. Previous research on

crystal growth of sucrose (Liang, Hartel, and Berglund, 1989) for example, gives

activation energy of growth rate as 28.9 to 33.1 kJ/mol for growth from pure

solutions, and 45.6 to 57.7 kJ/mol for growth from solutions having raffinose as an

impurity.
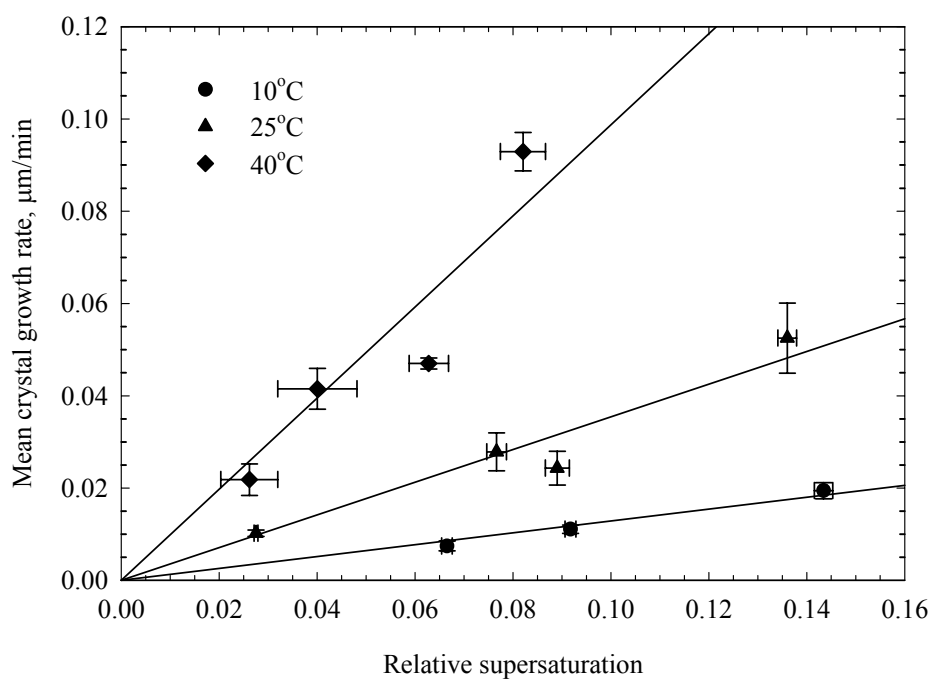
Figure 5.12 Mean size crystal growth rates for α-glucose monohydrate as a function

of relative supersaturation.
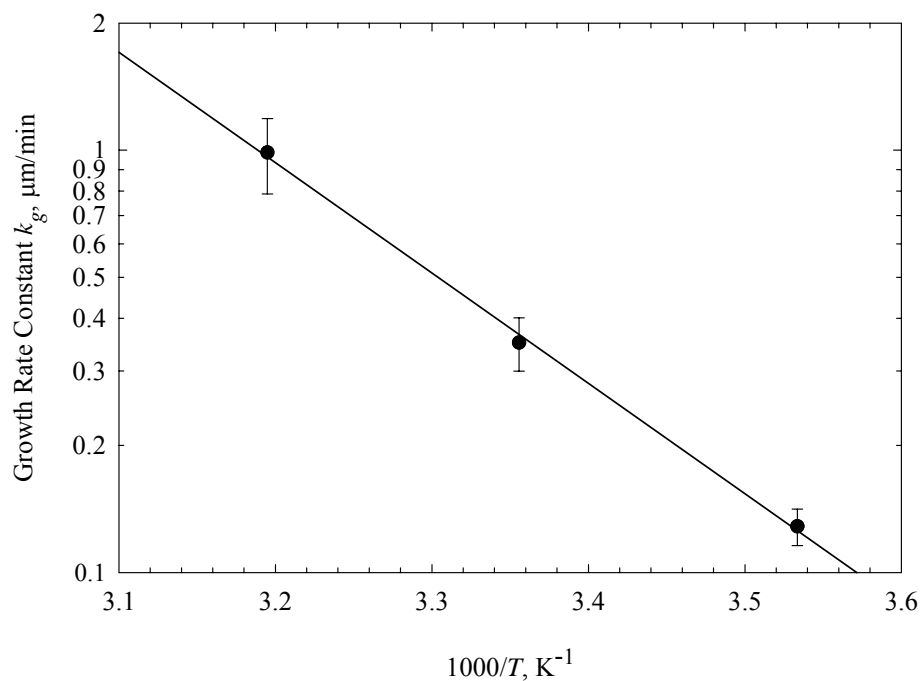
Figure 5.13 An Arrhenius plot of the growth rate constants.

5.4.3 Comparisons of Crystal Growth Rates

The crystal growth rates of other sugars (from literature data) are presented in Figure 5.14. The data are taken from various research groups as follows: glucose monohydrate (this work), glucose anhydrous grown at 41, 46, and 50°C (Elankovan and Berglund, 1987); glucose anhydrous at 60, 70, and 75°C (Kraus and Nývlt, 1994); fructose (Shiau and Berglund, 1987); and xylose (Gabas and Laguerie, 1991) with the rearranged growth equation by Addai-Mensah (1992).
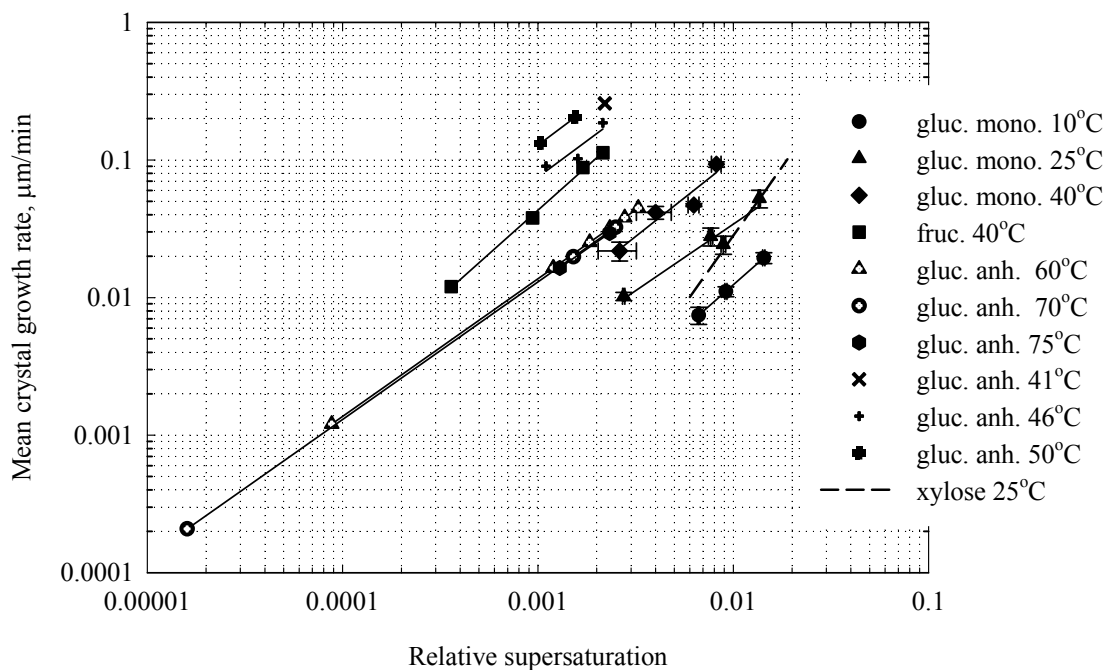
Figure 5.14 Crystal growth rates of sugars in aqueous solutions.

5.4.4   Crystal Growth Rate Dispersion

Crystal growth rate dispersion (GRD) in the batch crystallizations was measured based on the time dependent number based PSDs. Figure 5.6 shows that on a log size scale, the shape of the PSD was unchanged as the crystals grew and so the seed was CH seed. The growth rates shown in Figures 5.11, 5.12, and 5.13 are for the number mean size crystal. The growth rates for other sizes are this value multiplied by the ratio of the size of the crystal to the mean crystal size. The range of growth rates for this sieved seed can be expressed by the CV (= standard deviation / mean growth rate) of the growth rate distribution which for CH seed is identical to the CV of the PSD. These can be on a number basis, as was used in the current study, or on a weight (volume) basis. The standard deviation of the number based PSD was

calculated by discretizing the volume based PSDs in 1 μm intervals and converting the results to a number basis. The geometric standard deviations of the volume based PSDs (on a log size scale) were constant throughout the experiments (Figure 5.15), but this transforms into significant increases in the standard deviations of the number based PSDs on a linear size scale, as the experiments progressed, where for CH seed, the standard deviation should be proportional to the mean size and the slope gives the associated CV. An example of a plot to determine the crystal growth rate dispersion is shown in Figure 5.15 for an experiment at 40ºC and relative supersaturation equal to 0.082. There was very good reproducibility between duplicate samples in individual experiments, and between duplicate experiments. Table 5.1 gives values of the crystal growth rate dispersion CV on a number basis for all conditions studied.
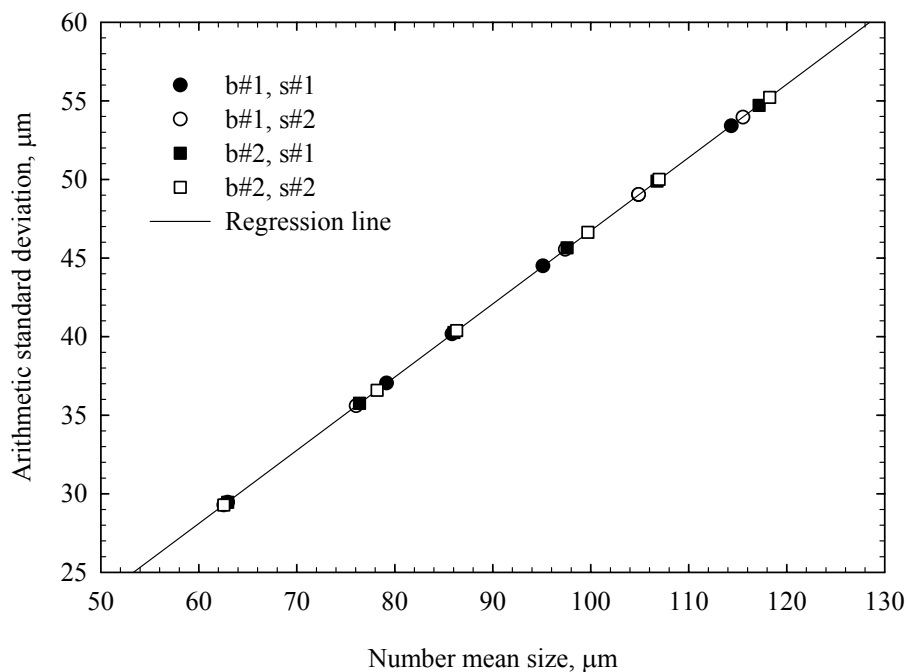
Figure 5.15 Plot of the arithmetic standard deviation of the number distribution against number mean size for the experiment at 40ºC and relative supersaturation equal to 0.082. b#1, b#2, s#1, and s#2 are batch 1, batch 2, sample 1, and sample 2, respectively.

Table 5.1 Crystal growth rate dispersion number based CVs for glucose monohydrate crystallized from aqueous solutions, all runs.

Temperature [°C]	Relative supersaturation [-]	CV (Batch 1) [-]	CV (Batch 2) [-]
10	0.067	0.50	0.50
	0.092	0.48	0.48
	0.143	0.46	0.46

Table 5.1 (Continued)

Temperature [°C]	Relative supersaturation [-]	CV (Batch 1) [-]	CV (Batch 2) [-]
25	0.027	0.56	0.56
	0.077	0.61	*a*
	0.089	0.62	*a*
	0.136	0.60	0.60
40	0.026	0.44	0.44
	0.040	0.44	0.44
	0.063	0.52	0.52
	0.082	0.47	0.47

a Only one batch was performed for these conditions.

The crystal growth rate dispersion CV is difficult to determine with very high accuracy due to the variability in the measured volume based PSDs. In the raw volume based PSD data there are small random changes in the geometric standard deviations through the experiment, but we have smoothed the data by assuming a constant geometric standard deviation, which is justified by the scaled volume based PSD plots, of which Figure 5.6 is an example. It is believed that the 95% confidence interval uncertainty on CV for a particular experiment is of the order of 0.10. Assuming that the CV measured come from identical distributions with the use of the same seed, it is possible to calculate the CV as 0.47 ± 0.06, for the results at 10 and 40°C (which used seed crystals from a single preparation), and 0.59 ± 0.05 for the seeds at 25°C, which had a wider PSD. These results can be used to determine

95% ranges of growth rates (G97.5%/G2.5%), for the two seeds. The seeds used in the 10 and 40ºC experiments had a 95% range of growth rates of 5.8 ± 1.0 times, and those used in the 25ºC experiment had a 95% range of growth rates of 8.5 ± 1.2 times. The bulk crystals, from which the CHS were prepared, had a number mean size of 91.33 μm and a number based standard deviation of 44.93 μm, resulting in a CV of 0.49. Thus, it can be concluded that the CV of the growth rate distributions predicted in the current study would be very similar to the CV of the growth rate distribution of the bulk particles from which the seeds were fractionated. Note that although the sieved fraction and the bulk material had similar CVs, the bulk had a mean size almost twice that of the sieved seed, so the mean growth rate would have been larger by the same ratio. That the CVs of bulk and fraction are similar is not implicit in the seed preparation method, but results from the coincidence that when the seed was prepared the reduction in the mean crystal size was by the same factor as the reduction in the standard deviation of the PSD: this resulted in an approximately constant value of the CV, and hence a similar 95% range of the growth rate distribution.

5.5 Conclusion

The crystallization of α-glucose monohydrate from aqueous solution should be operated within the SNT region if nucleation is to be avoided. The crystal growth rate order is 1, and the growth rate is temperature dependent with the activation energy of 50 ± 2 kJ/mol. Growth rate dispersion was observed. For the sieved seeds used, the 95% range of growth rates (G$_{97.5\%}$/G$_{2.5\%}$) was 5.8 ± 1.0 for crystallizations using the seeds prepared for the 10 and 40°C experiments, and 8.5 ± 1.2 for the seeds

prepared for the 25°C experiments, which had a slightly wider initial PSD. This is evidence that growth rate dispersion is significant for the system. The seeds were prepared from a sieve fraction from commercial α-glucose monohydrate, which had a similar CV value to that of the seeds, suggesting that the 95% range of growth rates for the commercial crystals is also nearly an order of magnitude. Mean crystal growth rates for the bulk crystals the seeds were prepared from will be approximately two times the rates measured in this work, because the mean size of the bulk crystals was approximately two times the mean size of the seeds. Based on the crystallization kinetics from the current work, and kinetics and equilibrium for the mutarotation reaction, it is probable that the mutarotation reaction kinetics will be significant for the industrial crystallization of glucose monohydrate when high seeding rates are employed.

5.6 References

Addai-Mensah, J. (1992). **Crystallization of D-Fructose from Aqueous Ethanolic Solutions.** Ph.D. Thesis, The University of Queensland, Brisbane, QLD, Australia.

Allen, T. (1997). **Particle Size Measurement: Volume 1 Powder Sampling and Particle Size Measurement** (5th ed.). the Dordrecht: Kluwer Academic.

Beckmann, W., Boje, G., Rössling, G. and Arlt, W. (1996). Crystallization of Galactose from Aqueous Solutions: Influence of the α- and β-Anomers. In B. Biscans, and J. Garside (eds.). **Proceeding of 13th Symp. on Industrial Crystallization** (pp 497-502). LGC-CNRS: Toulouse, France.

Boje, G., Beckmann, W., Arlt, W., and Rössling, G. (1997). A Model for the Batch Cooling Crystallization of α- and β-**D**-Pyrano-Galactoses from Aqueous Solutions. In J. Ulrich (ed.). **Proceeding of Fourth Int. Workshop on Crystal Growth of Organic Materials** (pp 342-349). Shaker Verlag: Aachen, Germany.

Butler, B. (1998). **Modelling Industrial Lactose Crystallization**. Ph.D. Thesis, The University of Queensland, Brisbane, QLD, Australia.

Elankovan, P. and Berglund, K. A. (1987). Contact Nucleation from Aqueous Dextrose Solutions. **AIChE. J.** 33(11): 1844-1849.

Flood, A. E., Johns, M. R., and White, E. T. (2000). Crystal Growth Rates and Dispersion for **D**-Fructose from Aqueous Ethanol. **AIChE J.** 46(2): 239-246.

Flood, A. E., Johns, M. R., and White, E. T. (1996). Mutarotation of **D**-fructose in aqueous-ethanolic solutions and its influence on crystallization. **Carbohydr. Res.** 288: 45-56.

Flood, A. E., Johns, M. R., and White, E. T. (2000). Crystal Growth Rates and Dispersion for **D**-Fructose from Aqueous Ethanol. **AIChE. J.** 46(2): 239-246.

Gabas, N. and Laguerie, C. (1991). Dispersion of Growth Rates of **D**-Xylose Crystals in Aqueous Solutions – Influence of the Presence of Ethanol as a Co-Solvent and of **D**-Mannose as a Co-Solute. **Chem. Eng. Sci.** 46(5/6): 1411-1418.

Goldberg, R. N. and Tewari, Y. B. (1989). Thermodynamic and Transport Properties of Carbohydrates and Their Monophosphates: The Pentoses and Hexoses. **J. Phys. Chem. Ref. Data**. 18(2): 809-880.

Jones, C. M. and Larson, M. A. (1999). Characterizing Growth-Rate Dispersion of NaNO$_3$ Secondary Nuclei. **AIChE. J.** 45(10): 2128-2135.

Kraus, J. and Nývlt, J. (1994). Crystallization of anhydrous glucose I. Mutarotation rate and solid-liquid phase equilibria. **Zuckerind**. 119(1): 24-29.

Kraus, J. and Nývlt, J. (1994). Crystallization of anhydrous glucose III. Shape factors and growth rates of crystals. **Zuckerind**. 119(4): 298-303.

Liang, B., Hartel, R. W., and Berglund, K. A. (1987). Growth Rate Dispersion in Seeded Batch Sucrose Crystallization. **AIChE J.** 33(12): 2077-2079.

Liang, B., Hartel, R. W., and Berglund, K. A. (1989). Effects of Raffinose on Sucrose Crystal Growth Kinetics and Rate Dispersion. **AIChE J.** 35(12): 2053-2057.

Lloyd, N. E. and Nelson, W. J. (1984). **Glucose- and Fructose-Containing Sweeteners from Starch: Chemistry and Technology** (2nd ed., pp. 611-660). San Diego: Academic Press.

Mueller, H. (1970). Isothermal crystallization of dextrose. U. S. Patent 3,547,696,

Mulvihill, P. J. (1992). Crystalline and Liquid Dextrose Products: Production, Properties, and Applications. In F. W., Schenck and R. E., Hebeda (eds.). **Starch Hydrolysis Products: worldwide technology production and applications** (pp. 121-176). New York: VCH.

Myerson, A. S. and Ginde, R. (2002). Crystals, Crystal Growth, and Nucleation. In A. S., Myerson (ed.). **Handbook of Industrial Crystallization** (2nd ed., pp.121-176). Boston: Butterworth-Heinemann.

Pantaraks, P. and Flood, A. E. (2005). Effect of Growth Rate History on Current Crystal Growth: A Second Look at Surface Effects on Crystal Growth Rates. **Crystal Growth & Design.** 5: 365-371.

Peres, A. M. and Macedo, E. A. (1997). Solid-Liquid Equilibrium of Sugars in Mixed Solvents. **Entropie.** 202/203: 71-75.

Randolph, A. D. and White, E. T. (1977). Modeling Size Dispersion in the Prediction of Crystal-Size Distribution. **Chem. Eng. Sci**. 32: 1067-1076.

Schenck, F. W. (1989). Glucose and Glucose-Containing Syrups. In **Ullmann's Encyclopedia of Industrial Chemistry** Vol. A 12 (pp 457-476). Weinheim: VCH.

Shanks, B. H. and Berglund, K. A. (1985). Contact Nucleation from Aqueous Sucrose Solutions. AIChE. J. 31(1): 152-154.

Shi, Y., Liang, B., and Hartel, R. W. (1990). Crystallization Kinetics of Alpha-Lactose Monohydrate in a Continuous Cooling Crystallizer. **J. Food Sci.** 55(3): 817-820.

Shiau, L. D. and Berglund, K. A. (1987). Growth Kinetics of Fructose Crystals Formed by Contact Nucleation. **AIChE. J.** 33(6): 1028-1032.

Srisa-nga, S. and Flood, A. E. (2004). Mutarotation Rates and Equilibrium of Simple Carbohydrates [CD]. In **Proceeding of the APCChE 2004** (paper no. 3C-10). Kitakyushu, Japan.

Young, F. E. (1957). D-Glucose-Water Phase Diagram. **J. Phys. Chem.** 61(5): 616-619,

CHAPTER VI

Modeling of the Effect of the Mutarotation Reaction on the Aqueous Crystallization of Glucose Monohydrate

6.1 Abstract

There are currently no models for industrial aqueous crystallization of glucose monohydrate, particularly where the mutarotation reaction is considered. This study aims to generate this model and specify the conditions where the mutarotation kinetics play an important role in the system. The model was generated based on the mutarotation and crystal growth parameters already measured in this study (Chapters III and V). Five ordinary differential equations were written to describe the system and then solved using the ODE45 routine in MATLAB together with the necessary initial conditions. The results show the mass deposition of glucose onto the crystal surface (which is implied from the crystal mass obtained) is faster in cases using small seed sizes, higher seeding rates, and higher temperatures. The depletion of α-glucose is rapid in cases using small seed size, high seeding rate, and low temperature. In summary, the conditions where the mutarotation may be the rate limiting step, or partially rate limiting, can be easily determined via the model.

Unfortunately, because of the small supersaturation values possible in this system (which are determined from the value of the long term secondary nucleation threshold) the reduction in the fraction of α-glucose monohydrate which results in

almost complete cessation of crystal growth is only approximately two percent from the equilibrium alpha fraction. A change in the anomer composition this small is not accurately measurable by ^{13}C-NMR, which makes the model predictions of the anomer compositions impossible to verify experimentally.

6.2 Introduction

6.2.1 General

Glucose is a commodity chemical that is used in a wide variety of food and pharmaceutical applications, as well as being a common feedstock for the chemical industry to produce citric acid, gluconic acid, and other commodity and specialty chemicals. The product is produced in large quantities both as aqueous solutions, and as anhydrous or monohydrate crystal forms.

Industrial crystallizations of glucose are usually carried out in batch crystallizers due to difficulty of crystal size control in continuous crystallization of the sugar. Typical patented processes can be found in the records of the patent office (Edwards, 1982; Mueller, 1970; Newkirk, 1925). Despite the importance of the processes to industrially crystallize glucose monohydrate and anhydrous glucose, there is still a limited amount of data on important kinetic data required to properly design the crystallization equipment.

6.2.2 Objectives of the Study

In the current study a model of the batch crystallization of glucose monohydrate in its range of crystallization (approximately –5 to 55°C) has been developed using the previously acquired data. The model predicts the crystal growth rates, crystal deposition rates, compositions of both α-glucose and β-glucose, and

other key operating parameters. This model will be used to specify whether mutarotation is the rate limiting step for the industrial crystallization of this sugar.

6.3 Materials and Methods

Experiments performed to collect data on the kinetic parameters used in the model have been described previously (Srisa-nga and Flood, 2004; Srisa-nga, Flood, and White, 2005) and shown in Chapter III and V, for mutarotation data and crystal growth kinetics, respectively. The secondary nucleation threshold (described in Chapter IV) and composition dependence of the crystal growth rates (under surface integration controlling conditions) were measured at 10, 25, and 40ºC to obtain models of the temperature and composition dependence of these variables in pure aqueous solutions over the approximate range of temperatures of α-glucose monohydrate crystallization. The temperature and composition dependence of the mutarotation kinetics and equilibria were measured in aqueous solutions in the same range of temperatures to model the temperature and composition dependence of these variables. There is also a reported effect of pH on the mutarotation rates (Nelson and Beegle, 1919), but this is not significant in the narrow range of pH used for the industrial crystallizations.

The solubility of the different crystal forms of glucose (α-glucose monohydrate, anhydrous α-glucose, and anhydrous β-glucose) in water are already well known (Young, 1957) and re-plotted in Figure 4.1 and also in Figure 4.10 where the metastable zone for secondary nucleation region is specified. The solubility (C^*, kg glucose/ 100 g solutions) in terms of the crystallization temperature T (in ºC) has been modeled by fitting a quadratic equation through the data of Young, giving

$$C^* = 0.01\ (33.82 + 0.6484\ T + 0.00135\ T^2) \tag{6.1}$$

The mutarotation reaction is modeled as a first order reversible reaction of α-to β-glucopyranose (a simplification which is well justified by the experimental results). The simplified kinetics are represented by Figure 5.1 (a), where the crystallization is not considered, with the forward reaction (from α-glucose to β-glucose) having a rate constant of k_1 (s^{-1}) and the backward reaction having a rate constant of k_2 (s^{-1}). The overall rate of reaction k (which is the apparent rate as fitted in a first order decay curve) is

$$k = k_1 + k_2 \tag{6.2}$$

The equilibrium constant (K) is represented by Equation 6.3 where x_β^* and x_α^* represents the equilibrium fractions of β- and α-glucose, respectively.

$$K = \frac{x_\beta^*}{x_\alpha^*} = \frac{k_1}{k_2} \tag{6.3}$$

The overall rate constant is modeled through the Arrhenius relationship, and there is no significant concentration dependence in the range of compositions we are modeling (as would be predicted for a true first order reaction), thus

$$\log k = 10.8 - \frac{4210}{T + 273.15} \tag{6.4}$$

The equilibrium constant may be assumed to be independent of both temperature and glucose composition, and have a value of 1.50. The previous relationships can be used to determine forward and reverse reaction rate constants

$$k_1 = \frac{kK}{1 + K} \text{ and } k_2 = k - k_1 \tag{6.5}$$

The last kinetic rate needed for the model is for the crystal growth kinetics. A large series of crystallization experiments has shown that the surface integration crystal growth kinetics is first order with respect to relative supersaturation defined in terms of weight fractions.

$$G = k_g \sigma \ \text{ with } \sigma = \frac{C_\alpha - C_\alpha^*}{C_\alpha^*} \text{ and } C_\alpha^* = \frac{C^*}{K+1} \tag{6.6}$$

Here, σ is the relative supersaturation, C_α and C_α^* are the concentrations of α-glucose at any time t and at equilibrium, respectively. There is no previously reported salting in or salting out of α-glucose monohydrate by β-glucose, so Equation 6.6 can be used as the equilibrium concentration. The crystal growth constant k_g depends only on the temperature, since we are considering surface integration controlled kinetics in pure solutions, and it can be adequately modeled using an Arrhenius relationship

$$\log k_g = 8.33 - \frac{2610}{(T + 273.15)} \tag{6.7}$$

Sugars are typically crystallized in seeded batch crystallizers operated within the secondary nucleation threshold to minimize the formation of false grain; hence the model assumes no nucleation occurs in the crystallizer. Figure 4.10 which is the glucose-water phase diagram also shows the valid region for this model (which is the region over the solubility line and under the metastable limit for secondary nucleation). In order to further simplify the modeling of the system, the seeds are treated as monosize seeds, and it is assumed that there is negligible growth rate dispersion. Crystal size is assumed to be the spherical average crystal diameter. These assumptions simplify the problem by allowing the crystal size distribution to be monodisperse, thus reducing the complexity of the population balance.

The differential equations used to describe a batch crystallization of α-glucose monohydrate, with a basis of 1 kg of solution, are:

1. The equation to describe the change in crystal size due to crystal growth

$$\frac{dL}{dt} = k_g \frac{C_\alpha - C_\alpha^*}{C_\alpha^*} = k_g \frac{x_\alpha C - x_\alpha^* C^*}{x_\alpha^* C^*}$$

(6.8)

This equation is derived from the crystal growth rate equation (Equation 6.6) with substitution of relative supersaturation based on the crystallizing anomer (α-glucose). The variable x_α is the fraction of glucose that is in the α-form, and can vary during the crystallization if the crystal deposition rate is higher than the rate of replacement through mutarotation. The variable C represents the total concentration of both forms of glucose. The term $x_\alpha^* C^*$ is constant over time. In the case of operation under a constant driving force, where the crystallization rate controls the overall rate in the system, $x_\alpha = x_\alpha^*$, and Equation 6.8 is equivalent to Equation 5.4, where the relative supersaturation is based on the total glucose concentration and a growth rate order is 1 confirmed by the experimental results.

2. The rate of change in crystal mass in the suspension (the mass of glucose deposited onto the crystal surface per time interval) is derived with the assumption that the crystal is spherical with a characteristic size L.

Mass of a sphere: $m_c = \rho_c \frac{\pi L^3}{6}$

(6.9)

The volume of a sphere is used because the sizing equipment used, the Malvern Mastersizer, represents size using the spherical average diameter. Spherical volume multiplied by glucose monohydrate crystal density, ρ_c (1,560 kg/m^3; Goldberg and Tewari, 1989), results in the mass of glucose monohydrate crystal, m_c. Differentiating

Equation 6.9 with respect to change in size L to $L + dL$ and from time t to $t + dt$ gives the change in total mass of N crystals due to the deposition of glucose as shown in Equation 6.10.

$$\frac{dm_c}{dt} = \frac{1}{2}\rho_c N\pi L^2 \frac{dL}{dt}$$
(6.10)

3. The rate of change in solution mass, m_s (Equation 6.11) is equal to the rate of mass lost by the deposition of crystalline material, which follows the mass conservation rule. The minus sign shows the mass change occurs in opposite directions, i.e. mass leaving the solution is equal to the mass deposition onto the crystal surface, but in the opposite direction.

$$\frac{dm_s}{dt} = -\frac{dm_c}{dt}$$
(6.11)

4. Because the crystal form is glucose monohydrate, the crystal contains just over 9% water in the lattice. Glucose monohydrate has the molecular weight of 198, whereas glucose anhydrous has a molecular weight of 180, so the portion of glucose in the glucose monohydrate crystal is equal to 180/198. Thus, the rate of change in the mass of glucose in solution, m_{gluc}, is equal to the rate of mass deposition onto the crystal surface corrected by the fraction of the crystal which is water, as Equation 6.12.

$$\frac{dm_{gluc}}{dt} = -\frac{180}{198}\frac{dm_c}{dt}$$
(6.12)

5. Considering Figure 5.1 (a), where the crystallizing species is considered to be only glucose monohydrate in the valid temperature range, and without any phase transformation, there are two reactions occurring simultaneously. These are the reversible mutarotation reaction and an irreversible crystallization process that

compete against each other in the system. Thus, the rate of change of the fraction of glucose in the α-form in solution is given by the difference between the rates away from this form (due to the forward mutarotation reaction and the crystallization) and the rates towards the form due to the backward mutarotation reaction from β-glucose to α-form.

$$\frac{dx_\alpha}{dt} = \frac{k_1}{K}(1 - x_\alpha) - k_1 x_\alpha + \frac{1}{C}\frac{dm_{gluc}}{dt} \tag{6.13}$$

The solution of the previous five differential equations requires the temperature of the batch to be known, as well as the following initial conditions

1. *L(t=0)*, which is determined by measurement of the sieved seed crystals. The number of seed crystals, which is also required by the model, is determined from the initial size and the mass of seed crystals added.

2. $m_c(t=0)$, the mass of seed added to the batch.

3. $m_s(t=0)$, the mass of solution in the batch before initiation of crystallization.

4. $m_{gluc}(t=0)$, the mass of glucose in the solution before initiation of crystallization, which may be calculated from the initial concentration.

5. $x_\alpha(t=0)$, the initial fraction of α-glucose in the crystallizer. Usually this is determined from the equilibrium constant, as industrial crystallizations will be initiated on equilibrium solutions. In research crystallizers, this fraction is determined by whether the α-form or the β-form was initially dissolved to create the solution, and the temperature-time profile of the cooling before the addition of seed crystals.

Other parameters necessary for modeling the crystallization, in particular the concentrations of particular species, can be determined using the variables found via solution of the equations above. The mathematical files are presented in Appendix D.

6.4 Results and Discussion

The model was used to simulate the crystallization of α-glucose monohydrate in a batch crystallizer for a range of different conditions, concentrating on the effect of variation in the size of seed crystals, the amount of seed crystals added, and the crystallization temperature. These three variables are the key to determining whether the rate of mutarotation reaction will be sufficiently low as to have crystallization inhibited by low levels of replacement of α-glucose. It is not reasonable to vary the initial α-fraction and observe the change in the other parameters since in industry the operation always starts with a solution at the mutarotational equilibrium. Initial glucose concentrations were set at 10% relative supersaturation, as this is a relatively high supersaturation for this system, but is within the short-term secondary nucleation threshold for all temperatures in the system.

6.4.1   The Effect of Seed Crystal Size

The effect of seed crystal size on the crystal growth of α-glucose monohydrate in a batch using 200 g seed/kg initial mother liquor, batch temperature equal to 10°C, and 10% initial relative supersaturation, is shown in Figure 6.1. The two parameters plotted are the mass of crystals in the vessel (showing the rate of crystal deposition) and the fraction of glucose that is in the α-form, as functions of

batch time, which is an indication of whether the rate of crystal mass deposition is faster than the rate of replacement by mutarotation.
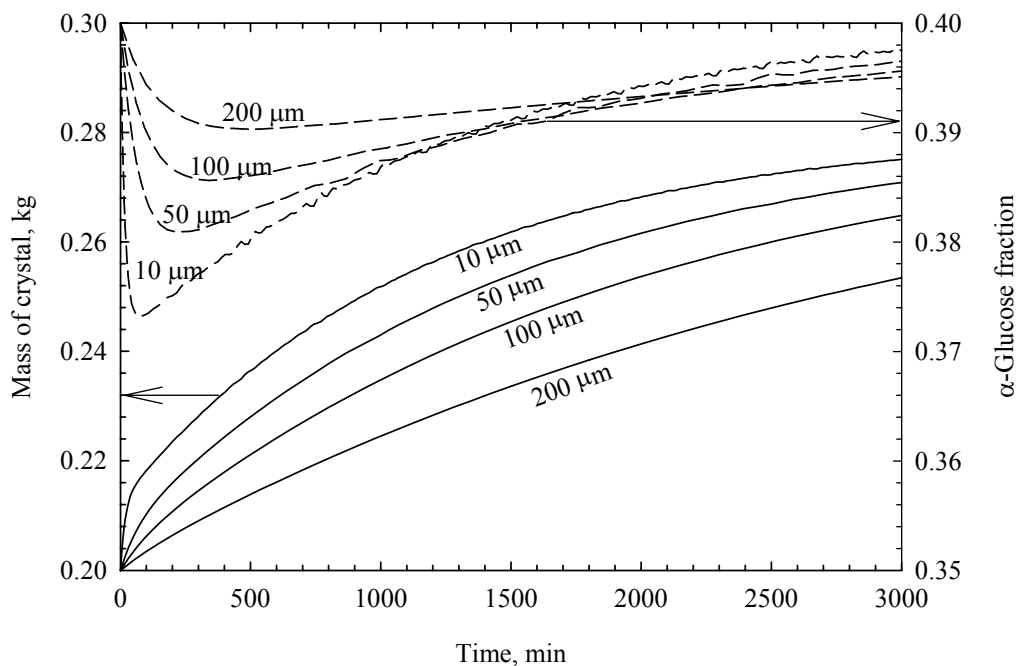
Figure 6.1 The effect of seed size on the change in crystal mass in the mother liquor and fraction of glucose in the α-form for batch aqueous crystallization of α-glucose monohydrate. Simulated conditions are, $T = 10°C$, initial relative supersaturation = 10%, and seeding rate = 200 g seed/kg of mother liquor.

The initial rate of crystal mass deposition is significantly higher for smaller seed crystals, based on the same mass of seed. The crystal deposition rate depends on the driving force (i.e. the supersaturation) and the surface area of the crystals in the liquor; the surface area of the small crystals is larger than the surface

area of larger crystals (for the same mass). The higher rate of mass deposition causes a significant decrease in the proportion of α-glucose in the crystallizer when 10 μm seeds are added. The change in the α-glucose fraction appears small, changing from the equilibrium value of around 0.4 down to a minimum of around 0.373 (at about 75 minutes), but this change is very significant with respect to the relative supersaturation, and therefore the crystal growth rate. The glucose concentration at this point is 0.4370 kg glucose/kg solution, with equilibrium of 0.4044 kg glucose/kg solution. The relative supersaturation of α-glucose at this point is 0.00803, while if the relative supersaturation is calculated on a total glucose basis it is 0.0806: the relative supersaturation in the crystallizer is effectively only 10% of what would be expected because of the removal of α-glucose without adequate replenishment from the β-form.

The difference between the true supersaturation (in terms of the α-glucose concentration) and the apparent supersaturation (measured in terms of total glucose in the crystallizer) is illustrated in Figure 6.2. Even for the simulation with a very small seed size, the total glucose concentration smoothly decreases towards the apparent glucose solubility, not approaching the solubility very closely even after 3000 minutes. The true supersaturation, that of α-glucose, decreases very rapidly however, and there is almost zero driving force for crystal growth very quickly during the batch using the 10 μm seed. After 100 minutes the crystallization is essentially entirely controlled by the mutarotation reaction giving up α-glucose for crystallization.
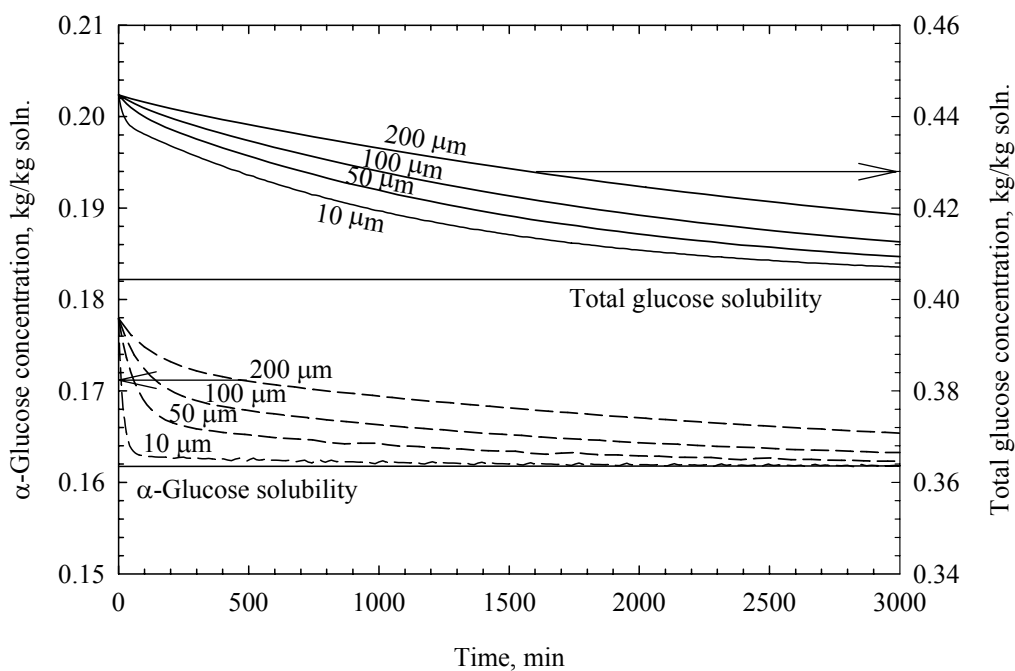
Figure 6.2 Plots of the concentrations of α-glucose and total glucose in the crystallization with reference to the solubility of the species during batch crystallization. Simulated conditions are, $T = 10°C$, initial relative supersaturation = 10%, and seeding rate = 200 g seed/kg of mother liquor.

6.4.2 The Effect of Seeding Rate

The effect of seeding rate (the amount of seed crystals added to the system) on the crystallization of α-glucose monohydrate is shown in Figure 6.3, where the crystallizer temperature is 10°C, the seed size is 100 μm, and the initial relative supersaturation is 10%. The seeding rates are varied from approximately 5 to 20% of fresh mother liquor which is the industrially used range (Mueller, 1970; Newkirk, 1925). This graph indicates the mutarotation reaction will be more

significant at higher seeding rates, which cause a more rapid depletion in the α-glucose anomer. A larger seed amount (with the same seed size) gives a larger surface area and therefore a higher mass transfer rate at a given value of the mass transfer flux, and this causes a faster crystal mass deposition rate. In this case, again, the conversion of the β-glucose anomer in the solution phase is not quick enough to replace the α-glucose anomer lost from the solution phase due to the crystallization process. This also causes a drop in the crystallization driving force in terms of the crystallizing species.

Normally in α-glucose monohydrate manufacturing, part of the crystalline suspension of the previous batch is left for the coming batch in order to induce the crystallization process. This seeding suspension is sometimes called "foots" (Newkirk, 1925) and the particles inside the solution act as seed for the coming batch. Preferred amount of foots (which is about 10 to 40% of solid) will be approximately 40% of the new batch, and this is used to calculate that the batch requires 4 to 16% seed. This value is close to that given by another patent (Mueller, 1970), which suggests 3 to 15% seed for the crystallization of this sugar.
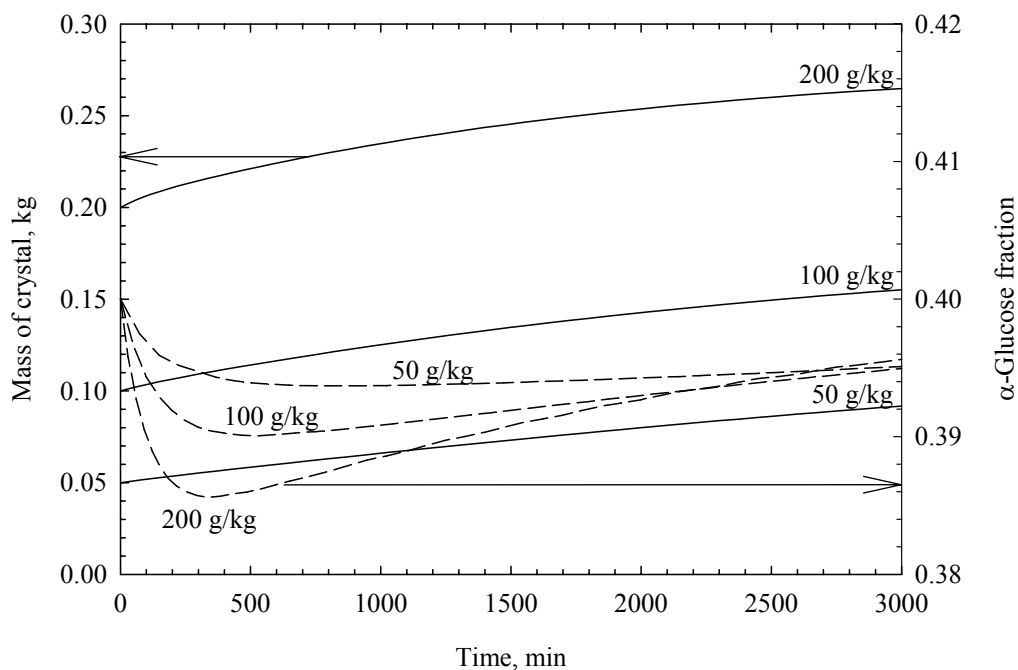
Figure 6.3 The effect of seed mass on the change in crystal mass in the mother liquor and fraction of glucose in the α-form for batch crystallization of α-glucose monohydrate. Simulated conditions are, $T = 10°C$, seed size = 100 μm, and initial relative supersaturation = 10%.

6.4.3   The Effect of Temperature

The effect of batch temperature on the crystallization of α-glucose monohydrate is shown in Figure 6.4 where the seeding rate is fixed at 200 g seed/kg solution, the seed size is 100 μm, and the initial relative supersaturation is 10%. The graph shows that at higher temperature, the crystal mass deposition is initially higher, which is due to the surface integration kinetics that will be higher at higher temperature (Myerson and Ginde, 2002). The other result observed from this graph is that the mass of crystal formed at higher temperatures is always higher than that at

lower temperatures at the same time, including at the equilibrium, even when the same amount of seed crystal is used. This is because there is higher solubility at higher temperature; therefore 10% relative supersaturation at 40°C represents a much higher amount of glucose able to be crystallized from solution than that at 25 and 10°C. From the calculation, at 10% relative supersaturation, there are approximately 0.04, 0.05, and 0.06 kg of glucose per kg of solution in excess of the equilibrium at 10, 25, and 40°C, respectively.

The change in α-fraction is more rapid and more pronounced at lower temperature, with a maximum depletion from the equilibrium value of 0.4 down to 0.384 at 10°C. At the conditions plotted in Figure 6.4 and at 40°C, the fraction of α-glucose is almost unchanged. The temperature changes both the crystallization kinetics and the mutarotation kinetics, but the mutarotation kinetics has a significantly higher value of the activation energy (the activation energy is 50 kJ/mol for crystallization kinetics and 80 kJ/mol for the mutarotation kinetics), and so the mutarotation rate increases far more than the crystallization rate as the temperature increases, thus making the system less mutarotation rate controlled.
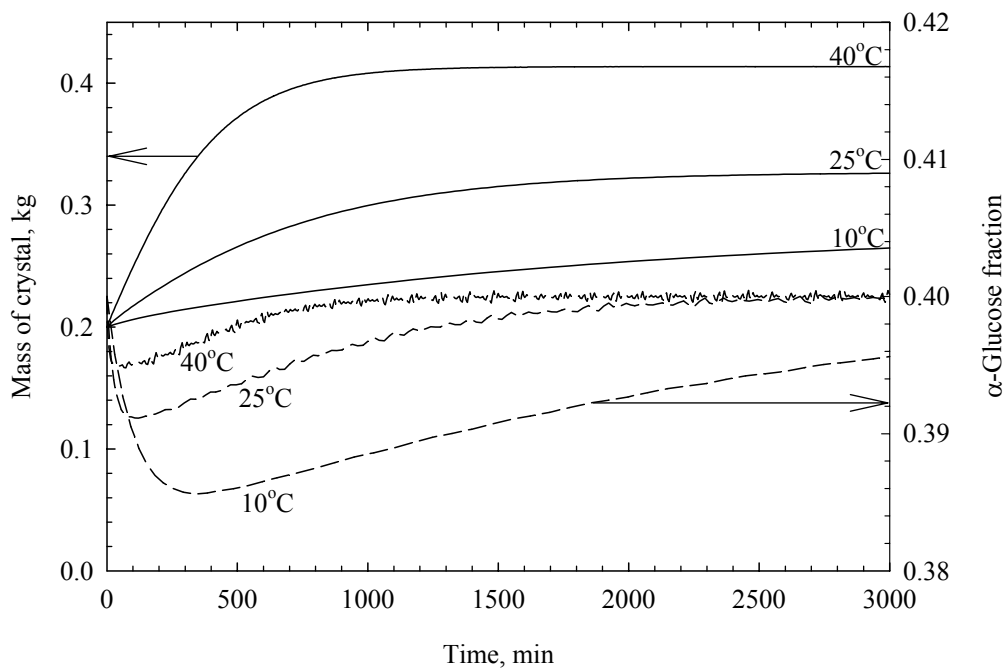
Figure 6.4 The effect of temperature on the change in crystal mass in the mother liquor and fraction of glucose in the α-form for batch crystallization of α-glucose monohydrate. Simulated conditions are, seed size = 100 μm, initial relative supersaturation = 10%, and seeding rate = 200 g seed/kg of mother liquor.

6.4.4   Comparison with Literature Results

There are a few literature models generated for the different sugars (Beckmann, Boje, Rössling, and Arlt 1996; Boje, Beckmann, Arlt, and Rössling, 1997; Flood, Johns, and White, 1996). Both groups generated simple mathematical models similar to that generated in this work but for batch cooling aqueous crystallization of galactose and seeded batch aqueous-ethanolic crystallization of fructose by Beckmann's group and White's group respectively. The models of both

groups were generated by a balance of the system considering both crystallization and the mutarotation reaction. Galactose and fructose undergo a complex mutarotation reaction concerning their tautomers. The group of Beckmann simplified mutarotation of galactose into simple kinetics concerning only the two main forms, that is the pyranose forms, and three forms for fructose, that are β-fructopyranose (the crystallizing anomer) and α- and β-fructofuranose were modeled by Flood et al. Both models found reasonable changes in the crystallizing anomer fraction in solution predicted by the model and the models also good agreement with the experimental results.

6.5 Conclusion

The current study has used previously measured kinetics for the mutarotation reaction of glucose, crystallization kinetics of α-glucose monohydrate in the temperature range that it is the stable crystal phase, and other data including secondary nucleation thresholds and solubility data to construct a model of the batch crystallization of this sugar.

Although the changes in the fraction of the α-glucose anomer are relatively small during most of the simulated batch crystallization, changing only from the equilibrium value of 0.40 to a minimum of about 0.37, this change is very significant when the relative supersaturation is considered. The relative supersaturation of α-glucose was as low as 10% of the supersaturation expected from the total concentration of glucose in the crystallizer. This indicates that under some conditions the crystallization is almost entirely mutarotation rate controlled. The main variables

affecting the response of the α-glucose anomer are the seed size, seeding rate, and the temperature. The mutarotation reaction may be the rate controlling step in processes where small seed sizes, higher seeding rates, and lower operating temperatures are used. This phenomenon must be taken into account when designing industrial crystallizers for this sugar, which typically has very high seeding rates because of the slow crystallization kinetics, although the situation in industrial crystallizers may be complicated by various impurities having an effect on the rates of both the mutarotation reaction and the crystallization.

6.6 References

Beckmann, W., Boje, G., Rössling, G. and Arlt, W. (1996). Crystallization of Galactose from Aqueous Solutions: Influence of the α- and β-Anomers. In B. Biscans, and J. Garside (eds.). **Proceeding of 13th Symp. on Industrial Crystallization** (pp 497-502). LGC-CNRS: Toulouse, France.

Boje, G., Beckmann, W., Arlt, W., and Rössling, G. (1997). A Model for the Batch Cooling Crystallization of α- and β-**D**-Pyrano-Galactoses from Aqueous Solutions. In J. Ulrich (ed.). **Proceeding of Fourth Int. Workshop on Crystal Growth of Organic Materials** (pp 342-349). Shaker Verlag: Aachen, Germany.

Edwards, L. W. (1982). Process for Continuous Crystallization of Alpha Monohydrate Dextrose Utilizing High Agitation. U. S. Patent 4,357,172

Flood, A. E., Johns, M. R., and White, E. T. (1996). Mutarotation of **D**-fructose in aqueous-ethanolic solutions and its influence on crystallization. **Carbohydr. Res.** 288: 45-56.

Goldberg, R. N. and Tewari, Y. B. (1989). Thermodynamic and Transport Properties of Carbohydrates and Their Monophosphates: The Pentoses and Hexoses. **J. Phys. Chem. Ref. Data**. 18(2): 809-880.

Mueller, H. (1970). Isothermal crystallization of dextrose. U. S. Patent 3,547,696

Myerson, A. S. and Ginde, R. (2002). Crystal, Crystal Growth, and Nucleation, In A. S., Myerson (ed.). **Handbook of Industrial Crystallization** (2nd ed., pp.121-176). Boston: Butterworth-Heinemann.

Nelson, J. M. and Beegle, F. M. (1919). Mutarotation of Glucose and Fructose. J. Am. Chem. Soc. 41: 559-575.

Newkirk, W. B. (1925). Manufacture of Dextrose. U. S. Patent 1,521,830

Srisa-nga, S. and Flood, A. E. (2004). Mutarotation Rates and Equilibrium of Simple Carbohydrates [CD]. In **Proceeding of the APCChE 2004** (paper no. 3C-10). Kitakyushu, Japan.

Srisa-nga, S., Flood, A. E., and White, E. T. (2006). The Secondary Nucleation Threshold and Crystal Growth of α-Glucose Monohydrate in Aqueous Solution. **Crystal Growth & Design.** 6(3): 795-801.

Young, F.E. (1957). D-Glucose-Water Phase Diagram. **J. Phys. Chem.** 61(5): 616-619.

CHAPTER VII

Conclusions and Recommendations

7.1 Conclusions

Glucose is one of the most significant commodity chemicals produced in the world currently. It is used in several industries such as the food, candy, soft drink, and pharmaceutical industries, and used as a precursor of many products including citric acid, lactic acid, and surfactants. It is used as a sweetener in glucose-containing syrup and used as the raw material for many low-calorie sweeteners and non-digested sweeteners. There are three crystalline forms of glucose, i.e. anhydrous α-glucose, α-glucose monohydrate, and anhydrous β-glucose. Of the three crystal forms, α-glucose monohydrate is the most important industrially, for several reasons including its high stability and ease of production.

The research aims to improve the knowledge of the kinetics of crystallization of this sugar in aqueous solution. This is done to better understand the process and allow for the improvement of the process designs and operations. The mutarotation reaction may complicate the crystallization kinetics and it is necessary to study its kinetics as well as equilibria. A generalized model has been generated and aims to apply to the crystallization of this sugar and also for all other sugars.

In order to achieve the research goal, a lot of data are necessary, i.e. the solubility, metastable limit, mutarotation rates and equilibrium, crystal growth kinetics, and crystal growth rate dispersion. However, in this research, some of the

data does not need to be measured: these data include the solubility data, where accurately literature values are already available, and the nucleation rate, which in industrial crystallization of glucose monohydrate is normally zero because crystallizations are seeded batch at low supersaturation. All the measured data are used in a mechanistic and balance equation model of this system, which was developed in the thesis.

The mutarotation rates of the simple sugars are temperature dependent and fall in narrow bands on an Arrhenius plot, depending on whether they are aldose or ketose sugars. Ketose sugars are significantly faster mutarotating in aqueous solutions than aldose sugars. The rate of mutarotation of disaccharides is similar to the rate of the constituent monosaccharide determining the anomeric form (ring containing the anomeric carbon). The sugar content has only a slight effect on the rate of mutarotation; this dependence is small enough that it can probably be neglected in models of the crystallization of sugars. The mutarotational equilibrium is more difficult to predict but is probably related to the steric effects between hydroxyl groups on the anomeric carbon and hydroxyl groups on adjacent carbons.

The secondary nucleation threshold of glucose monohydrate in aqueous solutions was measured and found to be large (16 g glucose / 100 g solution for an instantaneous limit), but decreases with increasing operating time (it reduces to 5 g glucose/100 g solution for a large time limit). The temperature does not have an effect on this parameter. The operating condition where crystals can grow without nucleation is specified in the phase diagram. This result will be used to decide the suitable condition for crystal growth experiments, and suitable regions for laboratory crystallizations.

The isothermal seeded batch crystallization of glucose monohydrate from aqueous solution is operated within the metastable region for secondary nucleation to avoid nucleation. The crystal growth rate found was abnormally high during the first one hour of the operation and then followed the normal linear tend. The crystal growth rate order is 1, and the growth rate is temperature dependent following the Arrhenius relationship with activation energy of 50 ± 2 kJ/mol. Growth rate dispersion of glucose monohydrate in this system is significant even when a carefully sieved seed is used.

A mathematical model has been constructed by using measured kinetics for the mutarotation reaction of glucose, crystallization kinetics of α-glucose monohydrate, and other data including secondary nucleation thresholds and solubility data. The model shows reasonable predicted results. The simulated results show the changes in the fraction of the α-glucose anomer are relatively small during most of the simulated batch crystallization but this change is very significant when the relative supersaturation is considered. The relative supersaturation of α-glucose was as low as 10% of the supersaturation expected from the total concentration of glucose in the crystallizer, which indicates that under some conditions the crystallization is almost entirely mutarotation rate controlled. The main variables affecting the response of the α-glucose anomer are the seed size, seeding rate, and the temperature. The mutarotation reaction may be the rate controlling step in processes where small seed sizes, higher seeding rates, and lower operating temperatures are used. This phenomenon must be taken into account when designing industrial crystallizers for glucose monohydrate, which typically has very high seeding rates because of the slow crystallization kinetics, although the situation in an industrial crystallizer may be

complicated by various impurities having an effect on the rate of both the mutarotation reaction and the crystallization.

7.2 Recommendations

7.2.1 Due to the assumptions that the crystallization in this thesis does not involve nucleation inside the crystallizer, i.e. no breakage and attrition, the nucleation rate is not studied and measured in this research. However, this kinetic rate may also be important in industrial crystallizations since the batch usually operates in a dense suspension system, which promotes the secondary nucleation mechanism. The batch is also usually operated under higher supersaturations to achieve higher solid yield, in which case the crystal shape is probably elongated. This elongated shape crystal is easy to break especially under very violent agitation. For this reason, the nucleation mechanism may be important to study further.

7.2.2 It is not possible to validate the model using the crystallization of glucose monohydrate from aqueous solution since the change in the α-fraction predicted by the model is very small (approximately 2%) and this is difficult to observe using the current equipment (^{13}C-NMR) because the accuracy of this technique is approximately ± 2%. The validation of the model should be performed with a sugar having low mutarotation rate and a high fraction of the crystallizing anomer at the mutarotation equilibrium. This means that the maximum change in the anomer content during the crystallization will be much greater than 2%. In this case, the crystallizing of β-maltose, β-cellobiose, and α-mannose from aqueous solution at low temperature would be good choices. Mannose would be the most convenient of these, as it is a common monosaccharide sugar.

7.2.3 The model should be used to optimize the crystallization of glucose monohydrate. This can be done if financial criteria such as the cost relationship between batch time, yield, operation process, are known. The system might be complex because the optimum process may not necessary be an isothermal operation (cooling or evaporation). This model can be used for this case, but it would involve a large amount of work to be able to optimize the process.

7.2.4 The correlation between the sugar types and the mutarotation rates and equilibrium is possible since the results from this work show that sugars within the same class of sugar (aldose or ketose) fall in the same band in an Arrhenius plot, which means that the activation energies are quite similar for similar types of sugars. The equilibrium values of aldose sugars are in the range of approximately $62 \pm 5\%$ for the stable form. These correlations may be difficult for ketose sugars since they usually undergo complex mutarotation kinetics.

Appendix A

Mutarotation Experimental

and Literature Data

A-1 Experimental data

Table A-1 The overall mutarotation rate constants of glucose in aqueous solutions.

Conc. [g/100g soln.]	Experimental temperature [°C]				
	7	15	20	24	35
22	0.627	1.592	2.347	5.786	15.161
		1.739*			14.773
33		1.430	2.480	4.844	12.922
				4.780	4.766*
44		1.464	2.357	3.833	12.924
50					14.120
					13.989
54					12.738
					13.309

* α-glucose anhydrous was dissolved.

Table A-2 The experimental mutarotation equilibrium compositions and the activation energies of studied sugars in aqueous solutions.

Sugar	Temp. [°C]	Conc. [%]	%β-pyr at equilibrium	E$^\bullet$ [kJ/mol]
D-glucose	7	22.0	65.68±4.191	79.93
	15	22.0-44.0	60.06±0.680	
	20	22.0-44.0	59.92±0.466	
	24	22.0-44.0	59.67±0.367	
	35	22.0-54.0	58.47±0.410	
D-galactose	15	10.0	67.33±1.657	89.86
	25	5.0-15.0	66.49±1.119	
	35	10.0	66.68±1.695	
D-cellobiose	15	8.0	59.60±4.466	74.22
	25	8.0	57.71±1.543	
	35	8.0	56.16±1.664	
D-maltose monohydrate	15	10.0-20.0	56.03±10.093	94.25
	25	10.0-30.0	59.21±1.407	
	35	10.0-30.0	58.91±1.345	
D-turanose	15	20.0	56.06±1.693	59.00
	25	20.0	55.96±0.969	
	35	20.0	57.08±0.741	

Table A-3 The overall mutarotation rate constants of glucose as a function of D_2O composition at 24°C.

%D_2O	$k \times 10^4$ [s^{-1}]	%α-glucose at equilibrium
0	5.5746	40.10
10	5.8196	40.02
20	5.5135	40.63
40	4.5727	40.83
60	3.2766	40.68
100	2.1674	42.84
100	2.4703	41.97

Table A-4 The overall mutarotation rate constants of studied sugars in aqueous solutions.

Temp. [°C]	$k \times 10^4$ [s^{-1}]				
	Glucose	**Galactose**	**Maltose**	**Cellobiose**	**Turanose**
7	0.6274				
15	1.5564	1.7775	0.9758	1.2992	21.5750
20	2.3949				
24	4.8060				
25		8.0602	3.9834	3.5114	70.7630
35	13.7420	20.2130	12.5450	9.7340	106.00

Note: Overall mutarotation rate constants are averaged from the experimental data with varying sugar concentrations.

A-2 Literature Survey Data

Table A-5 Mutarotation literature data of glucose in aqueous solutions.

Researcher	Method	Conc. [g/100 ml]	Temp. [°C]	%β-pyr at equilibrium	$k \times 10^4$ [s^{-1}]
Hudson and Dale (1917)	Polarimetry	< 10	0.7	N/A	0.12
			5		0.25
			10		0.37
			15		0.63
			20		1.09
			25		1.76
			30		2.80
			40		6.58
Nelson and Beegle (1919)	Polarimetry	N/A	0.15	N/A	0.13
			15		0.69
			25		1.73
			37		5.00
Nelson and Johnson(1976)	Circular Dichroism	N/A	20	N/A	1.17
Pigman and Isbell (1968)	Polarimetry	3.9	0.2	63.8	0.12
			20.0		1.04

Table A-5 (Continued)

Researcher	Method	Conc. [g/100 ml]	Temp. [°C]	%β-pyr at equilibrium	$k \times 10^4$ [s^{-1}]
Lee et al. (1969)	Polarimetry	N/A	25	N/A	1.85
			35		4.53
	GLC	N/A	25	N/A	1.70
			35		4.52
Kraus and Nývlt (1994)	Dissolution excepted at 24°C using polarimetry	N/A	24	N/A	2.5
			55		25.3
			60		38.5
			70		51.4
Barc'H et al. (2001)	GLC	40.0-52.2	30	60.15±0.50	5.86
		43.8-56.0	35	59.49±0.51	7.44
		50.0-60.0	40	59.28±0.56	8.00
		52.1-62.4	45	58.50±0.46	12.47

Table A-6 Literature mutarotation rate of mannose.

Researcher	Method	Conc. [g/100 ml]	Temp. [°C]	$k \times 10^4$ [s^{-1}]
Hudson and Sawyer (1917)	Polarimetry	N/A	4.8	0.68
			9.7	1.07
			14.7	1.82
			19.7	2.95
			24.8	4.95
			29.7	7.73
			34.8	11.37
			39.7	17.70
			44.8	28.5
Pigman and Isbell (1968)	Polarimetry	4.0	0.3	0.36
			20	2.97
Lee et al. (1969)	Polarimetry	N/A	15	2.43
			25	6.82
	GLC	N/A	15	2.53
			25	6.82

Table A-7 Literature mutarotation rate of galactose.

Researcher	Method	Conc. [g/100 ml]	Temp. [°C]	$k \times 10^4$ [s^{-1}]
Pigman and Isbell (1968)	Polarimetry (slow rxn.)	4.0-4.1	0.0	0.15
			20	1.33
Pigman and Isbell (1968)	Polarimetry (fast rxn.)	4.0-4.1	0.0	2.78
			20	14.72
Nelson and Johnson(1976)	Circular Dichroism	N/A	20	1.35
Wertz et al. (1981)	Polarimetry (slow rxn.)	N/A	15	2.00
			20	3.00
			25	5.00

Table A-8 Literature mutarotation rate of ketose sugars.

Ketose	Researcher	Method	Conc. g/100 ml	Temp. [°C]	$k \times 10^4$ [s^{-1}]
D-fructose	Nelson and Beegle (1919)	Polarimetry	N/A	0.15	1.42
				15	6.17
				25	13.83
				37	33.17
L-sorbose (fast rxn.)	Pigman and Isbell (1968)	^{13}C-NMR	11.3-11.6	0.4	5.00
				20	41.67

Table A-8 (Continued)

Ketose	Researcher	Method	Conc. g/100 ml	Temp. [°C]	$k \times 10^4$ [s^{-1}]
L-sorbose (slow rxn.)	Pigman and Isbell (1968)	^{13}C-NMR	11.3-11.6	0.4	0.92
				20	6.67

Table A-9 Literature equilibrium compositions of aldoses (Boons, 1998) and ketoses

(Que and Gray, 1974).

Sugar Type	Sugar	pyranose [%]		furanose [%]	
		α	β	α	β
Aldose	**D**-glucose	38	62	0.1	0.2
	D-mannose	65.5	34.5	-	-
	D-gulose	0.1	78	< 0.1	22
	D-idose	39	36	11	14
	D-galactose	29	64	3	4
	D-altrose	27	43	17	13
	D-talose	40	29	20	11
	D-xylose	36.5	63	< 0.5	
	D-lyxose	70	28	1.5	0.5
	D-ribose	21	59	6	14

Table A-9 (Continued)

Sugar Type	Sugar	pyranose [%]		furanose [%]	
		α	β	α	β
Ketose	**D**-fructose	0	72	5	23
	D-psicose	26	21	38	15
	L-sorbose	95	0	5	0
	D-tagatose	71	15	5	9
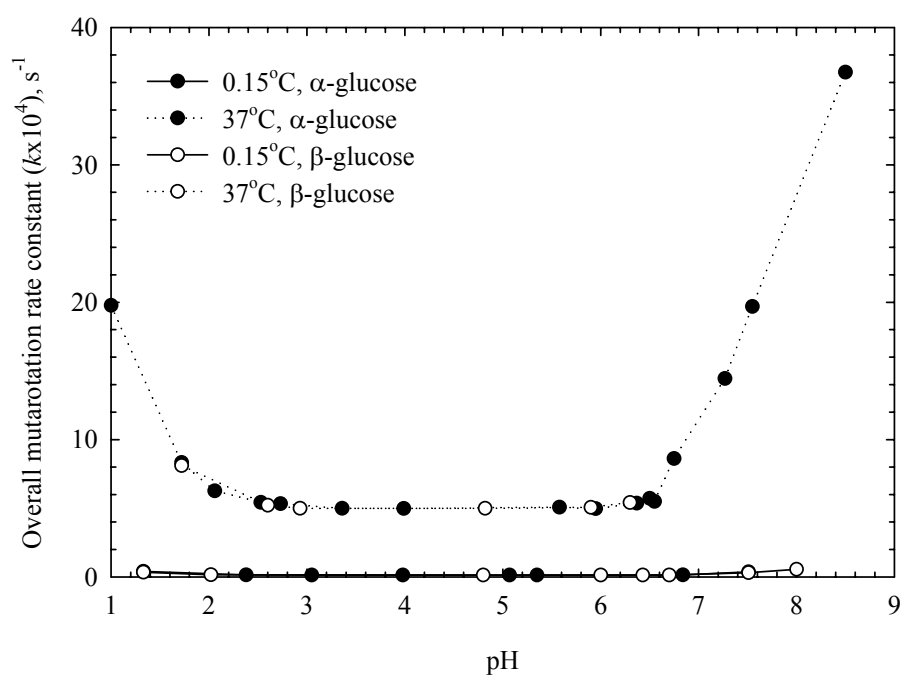
Figure A-1 Glucose mutarotation rate constants as a function of pH (Nelson and

Beegle, 1919). β-glucose and α-glucose represent the dissolved forms.
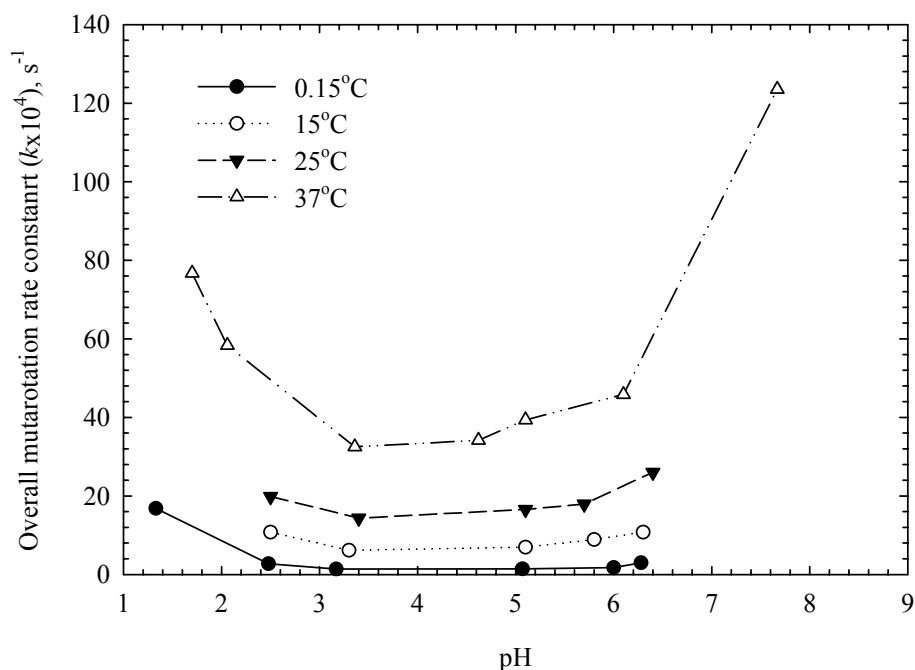
Figure A-2 Fructose mutarotation rate constants as a function of pH (Nelson and Beegle, 1919).

A-3 References

Barc'H, N. L., Grossel, J. M., Looten, P., and Mathlouthi, M. (2001). Kinetic study of the mutarotation of D-glucose in concentrated aqueous solution by gas-liquid chromatography. **Food Chem.** 74: 19-124.

Boons, G.-J. (1998). Mono- and oligosaccharides: structure, configuration and conformation. In G.-J. Boons (ed.). **Carbohydrate Chemistry** (pp 1-20). London: Blackie Acadamic & Professional.

Hudson, C. S. and Dale, J. K. (1917). Studied on the forms of D-glucose and their mutarotation. **J. Am. Chem. Soc.** 39: 320-328.

Hudson, C. S. and Sawyer, H. L. (1917). The preparation of pure crystalline mannose and a study of its mutarotation. **J. Am. Chem. Soc.** 39(3): 470-478.

Kraus, J. and Nývlt, J. (1994). Crystallization of anhydrous glucose I. Mutarotation rate and solid-liquid phase equilibria. **Zuckerind**. 119(1): 24-29.

Lee, C. Y., Acree, T. E., and Shallenberger, R. S. (1969). Mutarotation of **D**-glucose and **D**-mannose in aqueous solution. **Carbohydr. Res.** 9: 356-360.

Nelson, J. M. and Beegle, F. M. (1919). Mutarotation of glucose and fructose. **J. Am. Chem. Soc.** 41: 559-575.

Nelson, R. G. and Johnson, W. C. Jr. (1976). Optical Properties of Sugar. 3. Circular Dichroism of Aldo-and Ketopyranose Anomers. **J. Am. Chem. Soc.** 98(14): 4290-4295.

Pigman, W. and Isbell, H. S. (1968). Mutarotation of sugars in solution. I History, basic kinetics, and composition of sugar solutions. **Adv. Carbohydr. Chem.** 23: 11-57.

Que, L. Jr. and Gray, G. R. (1974). 13C nuclear magnetic resonance spectra and the tautomeric equilibria of ketohexoses in solution. **Biochem.** 13(1): 146-153.

Wertz, P. W., Garver, J. C., and Anderson, L. (1981). Anatomy of a complex mutarotation. Kinetics of tautomerization of α-**D**-galactopyranose and β-**D**-galactopyranose in water. **J. Am. Chem. Soc.** 103: 3916-3922.

Appendix B

Nucleation Experimental Data

The SNT experiments involved a simple observation of supersaturated solutions to determine if nucleation had occurred. Symbols used to convey the results are as follow:

√ nucleated

× not nucleated

? unsure.

Table B-1 Nucleation at 10°C set#1.

Concentration [g/100g soln.]	Inspection time [hr]										
	0.5	1.0	1.5	2.5	3.0	4.0	5.0	6.0	7.0	8.0	23.0
41.11	×	×	×	×	×	×	×	×	×	×	?
44.93	×	×	×	×	×	×	×	×	×	×	?
47.43	×	×	×	×	×	×	×	×	×	×	√
50.01	×	×	×	×	×	×	×	×	?	√	√
52.46	×	×	×	×	×	×	×	×	?	√	√
54.97	×	×	×	×	×	?	√	√	√	√	√
57.48	×	×	?	√	√	√	√	√	√	√	√
60.02	×	×	√	√	√	√	√	√	√	√	√

Table B-2 Nucleation at 10°C set#2.

Concentration [g/100g soln.]	Inspection time [hr]								
	0.5	1.0	2.0	3.0	4.0	5.0	6.0	7.0	8.0
43.01	×	×	×	×	×	×	×	×	?
44.94	×	×	×	×	×	×	×	√	√
46.92	×	×	×	×	×	×	×	?	√
49.02	×	×	×	×	×	×	×	√	√
50.99	×	×	×	×	√	√	√	√	√
52.94	×	×	×	×	×	×	?	√	√
54.98	×	×	×	?	?	√	√	√	√
57.00	×	×	?	√	√	√	√	√	√

Table B-3 Nucleation at 10°C set#3.

Concentration [g/100g soln.]	Inspection time [hr]													
	0.5	1.0	1.5	2.0	2.5	3.0	3.5	4.0	4.5	5.0	5.5	6.0	7.0	21.5
43.08	×	×	×	×	×	×	×	×	×	×	×	×	×	√
44.06	×	×	×	×	×	×	×	×	×	?	×	×	×	√
45.05	×	×	×	×	×	×	×	×	?	?	?	√	√	√
45.96	×	×	×	×	×	×	×	×	?	×	×	×	?	√
46.96	×	×	×	×	×	×	×	×	?	×	×	×	?	√
47.98	×	×	×	×	×	×	×	×	×	×	×	×	×	√
49.04	×	×	×	×	×	×	×	×	×	×	×	×	×	√
50.16	×	×	×	×	×	×	×	×	×	×	×	×	×	?
51.01	×	×	×	×	×	×	×	×	×	×	×	×	√	√
51.97	×	×	×	×	?	√	√	√	√	√	√	√	√	√
52.97	×	×	×	×	×	×	×	?	?	√	√	√	√	√

Table B-3 (Continued)

Concentration	Inspection time [hr]													
[g/100g soln.]	0.5	1.0	1.5	2.0	2.5	3.0	3.5	4.0	4.5	5.0	5.5	6.0	7.0	21.5
53.96	×	×	×	×	×	×	×	×	×	×	×	×	√	√
54.93	?	√	√	√	√	√	√	√	√	√	√	√	√	√
55.98	√	√	√	√	√	√	√	√	√	√	√	√	√	√
56.94	×	×	×	√	√	√	√	√	√	√	√	√	√	√

Table B-4 Nucleation at 25°C set#1.

Concentration	Inspection time [hr]											
[g/100g soln.]	0.5	1.5	2.0	4.0	6.0	8.0	21.0	24.0	31.0	33.0	34.0	48.0
52.30	×	×	×	×	×	×	×	×	×	×	×	×
54.97	×	×	×	×	×	×	×	×	×	×	×	√
57.55	×	×	×	×	×	×	×	×	?	√	√	√
60.00	×	×	×	×	?	×	?	?	√	√	√	√
62.57	×	×	×	×	?	?	√	√	√	√	√	√
64.97	×	×	×	√	√	√	√	√	√	√	√	√
67.35	?	√	√	√	√	√	√	√	√	√	√	√
70.00	√	√	√	√	√	√	√	√	√	√	√	√
72.46	√	√	√	√	√	√	√	√	√	√	√	√
74.00	√	√	√	√	√	√	√	√	√	√	√	√

Table B-5 Nucleation at 25°C set#2.

Concentration [g/100g soln.]	Inspection time [hr]									
	0.5	1.0	2.0	4.0	6.0	7.0	18.5	22.0	24.0	27.0
55.46	×	×	×	×	×	×	?	?	?	√
57.94	×	×	×	×	×	×	?	?	√	√
59.06	×	×	×	×	×	?	√	√	√	√
59.98	×	×	×	×	×	×	√	√	√	√
61.01	×	×	×	×	×	?	√	√	√	√
61.99	×	×	×	×	?	√	√	√	√	√
67.49	×	×	√	√	√	√	√	√	√	√

Table B-6 Nucleation at 40°C set#1.

Concentration [g/100g soln.]	Inspection time [hr]									
	0.5	1.0	1.5	2.0	2.5	3.0	4.0	5.0	6.0	21.5
64.65	×	×	×	×	×	×	?	?	?	√
67.14	×	×	×	×	×	×	×	?	?	√
69.96	×	×	×	×	×	?	?	√	√	√
72.49	×	×	×	×	×	?	?	√	√	√
74.86	×	×	√	√	√	√	√	√	√	√
77.43	×	×	√	√	√	√	√	√	√	√
80.00	×	√	√	√	√	√	√	√	√	√

Table B-7 Nucleation at 40°C set#2.

Concentration	Inspection time [hr]									
[g/100g soln.]	0.5	1.25	2.0	2.5	3.0	4.0	5.0	6.0	7.0	19.5
62.96	×	×	?	?	?	?	?	?	?	√
63.98	×	×	?	?	?	?	?	?	?	√
65.06	×	×	?	?	?	?	?	?	?	√
65.95	?	?	?	?	?	?	?	?	?	√
66.96	?	?	√	√	√	√	√	√	√	√
67.85	×	×	×	√	√	√	√	√	√	√
68.77	×	×	×	?	?	?	√	√	√	√
69.99	×	×	×	?	?	√	√	√	√	√
70.78	×	×	×	?	?	√	√	√	√	√
72.01	×	?	√	√	√	√	√	√	√	√
72.98	×	?	√	√	√	√	√	√	√	√
73.99	×	√	√	√	√	√	√	√	√	√
74.92	×	?	√	√	√	√	√	√	√	√
76.05	×	√	√	√	√	√	√	√	√	√
76.66	×	√	√	√	√	√	√	√	√	√

Table B-8 Nucleation at 40°C set#3.

Concentration [g/100g soln.]	Inspection time [hr]									
	0.5	1.0	1.5	2.0	3.0	4.0	5.0	5.5	20.5	24.0
61.98	×	×	×	×	×	×	×	×	×	×
63.83	×	×	×	×	×	×	×	×	×	×
66.02	×	×	×	×	×	×	×	×	×	?
69.92	×	×	×	×	×	×	×	×	√	√
72.06	×	×	×	×	×	?	?	√	√	√
73.91	×	√	√	√	√	√	√	√	√	√
75.94	×	√	√	√	√	√	√	√	√	√

Appendix C

Crystal Growth Experimental Data

C-1 Operating Conditions

This section contains the crystal growth operating conditions discussed in Chapter V.

Table C-1 The crystallization operating conditions.

Exp. Temp. [°C]	Run no.	Conc. [g/100g soln.]	Mass of Seed [g]	Mass of Soln. [g]	Exp. Time [hr]
10	1	43.13±0.044	0.86±0.172	500	34
	2				
	3	44.15±0.045	0.85±0.137	500	24
	4				
	5	46.24±0.076	0.68±0.029	500	24
	6				
25	7	55.40±0.125	0.482	500	24
	8	54.77±0.103	8.383	1000	24
	9	57.79±0.098	1.32±0.040	500	6
	10				
	11	52.27±0.020	0.78±0.125	500	26
	12				
25	13	57.55±0.036^a	1.212	500	6
	14	57.52±0.010^b	1.120	500	6

Table C-1 (Continued)

Exp. Temp. [°C]	Run no.	Conc. [g/100g soln.]	Mass of Seed [g]	Mass of Soln. [g]	Exp. Time [hr]
40	15	63.54 ± 0.360^{c}	1.02 ± 0.186	500	24
	16	64.40 ± 0.500^{d}			
	17	65.81 ± 0.250	0.95 ± 0.088	500	24
	18				
	19	67.00 ± 0.285	1.85 ± 0.346	500	8
	20				

Remark: [a] Operating speed of 400 rpm, [b] Operating speed of 550 rpm, [c] at 1-10 hour, [d] at 10-24 hour.

C-2 Data Interpretation

This section contains the data interpretation of crystal growth results discussed previously in Chapter V. In this section b#1, b#2, s#1, and s#2 are referred to batch no. 1, batch no. 2, sample (or replicate) no. 1, and sample no. 2, respectively. σ_g is geometric standard deviation obtained from the fitting with log-normal distribution) and σ is an arithmetic standard deviation calculated from the second moment about mean ($\sigma = \sqrt{m_2}$).

Table C-2 Volume median size of run no. 1, averaged $\sigma_g = 0.4699$ μm.

Time	Volume median size [μm]		σ [μm]	
[hr]	s#1	s#2	s#1	s#2
0.00	102.24	99.05	29.26	28.34
0.50	104.11	-	29.80	-
1.00	100.53	105.97	28.77	30.33
2.50	118.08	109.57	33.79	31.36
4.00	112.78	113.80	32.28	32.57
6.00	114.54	114.43	32.78	32.75
10.00	118.32	120.71	33.86	34.54
24.00	128.09	128.23	36.65	36.70
34.00	140.20	141.30	40.11	40.43

Table C-3 Volume median size of run no. 2, averaged $\sigma_g = 0.4690$ μm.

Time	Volume median size [μm]		σ [μm]	
[hr]	s#1	s#2	s#1	s#2
0.00	102.24	99.05	29.26	28.34
0.50	110.80	-	31.71	-
1.00	106.46	110.62	30.47	31.66
2.50	113.51	115.92	32.49	33.18
4.00	112.44	114.58	32.18	32.79

Table C-3 (Continued)

Time	Volume median size [μm]		σ [μm]	
[hr]	s#1	s#2	s#1	s#2
6.00	115.91	120.65	33.17	34.53
10.00	122.69	125.28	35.11	35.85
24.00	128.56	126.13	36.77	36.03
34.00	133.32	142.73	38.15	40.83

Table C-4 Volume median size of run no. 3, averaged $\sigma_g = 0.458$ μm.

Time	Volume median size [μm]		σ [μm]	
[hr]	s#1	s#2	s#1	s#2
0.00	97.16	96.07	27.78	27.47
1.00	105.01	107.37	30.03	30.70
2.50	109.84	111.62	31.41	31.92
4.00	111.52	114.72	31.89	32.80
6.00	115.31	112.86	32.97	32.27
8.00	117.45	116.64	33.58	33.35
24.00	136.53	134.68	39.03	38.50

Table C-5 Volume median size of run no. 4, averaged $\sigma_g = 0.458$ μm.

Time	Volume median size [μm]		σ [μm]	
[hr]	s#1	s#2	s#1	s#2
0.00	97.16	96.07	27.78	27.47
1.00	105.62	104.67	30.20	29.93
2.50	109.56	112.75	31.33	32.24
4.00	115.52	115.08	33.03	32.90
6.00	114.78	117.32	32.82	33.55
8.00	118.58	120.82	33.91	34.55
24.00	135.98	135.40	38.87	38.71

Table C-6 Volume median size of run no. 5, averaged $\sigma_g = 0.438$ μm.

Time	Volume median size [μm]		σ [μm]	
[hr]	s#1	s#2	s#1	s#2
0.00	97.86	97.49	27.86	27.75
1.00	112.64	112.87	32.07	32.13
2.50	119.34	119.80	33.98	34.10
4.00	124.00	127.71	35.30	36.35
6.00	132.92	133.36	37.83	37.96
8.00	135.69	135.56	38.62	38.57
10.00	140.56	140.90	40.01	40.10

Table C-6 (Continued)

Time	Volume median size [μm]		σ [μm]	
[hr]	s#1	s#2	s#1	s#2
24.00	163.30	168.64	46.46	47.96

Table C-7 Volume median size of run no. 6, averaged $\sigma_g = 0.438$ μm.

Time	Volume median size [μm]		σ [μm]	
[hr]	s#1	s#2	s#1	s#2
0.00	97.86	97.49	27.86	27.75
1.00	110.01	115.31	31.32	32.82
2.50	121.61	122.90	34.62	34.98
4.00	125.22	123.38	35.64	35.12
6.00	133.23	132.05	37.92	37.59
8.00	138.26	135.03	39.35	38.43
10.00	137.14	139.10	39.03	39.59
24.00	162.26	157.99	46.16	44.95

Table C-8 Volume median size of run no. 7, averaged $\sigma_g = 0.566$ μm.

Time [hr]	Volume median size [μm]		σ [μm]	
	s#1	s#2	s#1	s#2
0.00	90.80	-	25.05	-
1.00	111.94	101.96	30.87	28.12
2.00	127.79	128.58	35.23	35.44
3.00	120.66	122.51	33.27	33.76
4.00	126.86	124.67	34.97	34.37
6.00	130.23	126.84	35.90	34.97
8.00	145.05	132.77	39.95	36.59
24.00	184.88	195.56	50.71	53.54

Table C-9 Volume median size of run no. 8, averaged $\sigma_g = 0.576$ μm.

Time [hr]	Volume median size [μm]		σ [μm]	
	s#1	s#2	s#1	s#2
0.00	100.50	95.92	27.50	26.25
0.33	129.27	136.79	35.35	37.39
0.67	134.14	147.01	36.67	40.16
1.00	147.00	144.01	40.15	39.34
2.00	146.81	-	40.10	-
3.00	-	157.59	-	43.01

Table C-9 (Continued)

Time	Volume median size [μm]		σ [μm]	
[hr]	s#1	s#2	s#1	s#2
4.00	168.01	173.89	45.80	47.37
8.00	191.58	177.27	52.05	48.27
21.00	214.70	239.22	58.04	64.20
24.00	235.60	240.26	63.30	64.46

Table C-10 Volume median size of run no. 9, averaged $\sigma_g = 0.555$ μm.

Time	Volume median size [μm]		σ [μm]	
[hr]	s#1	s#2	s#1	s#2
0.00	106.91	108.00	29.72	30.03
1.00	124.16	121.67	34.51	33.82
2.00	128.18	131.16	35.62	36.44
3.00	130.92	139.73	36.38	38.81
4.00	143.12	148.83	39.74	41.32
6.00	148.15	154.51	41.13	42.88

Table C-11 Volume median size of run no. 10, averaged $\sigma_g = 0.555$ μm.

Time	Volume median size [μm]		σ [μm]	
[hr]	s#1	s#2	s#1	s#2
0.00	106.91	108.00	29.72	30.03
1.00	-	117.17	-	32.57
2.00	-	127.26	-	35.37
3.00	135.18	136.06	37.56	37.80
4.00	146.77	144.01	40.75	39.99
6.00	156.97	156.03	43.55	43.29

Table C-12 Volume median size of run no. 11, averaged $\sigma_g = 0.522$ μm.

Time	Volume median size [μm]		σ [μm]	
[hr]	s#1	s#2	s#1	s#2
0.00	91.62	96.48	25.95	27.32
1.00	92.99	93.78	26.33	26.56
2.00	94.07	95.67	26.64	27.09
3.00	95.96	96.60	27.17	27.35
4.00	96.08	98.32	27.21	27.84
6.00	98.95	98.94	28.02	28.02
8.00	103.26	104.29	29.24	29.53
26.00	127.97	123.04	36.22	34.83

Table C-13 Volume median size of run no. 12, averaged $\sigma_g = 0.522$ μm.

Time	Volume median size [μm]		σ [μm]	
[hr]	s#1	s#2	s#1	s#2
0.00	91.62	96.48	25.95	27.32
1.00	94.53	95.16	26.77	26.95
2.00	94.11	92.83	26.65	26.29
3.00	94.44	94.51	26.74	26.76
4.00	98.31	96.44	27.84	27.31
6.00	98.72	98.17	27.95	27.80
8.00	100.08	97.56	28.34	27.63
26.00	122.99	120.43	34.82	34.10

Table C-14 Volume median size of run no. 13, averaged $\sigma_g = 0.414$ μm.

Time	Volume median size [μm]		σ [μm]	
[hr]	s#1	s#2	s#1	s#2
0.00	116.01	115.69	32.68	32.59
1.00	138.28	140.14	38.95	39.47
2.00	151.97	149.82	42.80	42.20
3.00	158.31	155.22	44.58	43.71
4.00	164.86	164.84	46.42	46.41
6.00	183.30	180.80	51.58	50.88

Table C-15 Volume median size of run no. 14, averaged $\sigma_g = 0.401$ μm.

Time	Volume median size [μm]		σ [μm]	
[hr]	s#1	s#2	s#1	s#2
0.00	116.01	115.74	32.41	32.34
1.00	140.36	140.69	39.22	39.31
2.00	151.14	147.99	42.26	41.35
3.00	157.41	162.17	43.97	45.30
4.00	163.41	168.85	45.64	47.16
6.00	181.36	183.09	50.63	51.12

Table C-16 Volume median size of run no. 15, averaged $\sigma_g = 0.422$ μm.

Time	Volume median size [μm]		σ [μm]	
[hr]	s#1	s#2	s#1	s#2
0.00	97.03	96.97	27.45	27.43
1.00	100.71	100.58	28.49	28.45
2.50	104.45	104.69	29.55	29.61
4.00	106.13	106.26	30.02	30.06
6.00	109.06	109.23	30.85	30.90
10.00	123.45	123.97	34.92	35.07
24.00	175.79	178.56	49.68	50.46

Table C-17 Volume median size of run no. 16, averaged $\sigma_g = 0.422$ μm.

Time	Volume median size [μm]		σ [μm]	
[hr]	s#1	s#2	s#1	s#2
0.00	97.03	96.97	27.45	27.43
1.00	101.63	102.52	28.75	29.00
2.50	103.37	-	29.24	-
4.00	104.88	107.31	29.67	30.35
6.00	110.39	108.63	31.22	30.73
10.00	117.11	115.35	33.12	32.63
24.00	169.53	173.61	47.92	49.07

Table C-18 Volume median size of run no. 17, averaged $\sigma_g = 0.491$ μm.

Time	Volume median size [μm]		σ [μm]	
[hr]	s#1	s#2	s#1	s#2
0.00	106.77	106.37	30.51	30.40
1.00	124.99	125.03	35.71	35.72
2.50	132.29	132.59	37.79	37.88
4.00	146.37	146.30	41.80	41.78
6.00	155.35	155.64	44.35	44.43
10.00	177.00	177.90	50.46	50.71
24.00	242.35	245.50	68.23	69.05

Table C-19 Volume median size of run no. 18, averaged $\sigma_g = 0.491$ µm.

Time	Volume median size [µm]		σ [µm]	
[hr]	s#1	s#2	s#1	s#2
0.00	106.77	106.37	30.51	30.40
1.00	125.01	124.15	35.72	35.47
2.50	134.23	132.34	38.35	37.81
4.00	142.34	144.20	40.74	41.18
6.00	153.62	153.85	43.86	43.92
10.00	173.98	175.69	49.61	50.09
24.00	243.42	245.97	68.51	69.17

Table C-20 Volume median size of run no. 19, averaged $\sigma_g = 0.445$ µm.

Time	Volume median size [µm]		σ [µm]	
[hr]	s#1	s#2	s#1	s#2
0.00	103.27	102.64	29.46	29.28
1.00	129.87	124.81	37.04	35.60
2.50	140.86	-	40.17	-
4.50	156.07	159.80	44.49	45.55
6.00	172.08	172.12	49.03	49.04
8.00	187.62	189.59	53.40	53.95

Table C-21 Volume median size of run no. 20, averaged $\sigma_g = 0.445$ μm.

Time [hr]	Volume median size [μm]		σ [μm]	
	s#1	s#2	s#1	s#2
0.00	103.27	102.64	29.46	29.28
1.00	125.35	128.31	35.75	36.59
2.50	141.16	141.62	40.26	40.39
4.50	160.13	163.61	45.64	46.63
6.00	175.18	175.55	49.90	50.01
8.00	192.28	194.07	54.71	55.21

Table C-22 Crystal contents of run no. 7.

Time [hr]	Crystal content [kg particle / kg suspension]	
	s#1	s#2
0.00	0.0008	
1.00	0.0020	0.0012
2.00	0.0027	0.0027
3.00	0.0025	0.0026
4.00	0.0029	0.0030
6.00	0.0099	0.0096
8.00	0.0123	0.0106
24.00	0.0261	0.0270

Table C-23 Crystal contents of run no. 8.

Time	Crystal content [kg particle / kg suspension]	
[hr]	**s#1**	**s#2**
0.00	0.0068	
0.33	0.0123	0.0142
0.67	0.0154	0.0198
1.00	0.0166	0.0166
2.00	0.0182	-
3.00	-	0.0213
4.00	0.0230	0.0254
8.00	0.0388	0.0291
21.00	0.0480	0.0593
24.00	0.0619	0.0614

Table C-24 Volume median size of run no. 9 and 10.

Time	Crystal content [kg particle / kg suspension]			
[hr]	**b#1, s#1**	**b#1, s#2**	**b#2, s#1**	**b#2, s#2**
0.00	0.0027		0.0026	
1.00	0.0093	0.0098	0.0069	0.0080
2.00	0.0115	0.0109	0.0091	0.0103
3.00	0.0110	0.0127	0.0119	0.0121

Table C-24 (Continued).

Time	Crystal content [kg particle / kg suspension]			
[hr]	b#1, s#1	b#1, s#2	b#2, s#1	b#2, s#2
4.00	0.0137	0.0149	0.0146	0.0136
6.00	0.0164	0.0169	0.0173	0.0173

Table C-25 Volume median size of run no. 11 and 12.

Time	Crystal content [kg particle / kg suspension]			
[hr]	b#1, s#1	b#1, s#2	b#2, s#1	b#2, s#2
0.00	0.0017		0.0014	
1.00	0.0048	0.0054	0.0055	0.0054
2.00	0.0057	0.0058	0.0054	0.0054
3.00	0.0056	0.0057	0.0057	0.0057
4.00	0.0060	0.0064	0.0066	0.0066
6.00	0.0067	0.0064	0.0065	0.0076
8.00	0.0082	0.0076	0.0073	0.0069
26.00	0.0140	0.0129	0.0201	0.0132

Table C-26 Particle size characteristics of bulk glucose monohydrate from bottle.

Distribution	Mean particle size [μm]	Standard deviation [μm]
Volume	157.08	0.465
Volume density	126.48	0.466
Number density	91.33	44.93
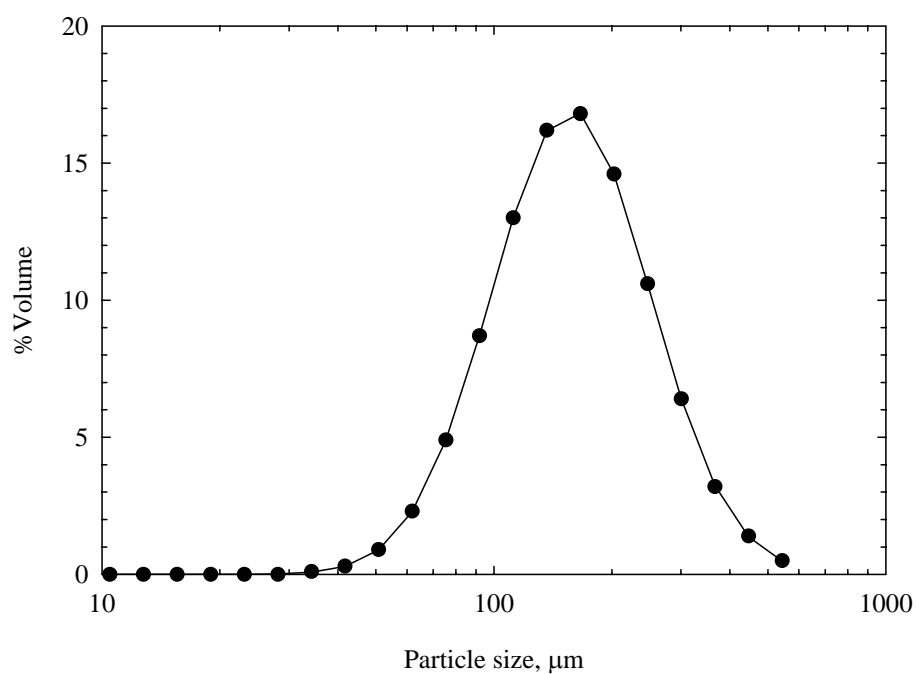
Figure C-1 Volume distribution of bulk glucose monohydrate from APS bottle.

Appendix D

Mathematical Model

The model generated in this work consists of two m file running through MATLAB version 5.3. These two m files are shown below.

File: optseed.m

```matlab
% The simulation of isothermal batch crystallization of glucose monohydrate

% The main program optseed.m is let the user to input the initial conditions

% as well as the experimental conditions

% The set of ODEs in "eqn1.m" will be called and ODE45 is used to solve the

% equations

% kg data based on number mean size

%

global kg K k1 CSAT N NP RHO

%

% format the digit

format short e

% Input the experimental temperature in C

disp('Please input the experimental temperature in degree C (0-40 C)')

T1 = input('Temperature(C)=');

% Calculation of temperature in K

T = T1+273.15; % K

% Calculation of the growth rate constant (kg) of glucose monohydrate

kg = (10^(8.33-2610./T))*10^-6; % m/min

CSAT = (33.82+0.6484*T1+0.00135*T1^2)/100.;        % kg glucose/kg solution
```

% Calculation of overall mutarotation rate (k) of glucose

k = (10^(10.8-4210./T))*60;   % 1/min.

% Average equilibrium constant from experimental results

K = 1.5;

% Calculation of forward mutarotation rate (k1)

k1 = k*K/(1+K);   % 1/min

N = 1.;   % growth order

RHO = 1560.;   % kg/m3 density of glucose monohydrate crystal

%

% INPUT the initial conditions

%   L   seed size

%   mgc   mass of seed

%   ms   mass of solution

%   mgs   mass of glucose in solution

%   x1   alpha glucose fraction

%   x0   vector of set of initial condition

%

% Input seed size in micron

L1 = input('Seed size (micron)=');

L = L1*10^-6 ;   % seed size in m

% Input mass of seed in g

m1 = input('Mass of seed added (g)=');

mgc = m1*10^-3;   % seed amount in kg

% Initial mass of solution

```
ms = 1.0;                              % mass of solution, kg

% Input the initial glucose concentration

C = input('Initial glucose concentration (kg glu/kg soln)=');

mgs = C*ms;                % calculate total amount of glucose in solution, kg

% Initial alpha glucose fraction

x1= 0.40;                              % equilibrium fraction of alpha

% Calculation of number of crystal

NP =  (mgc*6.)/(pi*RHO*L^3);

x0 =  [L; mgc; ms; mgs; x1];

t0 = 0.0;  tf = 3000.0;                % t in min

[t,x] = ode45('eqn1', [t0 tf],x0);

xdot1 = zeros(length(t),1);

for ii = 1:length(t)

  xdot = eqn1(t(ii),x(ii,:));

  xdot1(ii) = xdot(1);

end
```

File: eqn1.m

```
function xdot = eqn1(t,x)
%
global kg K k1 CSAT N NP RHO
%
% xdot(1) is the rate of change of crystal size (G), m/min

% xdot(2) is the rate of crystal mass deposition, kg/min

% xdot(3) is the rate of decrease of total free solution mass, kg/min

% xdot(4) is the rate of decrease of the mass of total glucose in solution, kg/min

% xdot(5) is the rate of change of alpha glucose fraction, 1/min

xdot(1) = kg*((x(5)*x(4)/x(3)-CSAT/(1+K)) /(CSAT/(1+K)))^N;

xdot(2) = 0.5*xdot(1)*pi*x(1)^2*NP*RHO;

xdot(3) = - xdot(2);

xdot(4) = -(180/198)*xdot(2);

xdot(5) = (k1/K)*(1-x(5))-k1*x(5)+xdot(4)/x(4);

xdot = [xdot(1);xdot(2);xdot(3);xdot(4);xdot(5)];
```

BIOGRAPHY

Miss Sukanya Srisa-nga was born on the 1st of October 1976 in Burirum province. She earned her Bachelor's degree in Chemical Engineering from Suranaree University of Technology (SUT), Nakhon Ratchasima, in 1999. After graduation, she worked as Quality Guarantee Engineer (QG Engineer) with Siam Tyre Industry Co., Ltd., Saraburi, for a year (During 1999-2000). She has received the RGJ-Ph.D. scholarship from the Thailand Research Fund (TRF) to study the doctoral degree in Chemical Engineering at SUT since year 2000.